NASA TM X-335

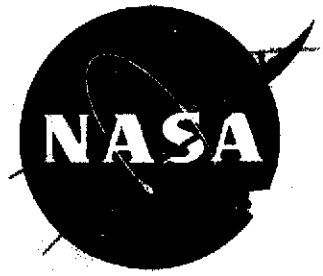

TECHNICAL MEMORANDUM

X-335

LONGITUDINAL STABILITY AND CONTROL CHARACTERISTICS OF MISSILE CONFIGURATIONS HAVING SEVERAL HIGHLY SWEPT CRUCIFORM FINS AND A NUMBER OF TRAILING-EDGE AND FIN-TIP CONTROLS AT MACH NUMBERS FROM 2.21 TO 6.01

By George C. Ashby, Jr., and Paul E. Fitzgerald, Jr.

Langley Research Center
Langley Field, Va.

CLASSIFICATION CANCELLED
Authority NASA TM-X-378 4/3/63
Date

(NASA-TM-X-335) LONGITUDINAL STABILITY AND CONTROL CHARACTERISTICS OF MISSILE CONFIGURATIONS HAVING SEVERAL HIGHLY SWEPT CRUCIFORM FINS AND NUMBER OF TRAILING EDGE AND FIN TIP CONTROLS (NASA) 125 p

N73-73881

Unclas
00/99 08034

NATIONAL AERONAUTICS AND SPACE ADMINISTRATION

WASHINGTON

January 1961

REPRODUCED BY
NATIONAL TECHNICAL
INFORMATION SERVICE
U.S. DEPARTMENT OF COMMERCE
SPRINGFIELD, VA 22161

1C

NATIONAL AERONAUTICS AND SPACE ADMINISTRATION

TECHNICAL MEMORANDUM X-335

LONGITUDINAL STABILITY AND CONTROL CHARACTERISTICS OF MISSILE CONFIGURATIONS HAVING SEVERAL HIGHLY SWEPT CRUCIFORM FINS AND A NUMBER OF TRAILING-EDGE AND FIN-TIP CONTROLS AT MACH NUMBERS FROM 2.21 TO 6.01*

L 8 37

By George C. Ashby, Jr., and Paul E. Fitzgerald, Jr.

SUMMARY

An investigation has been made in the Langley 20-inch Mach 6 tunnel to determine the longitudinal stability and control characteristics of missile configurations employing a series of low-aspect-ratio, highly swept, cruciform fins and a number of fin-tip and trailing-edge controls. Data are presented for an angle-of-attack range of -4° to 30°, control deflections of 0° to -30°, roll angles of 0° and 45°, and a Reynolds number of 6×10^6 per foot. Previously unpublished data from the Jet Propulsion Laboratory of these same configurations at Mach numbers of 2.21, 3.50, and 4.76 are also presented.

Test results show that at Mach number 6.01 fins having flat-plate profiles are more stable and produce more normal force than the fins having double-wedge or modified-hexagonal profiles. At Mach numbers of 2.21, 4.76, and 6.01, the slope of the normal-force curve over the angle-of-attack ranges of 0° to 10° and 10° to 20° can be considered to be a linear function of total planform area and is essentially independent of planform, fin position, and roll angle.

Diamond-profile trailing-edge controls were found to be more effective in producing pitching moment than flat-plate trailing-edge controls at all angles of attack of the tests and more effective than the fin-tip controls at angles of attack above 8°. Rolling the model to 45° had little influence on the pitching effectiveness of the trailing-edge controls but significantly increased the effectiveness of the tip controls.

*Title, Unclassified.

INTRODUCTION

Operational fighters and long-range missiles are flying at high supersonic speeds. Ground-to-air and air-to-air missiles which are to intercept such targets must operate at hypersonic speeds and are required to be highly maneuverable. References 1 to 3 present results from tests of configurations that apparently satisfy the condition of maneuverability at supersonic speeds. These configurations were missiles with highly swept, low-aspect-ratio wings having comparatively low drag penalty when the leading edges were blunted to reduce aerodynamic heating rates, small induced rolling moments, small center-of-pressure shifts, and longitudinal and directional stability.

In order to provide information on the longitudinal stability and control characteristics of such configurations in the hypersonic speed range, a series of fin-body configurations has been tested in the Langley 20-inch Mach 6 tunnel. The primary configuration investigated consisted of an ogive-cylinder body in combination with cruciform fins of various spans, chords, profiles, and planforms. The majority of the configurations was tested with the fins in two different longitudinal locations on the body. Several of the fin-body configurations were tested with fin-tip or trailing-edge controls. In addition, the nose fineness ratio was changed on two configurations and the afterbody fineness ratio on another.

The present paper presents the normal-force and pitching-moment characteristics of the various configurations at a Reynolds number of 6×10^6 per foot and a Mach number of 6.01 for angles of attack from -4° to 30°, control-deflection angles from 0° to -30°, and roll angles of 0° and 45°. In addition, longitudinal stability and control characteristics obtained from previously unpublished data from the Jet Propulsion Laboratory of these same configurations at Mach numbers of 2.21, 3.50, and 4.76 are presented to show variation with Mach number.

SYMBOLS

The aerodynamic moments were taken about the 59-percent, 55.6-percent, and 58.7-percent station of bodies I, II, and III, respectively. Coefficients are referenced to the body-axis system as shown in figure 1.

A	cross-sectional area of cylindrical section of body, sq in.
A'	total planform area of configuration for $\phi = 0^\circ$, sq in.

A''	planform area of two longitudinal controls, sq in.
C_N	normal-force coefficient based on body cross-sectional area, F_N/qA
C_N'	normal-force coefficient based on total planform area, F_N/qA'
$\Delta C_N''$	normal-force control-effectiveness coefficient based on control planform area, $\Delta F_N/qA''$
C_m	pitching-moment coefficient based on body cross-sectional area and body diameter, M_Y/qAd
C_m'	pitching-moment coefficient based on total planform area and root chord, $M_Y/qA'c_r$
$\Delta C_m''$	pitching-moment control-effectiveness coefficient based on control planform area and centroid location, $\Delta M_Y/q\bar{x}_c A''$
c_r	exposed fin root chord, in.
F_N	normal force
ΔF_N	change in normal force due to control deflection, $(F_N)_\delta - (F_N)_{\delta=0}$
M	Mach number
M_Y	pitching moment
ΔM_Y	change in pitching moment due to control deflection, $(M_Y)_\delta - (M_Y)_{\delta=0}$
d	diameter of cylindrical section of body, in.
l	length of body, in.
X,Y,Z	body axes as shown in figure 1
$\bar{x}$	centroid of fin planform area measured from tip of body nose
$\bar{x}_c$	centroid of control planform area measured from moment reference center of body

L 8 3 7

x_{cp} distance from nose of body to center of pressure, in.

r radius, in.

q free-stream dynamic pressure, lb/sq in.

α angle of attack of body center line, deg

δ_Y deflection angle of control in the XZ-plane, negative when trailing edge is up, deg

δ_Z deflection angle of control in the XY-plane, negative when trailing edge is up, deg

ϕ angle of roll about the body center line, deg

C_{N_α} slope of normal-force curve, $dC_N/d\alpha$

APPARATUS AND METHODS

Tunnel

The tests were made in the Langley 20-inch Mach 6 tunnel. A schematic drawing of the tunnel system and the tunnel is shown in figure 2. The tunnel is of the blowdown-to-atmosphere type capable of operation at a maximum stagnation pressure of 580 lb/sq in. and a maximum stagnation temperature of 600° F.

The 135,000 cubic-foot tank field from which the flow emanates is charged and maintained at 600 lb/sq in. during operation by a 6-stage centrifugal compressor. The air is dried by an activated alumina dryer designed to provide a dewpoint temperature of -40° F at a pressure of 600 lb/sq in. Before the flow enters the settling chamber, it passes through a heat exchanger to be heated to a temperature high enough to avoid air liquefaction in the test section. The heat exchanger is designed to heat the air to a temperature as high as 600° F.

The settling chamber of the tunnel is fitted with a perforated cone and screens which serve to filter the flow as well as uniformly distribute the flow to the first minimum. The perforated cone distributes the entering flow more uniformly to the screens and prevents damage to them. The test section is nearly square being 20.5 inches high by 20 inches wide, and the convergence and divergence of the nozzle from the settling chamber to the test section is in the vertical plane only. In order to allow lower starting and operating pressures, the tunnel is equipped

with an annular ejector and a variable second minimum. The contraction to and the expansion after the second minimum are in the horizontal plane only; however, for convenience they are shown in figure 2 in the vertical plane.

The models were supported in the tunnel by the "goose-neck" support shown in figure 3. With the support mounted from the top as shown, the horizontal plane is the angle-of-attack plane. An optical system was used to set the angle of attack, thereby eliminating the need for balance- or sting-deflection corrections or both. A combination of a lens and a right-angle prism with a focal length of 60 inches was imbedded in the model surface at the center of rotation of the support system. The reflection of the light of a 25-watt mercury-arc-point source by the prism was projected on a screen, and the location of the light on the screen was calibrated as a function of angle of attack. The prism has the advantage over a mirror in that rotation of the prism about its axis (such as, when the model is rolled) has no effect on the direction of the light reflection for roll angles up to 42°. The prism was mounted 22.5° above the horizontal plane when the model was in the position of $\phi = 0^\circ$. This placed the prism 22.5° below the horizontal plane when the model was rolled to a position of $\phi = 45^\circ$, thus keeping it well within the maximum 42° deflection.

Normal force and pitching moment were measured with a two-component, water-cooled, internal, strain-gage balance.

Model Configurations

The geometric characteristics of the bodies, fins, and controls are given in table I and figure 4. The configurations shown in figure 5 were formed by attaching the various combinations of forebodies, fins, and controls to a basic cylindrical afterbody. The configurations are identified by a three digit code. The first, second, and third digits correspond to the body, the fin, and the control numbers, respectively, which are given in figure 4. The fins could be positioned at two longitudinal locations on the body, one body diameter apart. Figure 6 is a photograph of the component parts of the model configurations.

Bodies.- The majority of the configurations employed a basic body having an ogive nose with a fineness ratio of 3.5 and a cylindrical afterbody with a fineness ratio of 9.83 (fig. 5). In some instances the nose fineness ratio was reduced to 2.5, and in another the afterbody fineness ratio was increased to 10.43.

Fins.- The nine sets of clipped-delta fins in figure 4 had various planforms, profiles, spans, and chords. All of the fins had rounded

leading edges and blunt trailing edges. The leading-edge sweep angle varied from approximately 73° to 81°.

Fins 1 and 2 have double-wedge profiles and have equal root and tip chords; however, fin 2 has a larger span and, therefore, a larger aspect ratio and a smaller sweep angle. Fin 3 is the same as fin 2 except it has a flat-plate profile. Fins 4 and 5 differ only in profile. Fin 4 has a modified hexagonal profile and fin 5 is a flat plate. Fin 6 is also a flat plate with the same sweep angle and aspect ratio as fin 5. However, its span and root chord have been reduced. Fins 7, 8, and 9 are all flat plates with cranked leading edges. Fin 8 differs from fin 7 only in chord. Both the root and tip chords of fin 8 are an equal amount less than those of fin 7. Fins 7 and 9 have equal root and tip chords; however, fin 9 has a larger span and a larger aspect ratio but a smaller sweep angle.

Controls.- Four sets of trailing-edge controls (controls 1, 2, 3, and 4) had the same chord. Controls 1, 2, and 3 also have the same span. Controls 1 and 2 are flat plates with the hinge line located at the 50-percent and 25-percent chord point, respectively. Control 3 has its hinge line at the 50-percent chord point also, but it has a diamond profile. Control 4 is similar to control 3 except it has a larger span. The flat-plate controls 1 and 2 had rounded leading edges and blunt trailing edges; whereas the leading and trailing edges of the diamond-profile controls 3 and 4 were sharp.

Two of the three sets of tip controls (controls 5 and 6) had the same double-wedge profile with a rounded leading edge and a blunt trailing edge and the same basic delta planform with a leading-edge sweep of 30°. However, the tip was clipped on one set (control 6), forming a trapezoidal planform. Control 7 had a delta-planform shape with a flat-plate profile and was attached to a trailing-edge flap. Both the leading and trailing edges were rounded. Controls 4 and 7 were the only ones not deflected in the tests.

TEST CONDITIONS AND ACCURACY

Tests

All tests were made at a stagnation temperature of 400° F, a stagnation pressure of 315 lb/sq in. absolute, and a Mach number of 6.01. The Reynolds number was 6.0×10^6 per foot, or based on body diameter it was 0.64×10^6. Tests were made through an angle-of-attack range from -4° to 30°, control deflection angles up to -30°, and roll angles of 0° and 45°.

Accuracy

The values presented in this section are the maximum errors that could have occurred in the tests. For the coefficients, the first term includes errors inherent in the balance and readout equipment, and the second term accounts for the maximum variation in tunnel stagnation pressure which was always positive. Because of the continuity of the data, it is believed that the actual accuracy is considerably better than that which these values infer.

C_N	$\pm \frac{0.2357 \text{ sq in.}}{A} + 0.01C_N$
C_N'	$\pm \frac{0.2357 \text{ sq in.}}{A'} + 0.01C_N'$
$\Delta C_N''$	$\pm \frac{0.2357 \text{ sq in.}}{A''} + 0.01\Delta C_N''$
C_m	$\pm \frac{0.2223 \text{ cu in.}}{Ad} + 0.01C_m$
C_m'	$\pm \frac{0.2223 \text{ cu in.}}{A'c_r} + 0.01C_m'$
$\Delta C_m''$	$\pm \frac{0.2223 \text{ cu in.}}{A''\bar{x}_c} + 0.01\Delta C_m''$
M	± 0.01
α, deg	± 0.10
δ, deg	± 1.00

PRESENTATION OF RESULTS

The following table presents a complete listing of the data figures in order to aid the reader in finding specific results. The figures are discussed in the subsequent sections.

	Figure
Aerodynamic characteristics of all configurations tested	7 to 38
Effect of fin or fin control profile on aerodynamic characteristics at $\phi = 0^\circ$	39
Effect of planform and planform area on aerodynamic characteristics at $\phi = 0^\circ$	40 to 44
Effect of fin longitudinal location on aerodynamic characteristics at $\phi = 0^\circ$	45
Effect of roll angle on aerodynamic characteristics	46
Effect of Mach number on aerodynamic characteristics at $\phi = 0^\circ$	47 to 51

DISCUSSION

The data of the report are divided into four sections. In section I all of the test data obtained for this program in the Langley 20-inch Mach 6 tunnel are presented as plots of C_m and α against C_N (figs. 7 to 38). Section II presents comparisons of longitudinal stability characteristics between configurations where fin profile, planform, span, chord, aspect ratio, roll angle, or fin longitudinal location is varied (figs. 39 to 51). In section III correlations of C_{N_α} with configuration total planform area for three angle-of-attack ranges are presented for all configurations at a Mach number of 6.01. Correlations of the center-of-pressure location of the fin with the centroid-of-area location of the fin are also presented for a Mach number of 6.01 (figs. 52 to 55). Section IV contains comparisons of both pitching-moment and trim effectiveness of trailing-edge controls having different hinge-line locations or profiles at two roll angles and a Mach number of 6.01. The effectiveness of tip controls is compared to that of the trailing-edge controls at the two roll angles at a Mach number of 6.0 (figs. 56 to 62). In addition, sections II, III, and IV contain previously unpublished test data from the Jet Propulsion Laboratory for Mach numbers 2.21, 3.50, and 4.76.

I. Basic Aerodynamic Characteristics of All Configurations at a Mach Number of 6.01

Because experimental data at hypersonic Mach numbers are not overly abundant, all the data obtained at a Mach number of 6.01 have been systematically shown in figures 7 to 38. Most of the data are discussed in connection with the comparison parts of sections II, III, and IV and are, therefore, presented in this section without comment.

II. Effect of Fin Configuration

All of the fins of the present investigation have blunted leading edges whose sweep is such that at a free-stream Mach number of 6.01, the Mach number normal to the leading edge is transonic. Reference 4 shows that for rounded leading edges at a Mach number of 5.8, the normal-force coefficient is not significantly affected by changing the Mach number normal to the leading edge from less than sonic to greater than sonic. Therefore, in the present tests there should be no significant effect of sweep-angle variation and leading-edge bluntness, and the data will be discussed only with respect to various profiles, planforms, spans, and chords.

Profile.- Figure 39 presents comparisons between configurations having the same planform and planform area but different fin profiles. In figure 39(a) a configuration having a fin with a double-wedge profile, configuration I-2, is compared with a configuration having a flat-plate profile, configuration I-3. The flat-plate profile (fin 3) produces the greatest normal-force coefficient and is more stable (larger restoring moment) than the double-wedge profile (fin 2) especially at the higher angles of attack. (Throughout the remainder of the discussion, references to stability will refer to the trends of the pitching-moment curve.) The reduction in stability when the profile is changed from a flat plate to a wedge is due to the forward shift of the center of pressure on the wedge in addition to the reduction in normal force. The reason for the reduction in normal force is not so obvious; therefore, a two-dimensional calculation using the shock-expansion method was made.

Since the pressure on the upper surface of a fin at angles of attack sufficient to shield the surface from the flow is nearly a vacuum in hypersonic flow, the normal force is almost wholly produced by the pressure on the lower surface. By using the shock-expansion method, the average pressures on the root section of the lower surfaces of fins 2 and 3 were determined for a Mach number of 6.01 and angles of attack up to 30°. Leading-edge bluntness was neglected because it was the same in both cases. The calculation shows that at angles of attack above about 20° the flat-plate fin has the larger lower surface pressure.

Further shock-expansion calculations showed that if the wedge half-angle were increased from 1.2° to a value above 3.00°, the double-wedge profile fin configuration would produce a larger average pressure than the flat plate throughout the angle-of-attack range from 0° to 30°. In this case, however, the stability of the double wedge would be decreased considerably.

In figure 39(b), a configuration having a fin with a modified-hexagonal profile, configuration I-4, is compared to a configuration having a flat-plate profile, configuration I-5. In addition, two configurations with fins and controls, I-1-1 and I-1-3, having the same total planform and planform area as the other two configurations are also presented in figure 39(b). The latter two configurations consisted of the same double-wedge-profile fin separated by a 0.050-inch gap from a flat-plate trailing-edge control in one case and a diamond-profile control in the other. The diamond-profile control had a sharp leading edge, and the flat-plate control had a rounded leading edge.

Again, the flat-plate-profile configuration I-5 produces the greatest normal-force coefficient and is more stable than the other configuration shown. Evidently the expansions on the lower surface of the modified-hexagonal profile, and the expansion and leakage through the gap on lower surfaces of the configurations with fins and controls reduce the average pressure over the lower surfaces below that over the lower surface of the flat plate.

Since the wedge half-angle of the modified-hexagonal profile (fin 4) is larger than that on the double-wedge profile in figure 39(a), it was decided to check the average pressure on the lower surface of the root section by the shock-expansion method to see if it would be smaller than that on a flat plate. Again, the average pressure was found to be less than that on a flat plate at a Mach number of 6.01 and angles of attack above about 20°. There is other evidence that the expansion on the lower surface is the cause of the normal force being less than on a flat plate. The expansion on the lower surface of the modified-hexagonal configuration of figure 39(b) occurs over a larger portion of the surface than on the double-wedge configuration of figure 39(a), and it is interesting to note that its normal-force coefficient is reduced a larger amount from the flat-plate value.

The stability and normal force of the configurations with fins and controls are not very much less than those of the flat plate. Evidently the reduction in normal force due to the expansion on the lower surface of the fin and leakage through the gap is alleviated somewhat by the compression over the control lower surface.

Planform and planform area.- The effect of cranking the leading edge of the fin while keeping the root and tip chords and span constant

is shown in figure 40. Cranking adds about 5 percent area in the forward-outboard region. The addition of area in this region produces an increase in normal-force coefficient and a forward shift of the center of pressure. It should be remembered that the coefficients are now based on the total planform area of the configuration.

Figure 41 shows a comparison between two configurations having the same basic fin to which an equal amount of area has been added. In one case, the area was added by cranking the leading edge while holding the root and tip chord and span constant. In the other case the area was added in the form of a delta tip control. The latter configuration (I-3-7) fouled at an angle of attack of 24°; that is, the strain-gage balance deflected enough for the trailing edge of the model to hit the support sting. However, the data at the lower angles of attack are sufficient to show that the addition of area at the tip is much more effective in producing normal force than the addition along the leading edge. Due to its more rearward position, it is also more stabilizing.

Figure 42 shows the effect of increasing the area by increasing the chord. In figure 42(a) the basic fin has a cranked leading edge and a flat-plate profile. The second configuration is formed from the first by adding a constant-span trailing-edge section as an integral part. The basic fin of figure 42(b), however, has a straight leading edge and a double-wedge profile. The second configuration is formed from the first by adding a constant-span, diamond-profile, trailing-edge control which was separated from the basic configuration by a 0.050-inch gap. The area added in both cases is the same.

The normal-force coefficient increases with increasing area the same amount in both figures. However, the stability is increased considerably more in the case in which the diamond control was added. This indicates that the center of pressure shifts further aft in the latter case. This would also occur if the control were a flat plate. (See fig. 39(b).)

Figure 43 presents the comparison between flat-plate fins having approximately the same exposed aspect ratio but different spans and chords. The comparison shows that the normal-force coefficients and pitching-moment coefficients are functions of the area. The pitching-moment coefficients are adjusted to account for the difference in fin longitudinal location by assuming that the center of pressure occurs at the centroid of area of each fin.

Aspect ratio.- The effect of increasing the aspect ratio by increasing the span while holding the root and tip chords constant is shown in figure 44 for three configurations. This change results in an increase of area and a decrease in sweep angle. As noted previously the effect of sweep was found to be negligible for similar configurations

in reference 4; therefore, the increase in normal force and pitching moment is a result of increased aspect ratio.

Fin location.- In figure 45, comparisons are made between the aerodynamic coefficients for two longitudinal locations of the fin on the body. The locations are one diameter of the body apart. The configurations for which the comparisons are made are representative of those of the present investigation.

The pitching-moment coefficient decreases as expected as the fin is moved forward; however, it is shown subsequently that it is not necessarily true that the center of pressure moves the same amount as the fin. There are only slight variations in the normal-force coefficient with changes in fin location. For the two shorter span configurations shown in figures 45(a) and 45(c), the normal-force coefficient for the fin forward is equal to or less than that for the fin rearward. For the larger spans (figs. 45(b) and 45(d)) the fin in the forward position produces the larger normal-force coefficient.

Roll angle.- Figure 46 presents comparisons of the aerodynamic characteristics of representative configurations at $\phi = 0^\circ$ and 45°. It should be noted that the normal force was always measured in the angle-of-attack plane, and at $\phi = 45^\circ$ the normal force measured is the sum of the components of the normal force of each fin in the angle-of-attack direction.

At $\phi = 45^\circ$ the projected area of the four fins in the horizontal plane is approximately 1.4 times that of the two fins at $\phi = 0^\circ$. However, for the configurations shown in figures 46(a) to 46(d), the normal-force coefficient at $\phi = 45^\circ$ is only slightly larger than that at $\phi = 0^\circ$ up to an angle of attack of 26°. For angles of attack above 26° the reverse is true. For configurations with tip controls (figs. 46(e) and 46(f)) the normal-force coefficient is larger at $\phi = 45^\circ$ than at $\phi = 0^\circ$ over the entire angle-of-attack range; however, there is a definite decrease in the amount that it is larger as angle of attack increases above 26°.

The effects of roll angle on normal force are a result of two influences: the influence of the body vortices, and the influence of the effective sideslip and effective angle of attack on the normal force of each fin (ref. 5).

When a cruciform-finned body at a given angle of attack is rolled about its longitudinal axis, the fins move relative to the body vortices and each pair of diagonally opposite fins is positioned in a combined angle of attack and sideslip flow. At any roll angle other than 45°, the two pair of fins would be influenced differently by the vortices and would have different values of angle of attack and sideslip;

however, in the present investigation the only roll angle was 45° and only one pair of fins, those in the XY-plane, will be discussed.

At 0° roll and an angle of attack greater than zero, the fins in the XY-plane are the only ones contributing to the normal force. When the body is rolled, one of these fins, herein referred to as the windward fin, moves away from the body vortex and is effectively sideslipped into the flow at a reduced angle of attack while the other, the leeward fin, moves towards the vortex and is effectively sideslipped away from the flow at the reduced angle of attack. The reduced effective angle of attack reduces the normal forces on both the windward and leeward fins, but the sideslip and the change of influence of the vortices increases the normal force on the windward fins and decreases it on the leeward fins. The net result is that compared to the fins at $\phi = 0°$, the fins on the leeward side of a rolled body will have their normal force reduced because of the body vortices, the reduced effective angle of attack, and the effective sideslip angle. The fins on the windward side will have their normal force reduced less because the vortices have less effect and the sideslip increases the normal force. The effect of reduced angle of attack was the same.

L
8
3
7

In the present investigation the sum of the components of normal force of the two pair of fins at a roll angle of 45° is approximately equal to the normal force of one pair at a roll angle of 0°; therefore, rolling the body 45° reduces the force normal to the fins in the XY-plane to 0.7 of its value at a roll angle of 0°. All of the configurations show a loss in stability with roll angle except for one of the configurations with the shortest span (fig. 46(g)) for which there is an increase in stability.

Mach number effect.- The variation of normal-force and pitching-moment coefficients with Mach number is shown in figures 47 to 51 for configurations representative of this investigation. Data for both the forward and rearward locations of the fins are presented for each configuration. Each figure contains data at roll angles of 0° and 45° when available and at angles of attack of 10°, 20°, and 28°.

The normal-force and pitching-moment coefficients generally decrease with increasing Mach number. This decrease in normal-force and pitching-moment coefficients would be expected from oblique-shock considerations. The rate of change of the coefficients is highest in the range of Mach numbers from 2.21 to 4.76. From Mach number of 4.76 to 6.01 the change is small. The rate of change of the coefficients with Mach number

generally increases as angle of attack increases especially in the Mach number range of 2.21 to 4.76.

III. Correlations of Aerodynamic Characteristics For All Configurations

Correlation of C_{N_α} with planform area.- In hypersonic flow the variation of normal-force coefficient is nonlinear with angle of attack. However, it is noted for the various configurations of the present investigation that for the three selected angle-of-attack ranges of 0° to 10°, 10° to 20°, and 20° to 30°, the average slope of the normal-force curve is quasi-linear. For the majority of the configurations, C_{N_α} is plotted in figure 52 against the ratio of total planform area at $\phi = 0°$ to body cross-sectional area for Mach numbers of 6.01, 4.76, and 2.21.

The correlations show that the slope of the normal-force curve in the angle-of-attack ranges of 0° to 10° and 10° to 20° can be considered a linear function of the total planform area and is nearly independent of fin planform, roll angle, and the longitudinal location of the fins on the body for all three Mach numbers. In the angle-of-attack range of 20° to 28° the slope is still a linear function of area but varies significantly with planform. (See fig. 52.) At a Mach number of 2.21, the scatter of the test points increases especially at angles of attack above 20°.

Figure 53 shows the slope of the correlation curves $\frac{dC_{N_\alpha}}{d(A'/A)}$ of figure 52 plotted against Mach number for the three angle-of-attack ranges. For angle-of-attack ranges of 0° to 10° and 10° to 20°, $\frac{dC_{N_\alpha}}{d(A'/A)}$ decreases as Mach number increases. However, the variation of $\frac{dC_{N_\alpha}}{d(A'/A)}$ with Mach number decreases as angle of attack increases becoming nearly zero in the angle-of-attack range of 20° to 28°.

Correlation of x_{cp}/l with centroid location.- Since stability is a function of the longitudinal location of the fin on the body, a correlation of the fin center-of-pressure location as a function of fin centroid-of-area location is presented in figure 54 for Mach numbers of 6.01, 4.76, and 2.21. The center-of-pressure values were based on body-fin data minus body-alone data; thus, the interference effects of the fins on the body were not considered. The figures include data for

both the forward and rear position of the fin on the body, for roll angles of both 0° and 45°, and for angles of attack of 4°, 10°, 20°, and 30°.

At a Mach number of 6.01 (fig. 54(a)) and a roll angle of 0°, the correlation shows that for all configurations except two the shift of the center of pressure with variation in angle of attack is less than 1 percent of the body length. One of the configurations for which the center of pressure shifted more was unstable, and the other had the shortest span fin. With the exception of the shortest span configuration, the center of pressure is within ±2.0 percent of the body length of the centroid of area for both roll angles. Rolling the body does, however, tend to move the center of pressure forward and increases the variation of its location with angle of attack.

L
8
3
7

As Mach number is reduced in figures 54(b) and 54(c), the center of pressure tends to move forward of the centroid-of-area location and the variation of its locations with angle of attack tends to increase at roll angles of both 0° and 45°. However, its location is always within 4 percent of the body length from the centroid except for configuration I-7 at an angle of attack of 4° and a roll angle of 45° (fig. 54(c)).

Figure 54 includes data points for both the forward and rearward locations of the fins on the body. However, because no distinction is made between the data points for the two different fin locations, the figures do not reveal the difference in location of center of pressure for the same configuration with different fin locations. This difference is shown in figure 55. This figure presents the ratio of the center-of-pressure movement to the centroid-of-area movement when the fins are moved against angle of attack for representative configurations of this investigation at 0° and 45° roll and Mach numbers 6.0, 4.76, and 2.21.

The figure indicates that at all three Mach numbers, for the majority of the cases, when the fin is moved longitudinally on the body the center of pressure of the fin shifts within ±10 percent of this longitudinal distance. The data points which are greater than ±10 percent are primarily at an angle of attack of 4° where the accuracy of the center-of-pressure location is less than that at the higher angles of attack.

IV. Control Effectiveness

Values of C_N and C_m for several missile configurations having different types of controls were obtained at angles of attack from -4° to 30°, control deflections from 0° to -30°, and roll angles of 0° and 45°. For the sake of comparing controls having different planform

areas, $\Delta C_N''$ and $\Delta C_m''$ values have been computed on the basis of individual control area and distance of control centroid from model moment reference center. These are, however, only effectiveness indicators and in comparing one control with another, it sometimes becomes difficult to say definitely that one control has a greater "total" effectiveness than the other. The dilemma arises when there is an attempt to attach some relative value to an amount of $\Delta C_N''$ lost and to compare it with an amount of $\Delta C_m''$ gained in a specific control deflection. In powered flight, it can be said that the $\Delta C_m''$ factor is more important than the $\Delta C_N''$ factor, but the amount of importance depends on the specific control manuever under consideration. For this reason, the majority of the data are presented as $\Delta C_N''$ and $\Delta C_m''$ plotted against δ and no attempt has been made to show "total" effectiveness. It will be seen in several instances, however, that some controls are obviously more effective than others.

Effect of control hinge-line location.- In order to determine the influence of a hinge-line shift on the effectiveness of the trailing-edge controls, two sets of controls, one having a hinge line at 50-percent chord (control 1) and the other at 25-percent chord (control 2) were tested. For both of these cases, data were obtained at control deflections of -5°, -15°, and -30°. The sign convention was chosen such that a negative deflection causes a positive increment in pitching moment.

It can be seen from figure 56(a) that at an angle of attack of 0° and a roll angle of 0°, the forward hinge-line control (control 2) is roughly twice as efficient in producing moment as the control with the rearward hinge line (control 1). The corresponding decrease in $\Delta C_N''$ at $\alpha = 0^\circ$ and $\phi = 0^\circ$ is also about twice as much for control 2 as for control 1. This was seen to be true at all tested control deflection angles and can be attributed to the fact that a greater percentage of the control surface of control 2 lies further outside the low-energy flow region directly behind the fin. It can be easily reasoned that as the control surface moves further out of this region, its effectiveness will increase (ref. 6).

The advantage of control 2 over control 1 decreases as the values of control deflection and angle of attack increase so that at control deflections above -14° and angles of attack above 14°, control 1 shows a clear advantage over control 2 in producing pitching moment. In view of the fact that many guided missiles are required to execute low-radius turns through fairly large turning angles, it can be said that, for this case, the rearward hinge-line, trailing-edge control is the more effective of the two controls. It should be noted, however, that control 2 retains an advantage over control 1 up to an angle of attack

of 30° for control deflections of less than -8°. It should also be noted that the opening between the fin and control 2 is smaller than that between the fin and control 1 when both controls are deflected the same amount. It will be shown subsequently that this opening size influences the control effectiveness, and there is some indication that if the gap size forward of control 2 were increased, the effectiveness of the control would also increase.

As can be seen in figure 56(b) what has been said about the comparative effectiveness of controls 1 and 2 at $\phi = 0°$ also holds true at $\phi = 45°$.

L
8
3
7

Effect of control profile.- In order to determine the relative merit of two common control profiles, a flat-plate control with circular leading edge (control 1) and a diamond-profile control (control 3) were tested, and the results of their influence on C_m and C_N of the missile were compared in figure 57. Both controls had the same planform area, aspect ratio, maximum thickness, and hinge-line position (50 percent control chord); the only difference was their profile.

It was seen that throughout the positive range of angle of attack and at all control deflections, the diamond profile (control 3) was more effective in producing changes in pitching moment. Figure 57(a) shows that at a roll angle of 0° the diamond profile is approximately twice as effective as the flat-plate control. The reason for this increased effectiveness is that the forward half of the upper surface of the diamond-profile control in the deflected position is always at a greater negative angle to the flow than the upper surface of the flat plate; thus, the local pressures are higher and there is a resulting increase in C_m and decrease in C_N (ref. 7). The opposite effect of this difference in surface angle, on the lower side of the control, is small due to the very low pressures in this leeward region.

Figure 57(b) shows essentially the same result at a roll angle of 45°.

Comparison of fin-tip and trailing-edge controls.- Since it has been seen in comparing the different trailing-edge controls that the diamond profile with the hinge line at 50 percent control chord was most effective, a comparison between this control and two fin-tip controls is shown in figure 58. The control-effectiveness parameters $\Delta C_m''$ and $\Delta C_N''$ for these three controls are again based on their respective control areas and control centroid distance from the moment reference center. Figures 58(a) and 58(b) show these values plotted against δ for the angle-of-attack range of -4° to 30° at roll angles of 0° and 45°, respectively.

It can be seen that for all angles of attack greater than 8°, control 3 is more effective than either of the two tip controls in producing pitching moment. This advantage in ΔC_m" increases with both angle of attack and control deflection. For angles of attack from 0° to 8°, the tip controls show some advantage over the diamond-profile trailing-edge control although at these low angles one tip control seems to have very little advantage over the other.

A comparison of figure 58 with figure 56 shows that the tip controls are more effective in producing pitching moment than either of the flat-plate trailing-edge controls up to an angle of attack of about 20°.

Rolling the missile to 45° has little effect on the comparison of tip with trailing-edge controls although there is a marked difference when the two tip controls are compared with each other. At a roll angle of 0° and angles of attack above 8°, control 6 shows an advantage over control 5 in producing pitching moment, but the opposite is true at a roll angle of 45°. As will be shown subsequently, the results of this comparison are not consistent with changes in Mach number.

Influence of roll on individual control effectiveness.- For both flat-plate trailing-edge controls (control 1 and control 2), the effect of roll was very nearly the same. Figures 59(a) and 59(b) show that at the lower angles of attack ($\alpha < 20°$) the controls at a roll angle of 45° were more effective in producing pitching moment, and there was a corresponding increased loss in normal force. This is true mainly because at a roll angle of 45° all four controls were deflected, and at the lower angles of attack this allows approximately 1.4 times as much effective control area as there is at a roll angle of 0° with only two controls deflected. However, at the higher angles of attack (α = 20° to 30°) the controls at a roll angle of 0° are more effective in producing pitching moment, and also the resulting loss in normal force is less than that for the controls at a roll angle of 45°. This would definitely indicate that for angles of attack greater than 20°, the controls are more effective at a roll angle of 0°. The obvious explanation for this is that when the missile is at a roll angle of 45° and at an angle of attack, the "upper" two control surfaces are partially shielded from the flow by the "lower" two fins. This effect becomes more pronounced as the angle of attack increases. It is also recalled that in figure 46 it was shown that the rate of change of the normal-force coefficient with angle of attack for various fin configurations decreased above an angle of attack of 26° at a roll angle of 45°; whereas at a roll angle of 0°, it continued to increase. Here again the gain in normal force due to the effective sideslip when the body is rolled does not increase at as high a rate above α = 26° as the body vortices and reduced effective angle of attack decreases it.

Figure 59(c) shows the data at the two roll angles plotted for control 3. Although there is a slight increase in $\Delta C_m''$ at a roll angle of 45°, there is also a corresponding slight decrease in normal force. It seems that the effect of roll on control 3 is small. This consistency of control effectiveness with roll angle might be considered as a slight advantage of the diamond-profile trailing-edge control.

The effect of roll on the wing-tip controls is considerably more significant than on any of the trailing-edge controls. Figures 59(d) and 59(e) show that with the exception of three cases, rolling the missile to 45° renders these controls more effective in changing the pitching moment of the missile. Gain in $\Delta C_m''$ and loss in $\Delta C_N''$ with increase in roll angle for the lower angle-of-attack range ($\alpha < 14°$) for both control 5 and control 6 is large and fairly consistent. At angles of attack above 20°, the delta tip control at a roll angle of 45° gives as much as 100-percent increase in $\Delta C_m''$ over the same control at a roll angle of 0°. The values of $\Delta C_m''$ for the clipped-delta control show the opposite trend at these higher angles of attack. At a control deflection of -25° and at angles of attack of 14°, 26°, and 30°, the control was less effective at a roll angle of 45° than at a roll angle of 0°.

L
8
3
7

Mach number influence on control effectiveness.- Figure 60 shows the influence of Mach number on the effectiveness of controls 1, 2, 5, and 6 for the Mach number range from 2.21 to 6.01. Unfortunately, control 3 was not tested at the lower Mach numbers and hence is not shown. Data were sampled at angles of attack of 0° and 20°, for roll angles of 0° and 45°, and control deflections from -5° to -30°.

As would be expected (ref. 8), the pitching-moment effectiveness of all controls generally decreased with increasing Mach number. The greatest decrease occurred at the lower Mach numbers for the trailing-edge controls; whereas the tip controls showed a random rate of decrease with Mach number. It should be noted that when the tip controls are compared, no one control is consistently more effective than the other as Mach number and roll angle vary. The trailing-edge controls lose about half of their effectiveness from a Mach number of 2.21 to 4.76, whereas the tip controls lose 1/3 or less in this Mach number range. From a Mach number of 4.76 to 6.01 the change in effectiveness for both types of controls is very small.

It is noted that, in general, as deflection angle is increased, the rate of change of effectiveness with Mach number in the lower Mach number range increases.

The rate of change with Mach number decreases as angle of attack increases from 0° to 20° only for a roll angle of 0°. For a roll angle of 45°, the rate of change remains the same or increases as angle of attack is increased.

Variation of $(C_N')_{trim}$ with control deflection.- Since $(C_N')_{trim}$ (C_N' at $C_m = 0$ for a particular δ) is also an indication of the effectiveness of a control, figure 61 shows this value plotted against δ for roll angles of 0° and 45°.

As would be expected, $(C_N')_{trim}$ values increase with control deflection for all controls tested. The higher values of $(C_N')_{trim}$ for control 3 again indicate the advantage of this control over the other two trailing-edge controls. The large increase in $(C_N')_{trim}$ with deflection angle for controls 1 and 3 is a result of the opening between the fin and control becoming large enough to allow unrestricted flow through it.

At the lower deflection angles, up to at least -12° for control 3, the opening is not large enough to allow unrestricted flow and the majority of the flow is deflected around the lower surface of the control and the control is effectively an integral part of the fin. However, between control-deflection angles of -12° to -24°, the opening becomes large enough for unobstructed flow to pass through and the control is effectively detached from the fin.

A comparison of figures 8 and 31 shows that this analysis is true. When control 3 is undeflected as in figure 31 it contributes some positive normal force over that of the fin alone as in figure 8. The comparison also shows that when the control is deflected -12°, it contributes no normal force at angles of attack below 20° and some positive normal force at the higher angles of attack. When the control is deflected -24°, however, it contributes a large amount of negative normal force.

Figure 31 shows that the effectiveness at a deflection angle of -24° is not only sufficient to overcome the restoring moment of the fin at an angle of attack of 0° but increases at the same rate as the restoring moment with increasing normal-force coefficient. However, at a deflection angle of -12° the effectiveness increases at a slower rate than the restoring moment of the fin as the normal force increases. The large increase in effectiveness at a deflection angle of -24° greatly increases the trim normal force.

Figure 61(b) shows that, with the exception of control 1 and control 3 at high control-deflection angles, all controls showed greater $(C_N')_{trim}$ for a roll angle of 45°.

Because the planform areas of the fin-tip controls are different from those of the trailing-edge controls, figure 61 is not intended as a comparison of the $C_{N_{trim}}$ values of the two types of controls.

Variation of $(C_N')_{trim}$ with Mach number.- Figures 62(a) and 62(b) show $(C_N')_{trim}$ plotted against Mach number at roll angles of 0° and 45°, respectively. The data taken at a Mach number of 3.50 are also previously unpublished results from the Jet Propulsion Laboratory. Control 3 was tested only at a Mach number of 6.01 and, therefore, does not appear in these plots.

With the one exception of control 1 at $\delta = -30°$, both trailing-edge controls show a definite decrease in $(C_N')_{trim}$ with Mach number at all control deflections. This would be expected since the boundary layer on the fins thickens with the increase in Mach number and, thus, more of the control surface in a low-pressure region is placed at the higher Mach numbers. The decrease is nonlinear, its slope decreasing with increasing Mach number.

In the case of the exception, control 1 at a deflection angle of -30°, the opening between the trailing edge of the fin and the leading edge of the control evidently is not large enough to pass unrestricted flow at the lower Mach numbers; therefore, the control pitching moment and trim effectiveness is greatly reduced.

The Mach number effect on both the fin-tip controls was found to be small in the range under discussion (i.e., $M = 2.21$ to 6.01). This control consistency with Mach number may be considered to be one advantage of the tip controls.

It can be seen by comparing figures 62(a) and 62(b) that the Mach number effects on $(C_N')_{trim}$ are quite different for the two roll conditions. For each control at each control deflection, the $(C_N')_{trim}$ values are greater at $\phi = 45°$ than at $\phi = 0°$.

It should be remembered that the controls vary in area; therefore, these plots show only variation of $(C_N')_{trim}$ with Mach number for each control and the reader should not attempt to compare the $(C_N')_{trim}$ values of the tip controls with those of the trailing-edge controls.

CONCLUSIONS

The longitudinal stability characteristics of missile configurations having low-aspect-ratio, highly swept, cruciform fins of various planforms, profiles, chords, and spans have been obtained. In addition, the longitudinal control characteristics of tip and trailing-edge controls were also obtained at Mach number 6.01.

An analysis of the results of this investigation and previously unpublished results obtained at the Jet Propulsion Laboratory for the same configurations at Mach numbers of 2.21, 3.50, and 4.76 indicate that:

L
8
3
7

1. The fins having flat-plate profiles produce more normal force and restoring moment at a Mach number of 6.01 than those having double-wedge or modified-hexagonal profiles.

2. At a Mach number of 6.01, increases in area increased the normal-force coefficient. Spanwise additions of area proved to be the most efficient way to increase normal force.

3. At Mach numbers of 2.21, 4.76, and 6.01 the slope of the normal-force curve over the angle-of-attack ranges of 0° to 10° and 10° to 20° can be considered quasi-linear functions of the total planform area and are independent of planform, span, roll angle, and longitudinal location of the fins on the body.

4. For the Mach number range between 2.21 and 6.01, the fin center of pressure varies from 4 percent of the body length forward of the fin centroid of area to 2 percent of the body length rearward of the fin centroid of area.

5. Longitudinal movement of the fins on the body at angles of attack above 10° and Mach numbers of 2.21, 4.76, and 6.01 resulted in a movement of the center of pressure of the fin within ± 10 percent of this longitudinal movement and has essentially no effect on the normal-force coefficient.

6. At a Mach number of 6.01 for roll angles of 0° and 45°, control deflections up to -14°, and angles of attack up to 14°, the flat-plate trailing-edge control with the hinge line at 25 percent control chord proves to be more effective in producing pitching moment. But above these values, the control with the hinge-line location at 50 percent control chord is more effective.

7. At a Mach number of 6.01 the diamond-profile trailing-edge control was found to be more effective than either of the flat plate

trailing-edge controls throughout the test range of angle of attack and more effective than the fin-tip controls at angles of attack greater than 8°. The fin-tip controls were more effective per unit control area than any of the trailing-edge controls at angles of attack less than 8°.

8. Roll has very little influence on the effectiveness of the trailing-edge controls, but it significantly increases the effectiveness of the delta tip control over the entire angle-of-attack range and the clipped-delta tip control at the lower angles of attack.

9. As Mach number increases, the effectiveness of all the controls decreases; the rate of change is greatest for Mach numbers below 4.76 and considerably less for Mach numbers from 4.76 to 6.01. Changes in Mach number influence the effectiveness of the trailing-edge controls more than that of the tip controls.

Langley Research Center,
National Aeronautics and Space Administration,
Langley Field, Va., July 11, 1960.

REFERENCES

1. Robinson, Ross B.: Aerodynamic Characteristics of Missile Configurations with Wings of Low Aspect Ratio for Various Combinations of Forebodies, Afterbodies, and Nose Shapes for Combined Angles of Attack and Sideslip at a Mach Number of 2.01. NACA RM L57D19, 1957.

2. Katzen, Elliott D., and Jorgensen, Leland H.: Aerodynamics of Missiles Employing Wings of Very Low Aspect Ratio. NACA RM A55L13b, 1956.

3. Jorgensen, Leland H., and Katzen, Elliott D.: Wing-Body Combinations With Wings of Very Low Aspect Ratio at Supersonic Speeds. NACA RM A56G16, 1956.

4. Nicholson, Kenneth F.: The Effects of Blunt Leading Edges on Delta Wings at Mach 5.8. Jour. of Aero./Space Sci., vol. 25, no. 12, Dec. 1958, pp. 786-787.

5. Spahr, J. Richard: Contribution of the Wing Panels to the Forces and Moments of Supersonic Wing-Body Combinations at Combined Angles. NACA TN 4146, 1958.

6. Bogdonoff, Seymour M., and Vas, Irwin E.: A Study of Hypersonic Wings and Controls. Paper no. 59-112, Inst. Aero. Sci., June 16-19, 1959.

7. McLellan, Charles H.: A Method for Increasing the Effectiveness of Stabilizing Surfaces at High Supersonic Mach Numbers. NACA RM L54F21, 1954.

8. Spearman, M. Leroy, and Robinson, Ross B.: Longitudinal Stability and Control Characteristics at Mach Numbers of 2.01, 4.65, and 6.8 of Two Hypersonic Missile Configurations, One Having Low-Aspect-Ratio Cruciform Wings With Trailing-Edge Flaps and One Having a Flared Afterbody and All-Movable Controls. NASA TM X-46, 1959.

L
8
3
7

TABLE I

MODEL DIMENSIONS

	I	II	III
Body:			
Length, in.	17.06	15.78	17.826
Diameter, in.	1.28	1.28	1.28
Cross-sectional area, sq in.	1.287	1.287	1.287
Fineness ratio of nose	3.5	2.5	3.5
Length-diameter ratio	13.328	12.326	13.925
Moment center location, percent length	59.00	55.6	58.7

	1	2	3	4	5	6	7	8	9
Fins:									
Area, exposed, two fins, sq in.	18.83	28.46	28.46	23.06	23.06	16.68	25.31	21.08	36.88
Root chord, in.	9.8	9.8	9.8	11.00	11.00	8.828	11.00	9.8	11.00
Tip chord, in.	0.9	0.9	0.9	2.10	2.10	2.10	2.10	0.9	2.10
Span, exposed, two fins, in.	3.52	5.32	5.32	3.52	3.52	3.05	3.52	3.52	5.32
Span total, two fins, in.	4.8	6.6	6.6	4.8	4.8	4.33	4.8	4.8	6.6
Taper ratio	0.092	0.092	0.092	0.191	0.191	0.238	0.191	0.092	0.191
Maximum thickness, root, percent chord	3.42	3.42	1.28	3.07	1.14	1.42	1.14	1.28	1.14
Maximum thickness, tip, percent chord	12.55	12.22	13.88	9.53	5.96	5.96	5.96	13.88	5.96
Aspect ratio, exposed	0.66	0.997	0.997	0.538	0.538	0.558	0.49	0.588	0.767
Leading-edge sweep, deg	78.85	73.35	73.35	78.85	78.85	77.20	80.50	80.50	75.00
Leading-edge radius, in.	0.040	0.040	0.0625	0.0625	0.0625	0.0625	0.0625	0.0625	0.0625
Trailing-edge thickness	0.335	0.335	0.125	0.100	0.125	0.125	0.125	0.125	0.125

	1	2	3	4	5	6	7
Controls:							
Area, exposed, two controls, sq in.	4.05	4.05	4.05	6.12	2.54	1.98	8.66
Area ratio (to fin)	0.216	0.216	0.216	0.216	0.111	0.086	0.305
Root chord, in.	1.15	1.15	1.15	1.15	2.10	2.10	2.10
Tip chord, in.	1.15	1.15	1.15	1.15	0	0.987	0
Span, exposed, two controls, in.	3.52	3.52	3.52	5.32	2.42	1.28	2.42
Maximum thickness, root, percent chord	10.87	10.87	8.69	8.69	9.53	9.53	5.96
Maximum thickness, tip, percent root chord	10.87	10.87	8.69	8.69	5.48	7.38	5.96
Aspect ratio, exposed	1.53	1.53	1.53	2.312	1.153	0.414	1.153
Leading-edge radius, in.	0.0575	0.0575			0.0575	0.0575	0.0625
Hinge-line location, percent root chord	50	25	50		50	50	
Trailing-edge thickness	0.125	0.125	0.000	0.000	0.100	0.100	0.125

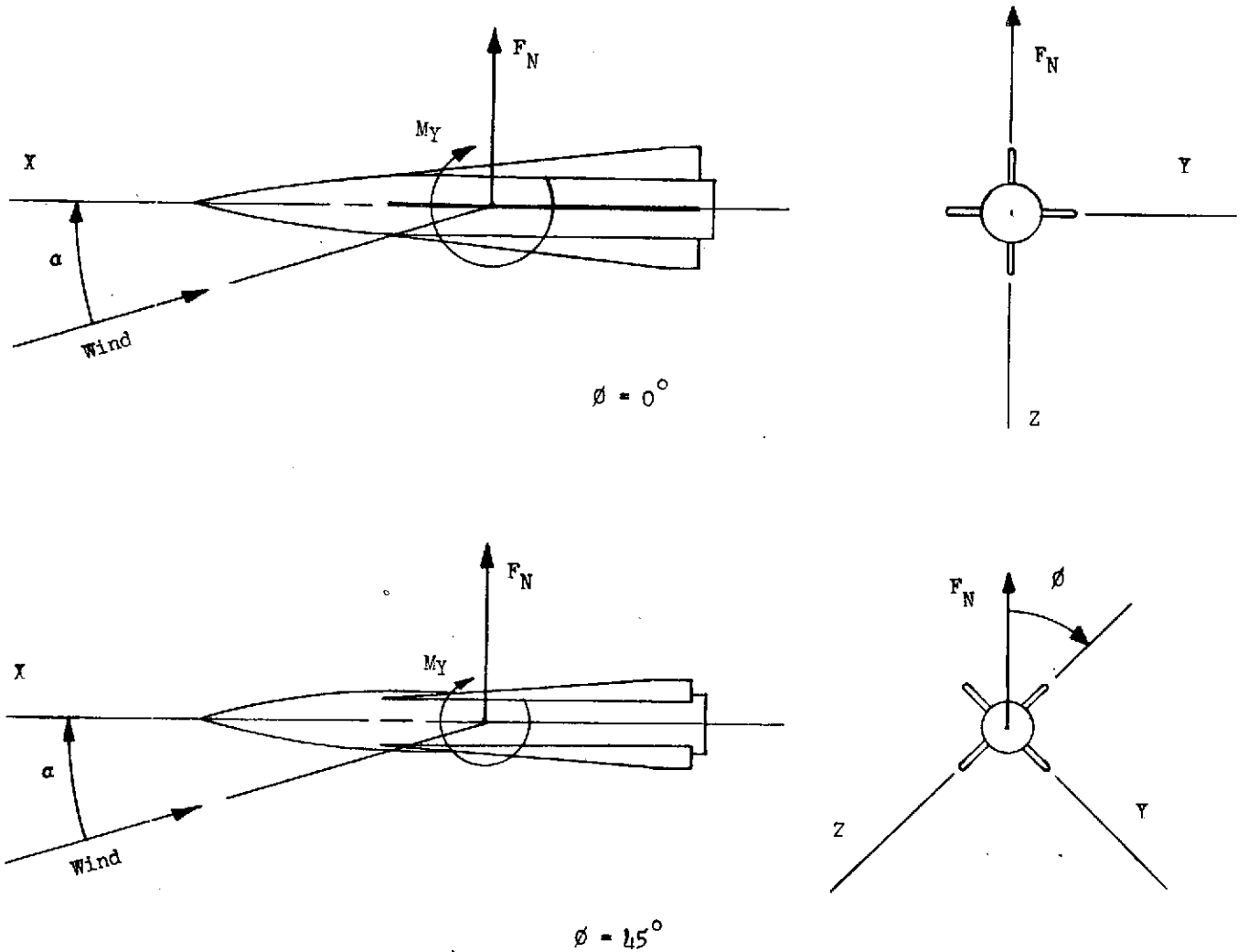

Figure 1.- Forces, moments, and axis system of present investigation. Arrows indicate positive directions of forces, moments, and angles.

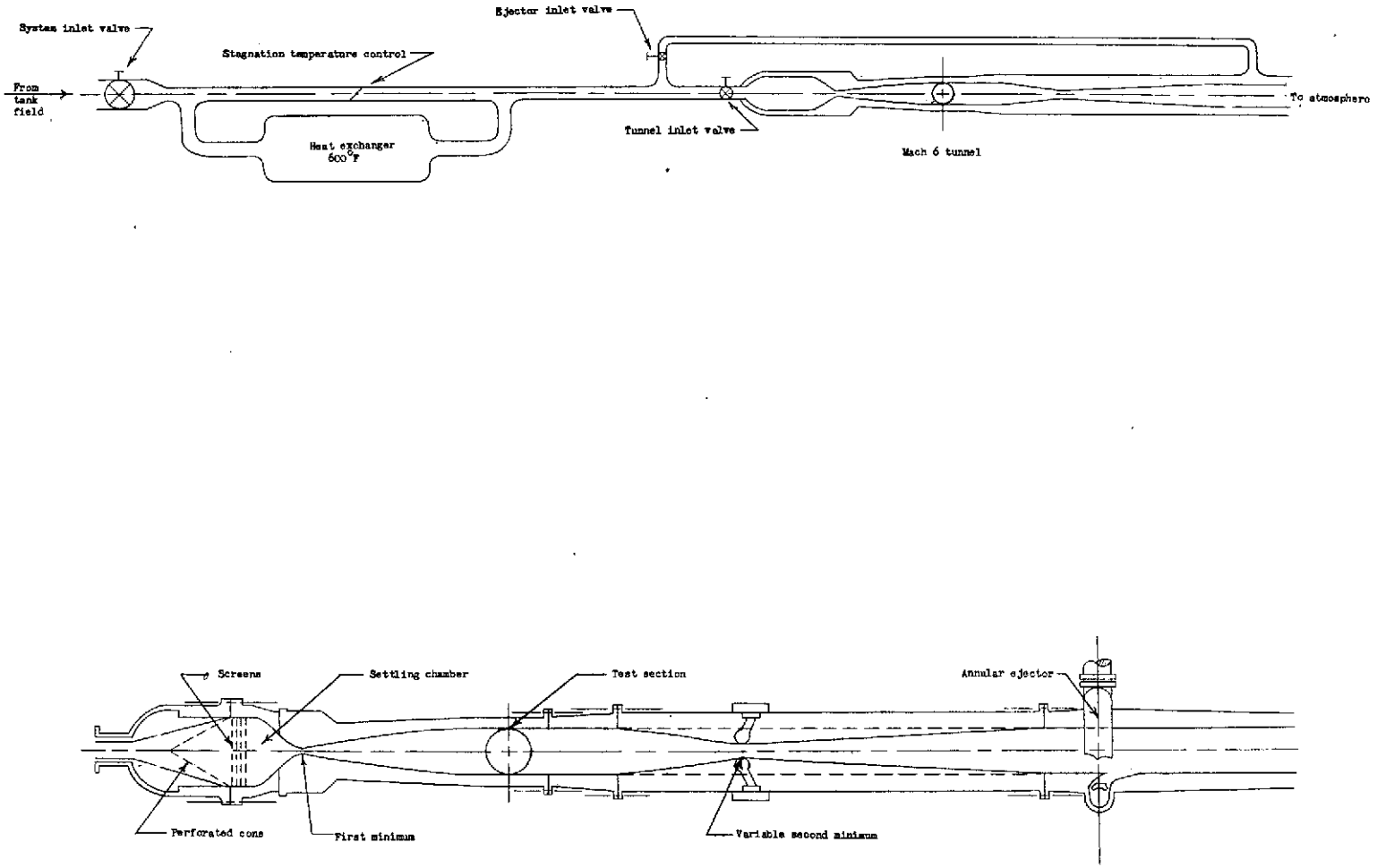

Figure 2.- Schematic diagram of 20-inch Mach 6 tunnel and its auxiliary equipment.

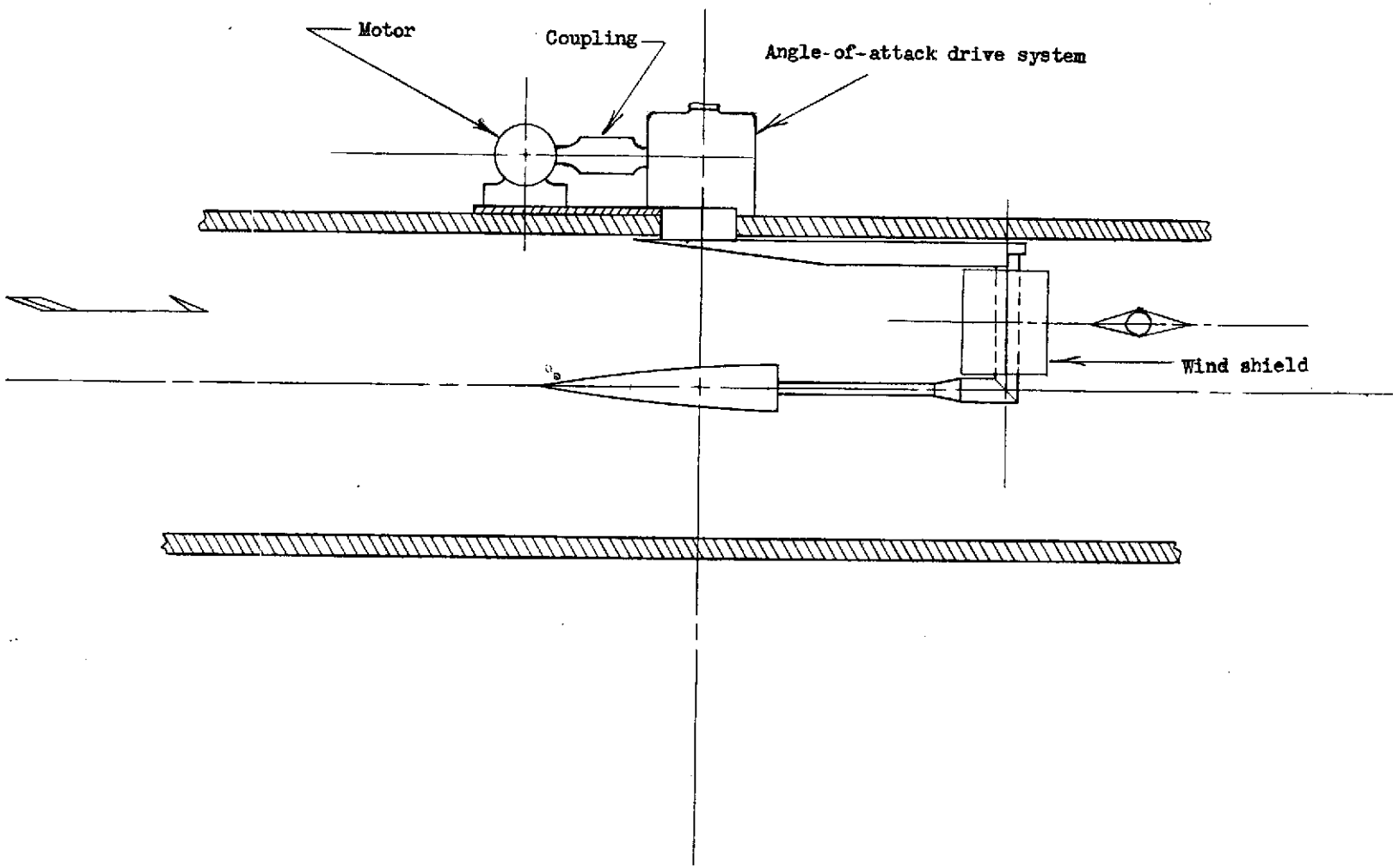

Figure 3.- Schematic diagram of the model support system.

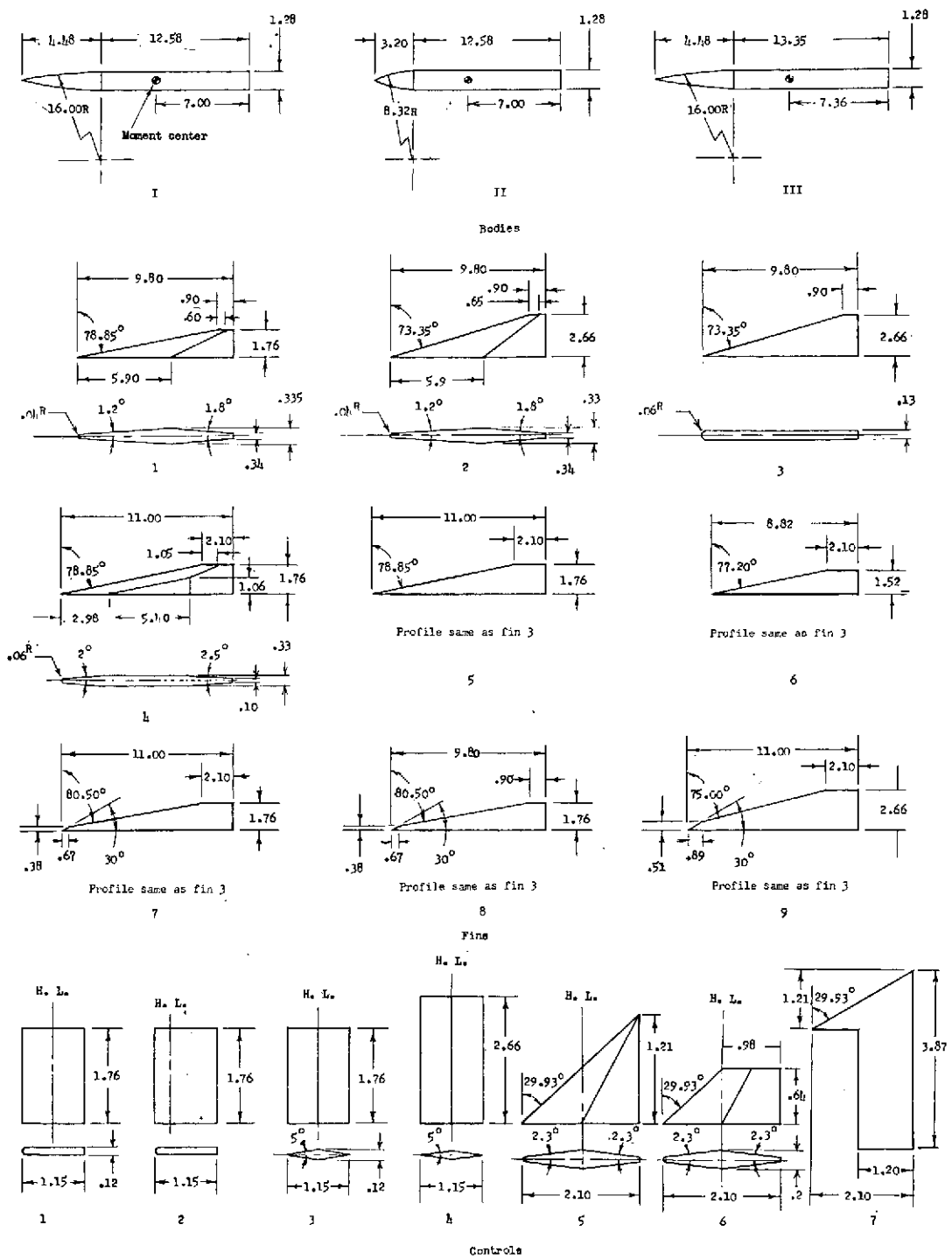

Figure 4.- Details of bodies, fins, and controls. Linear dimensions are in inches.

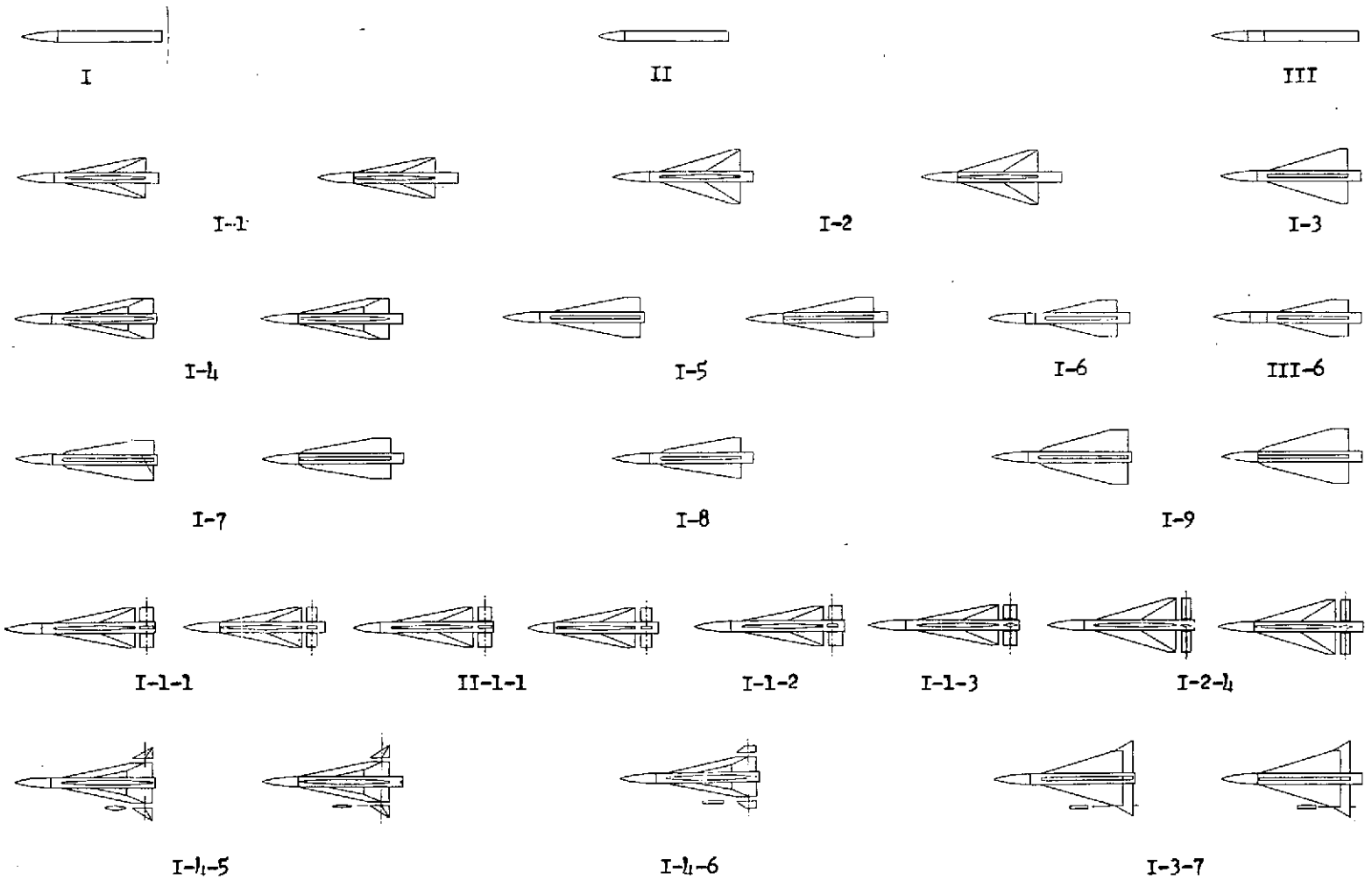

Figure 5.- Sketches and identification of model configurations. The same identification is used for the fins located forward and rearward.

L-837

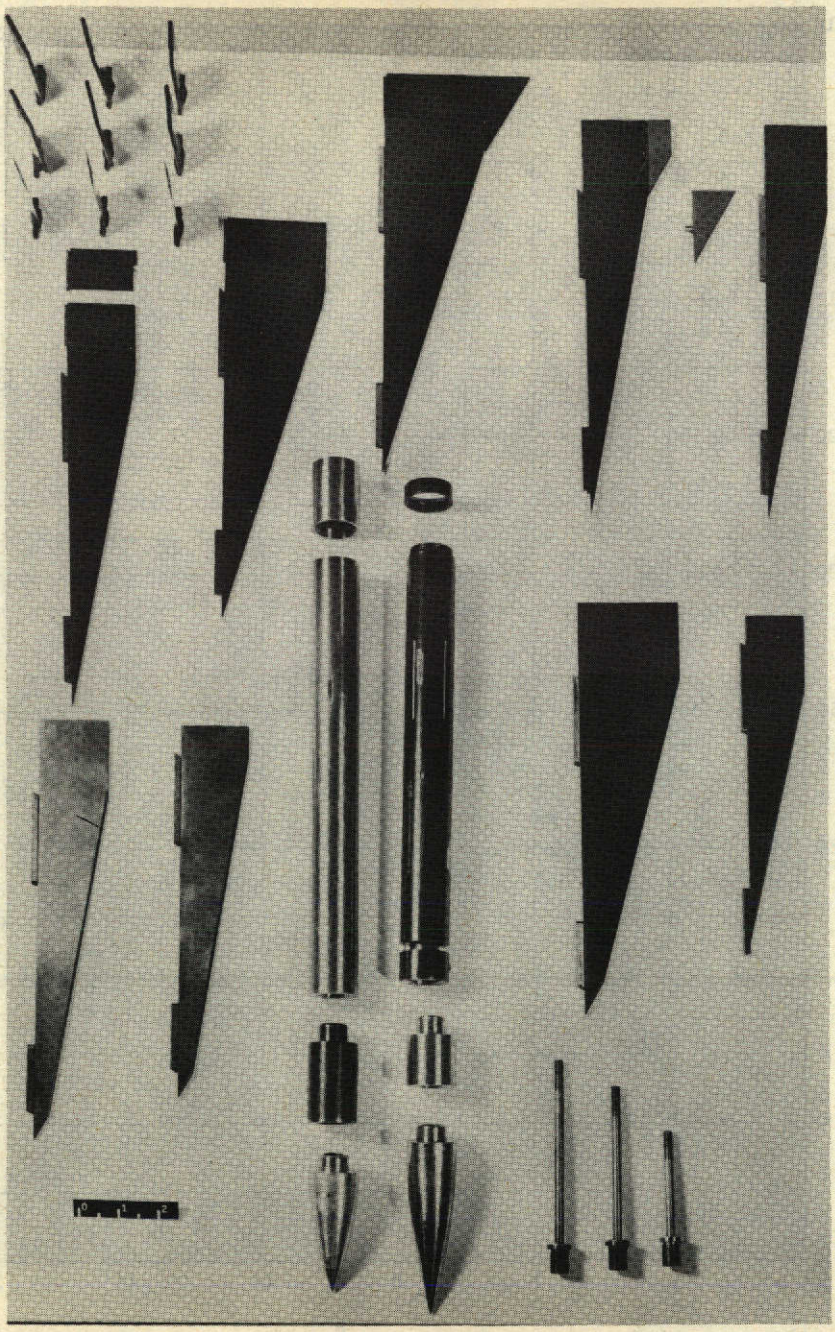

L-58-795a

Figure 6.- Photograph of the component parts of the model configurations showing ogive noses, cylindrical afterbodies, fastening bolts, and one of each of the fins and controls.

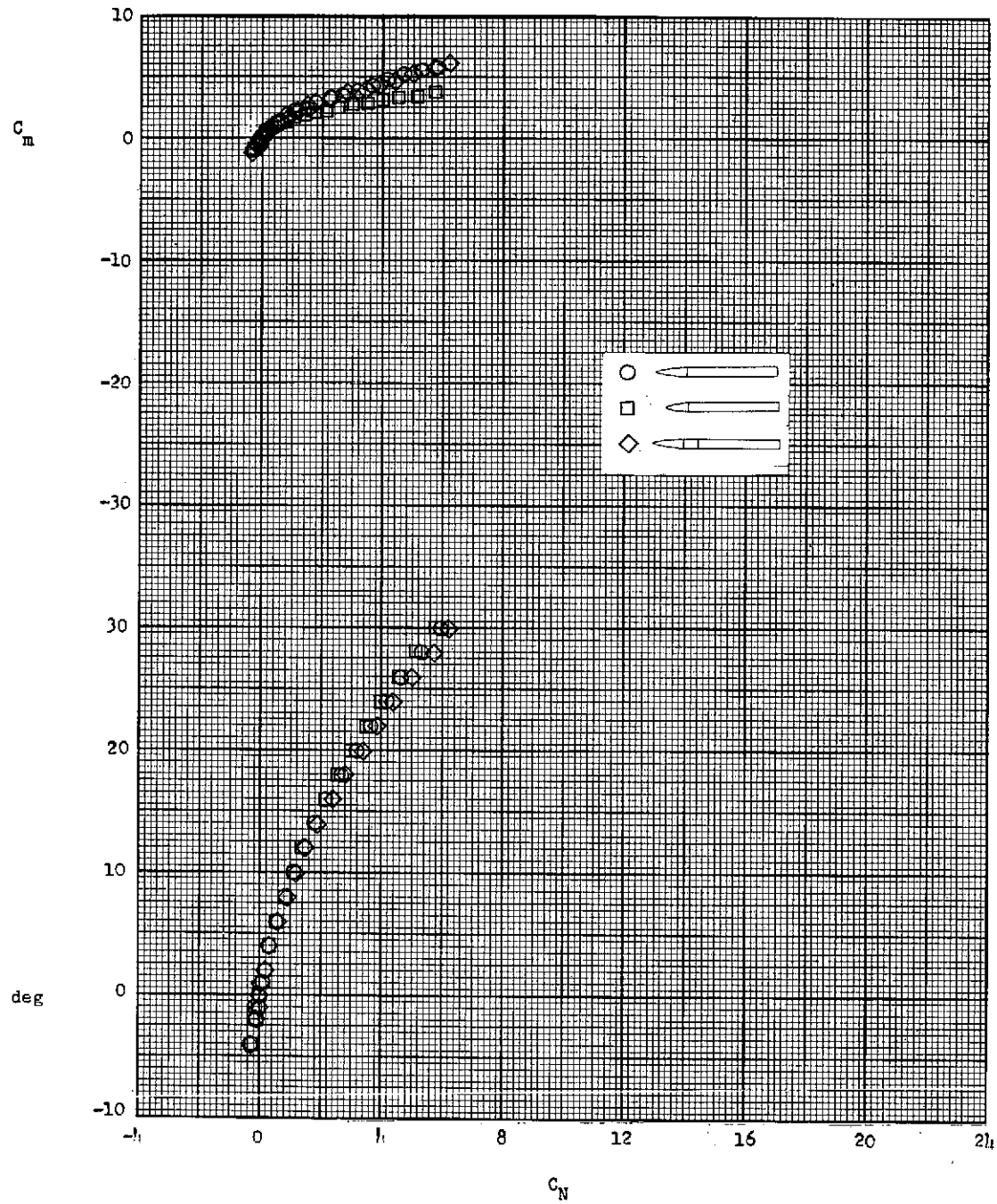

Figure 7.- Aerodynamic characteristics of configurations I, II, and III in pitch at a Mach number of 6.01.

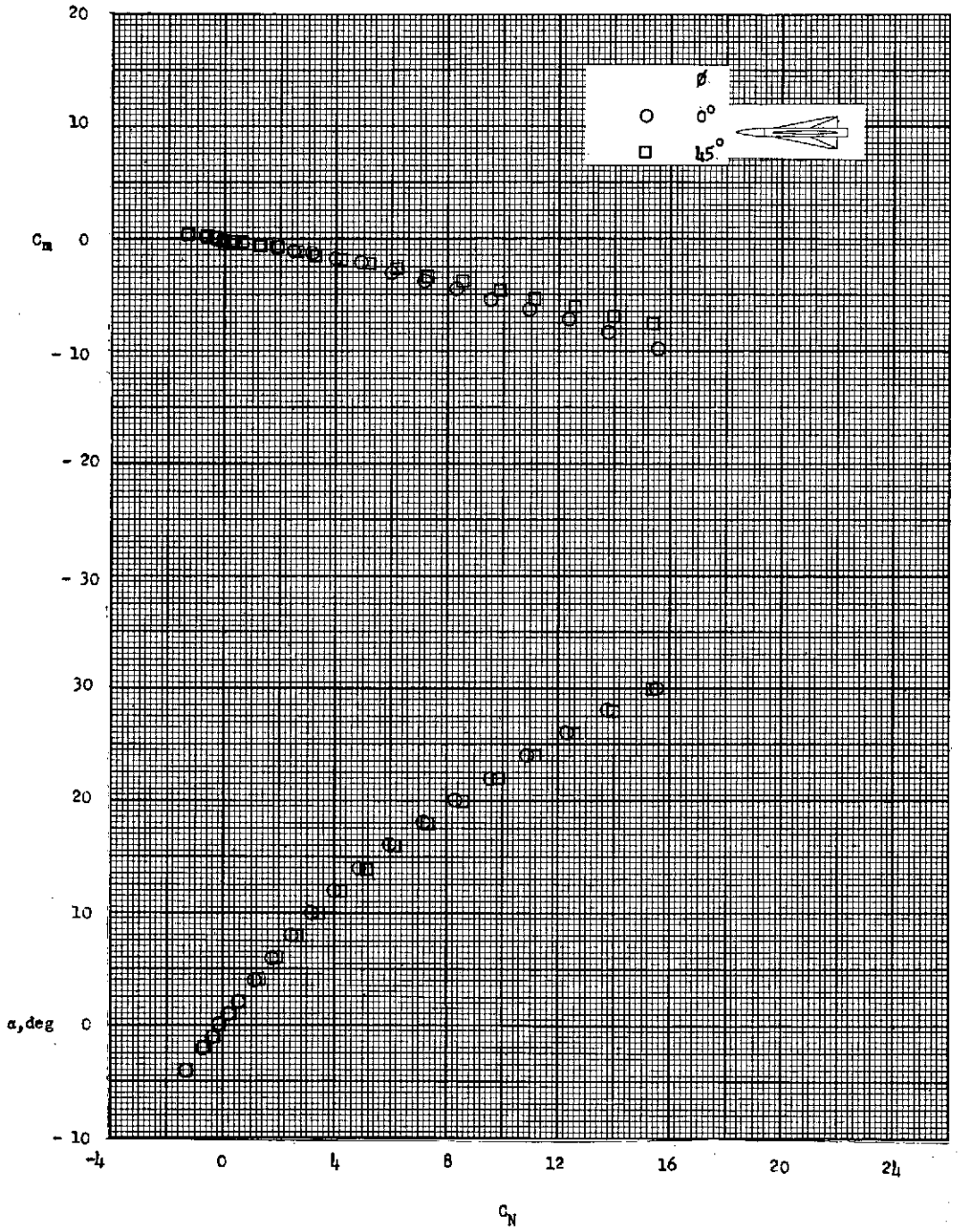

Figure 8.- Aerodynamic characteristics of configuration I-1 in pitch at roll angles of 0° and 45° and a Mach number of 6.01. Fins are in rear position.

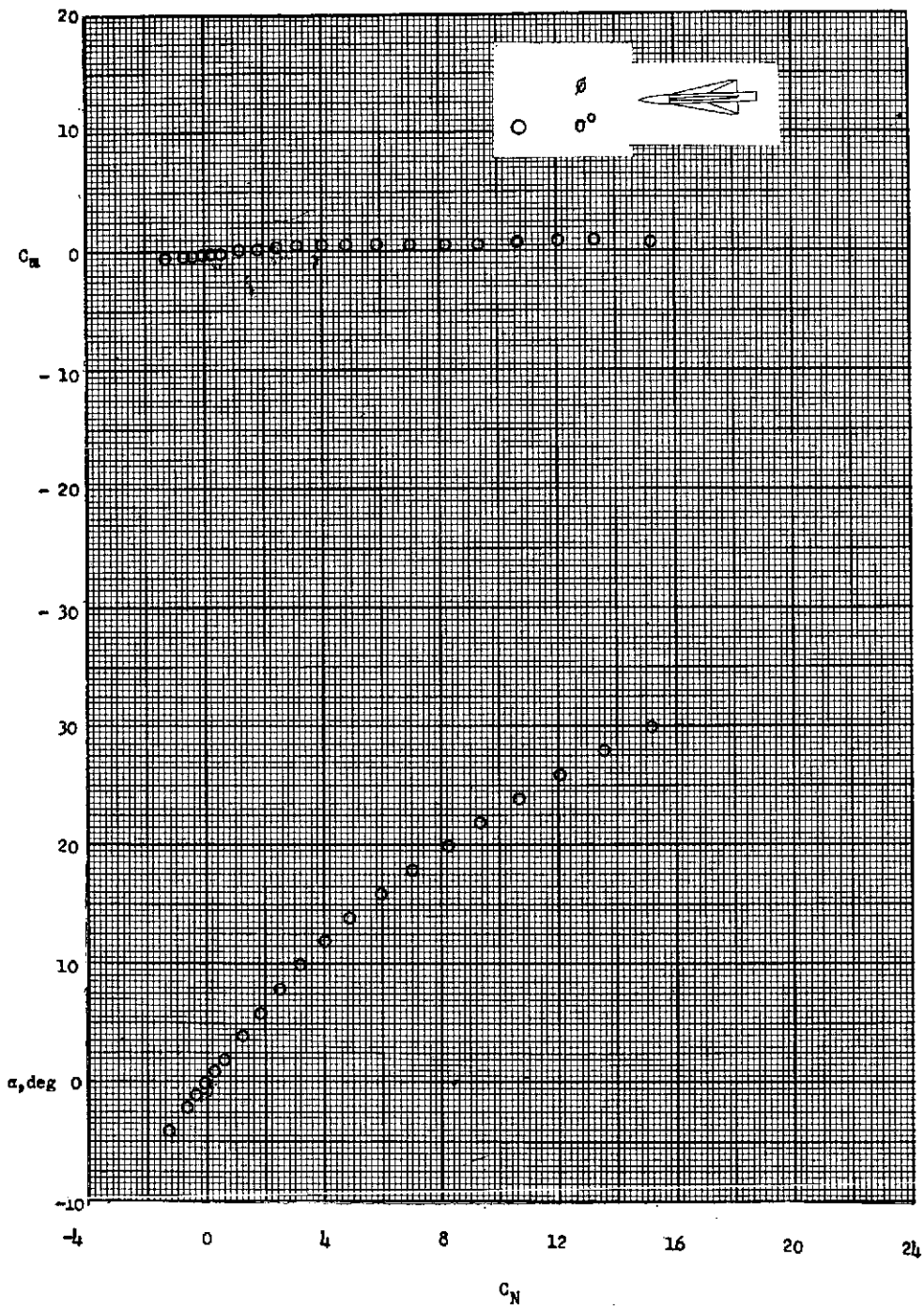

Figure 9.- Aerodynamic characteristics of configuration I-1 in pitch at a roll angle of 0° and a Mach number of 6.01. Fins are in forward position.

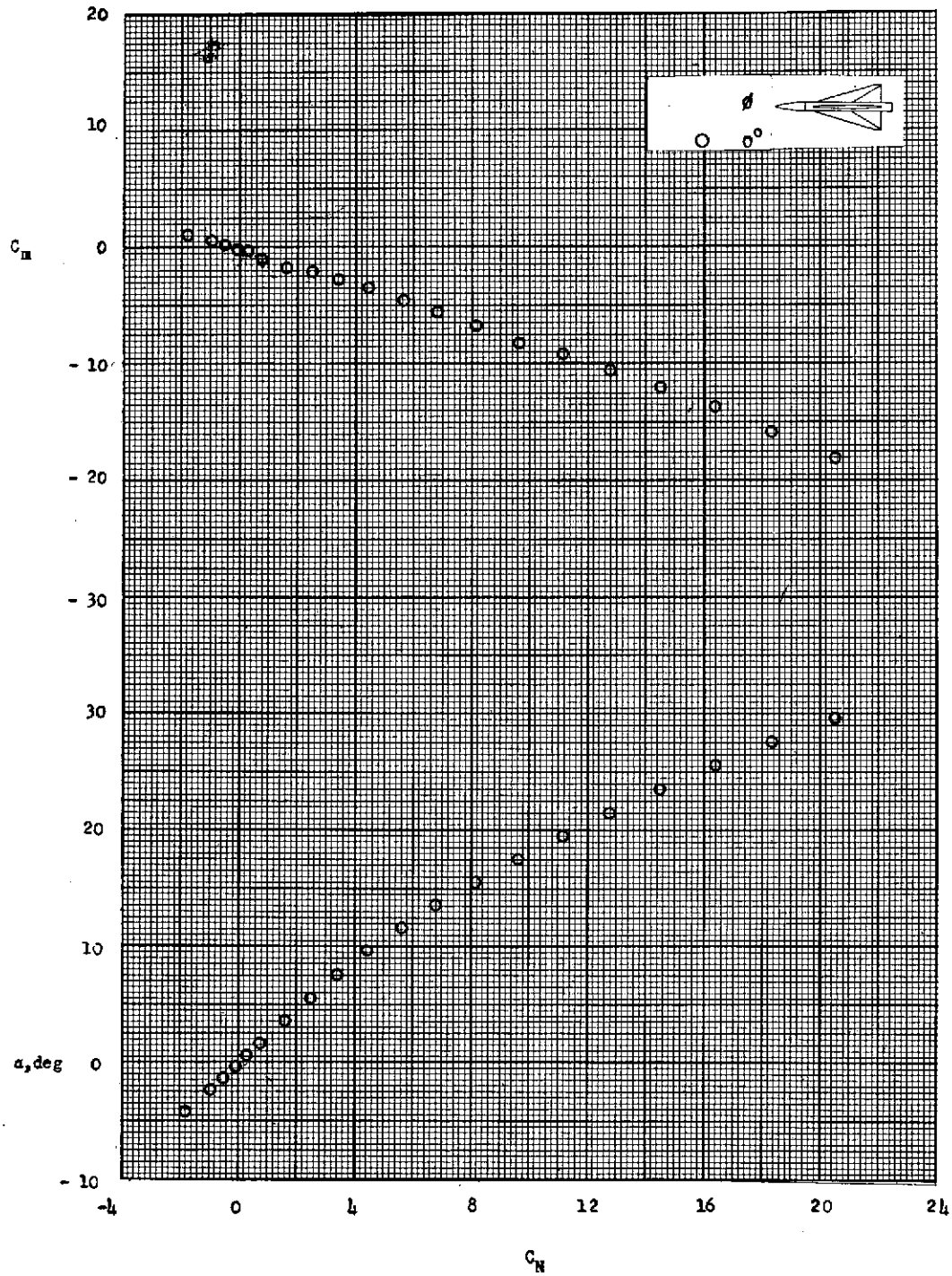

Figure 10.- Aerodynamic characteristics of configuration I-2 in pitch at a roll angle of 0° and a Mach number of 6.01. Fins are in rear position.

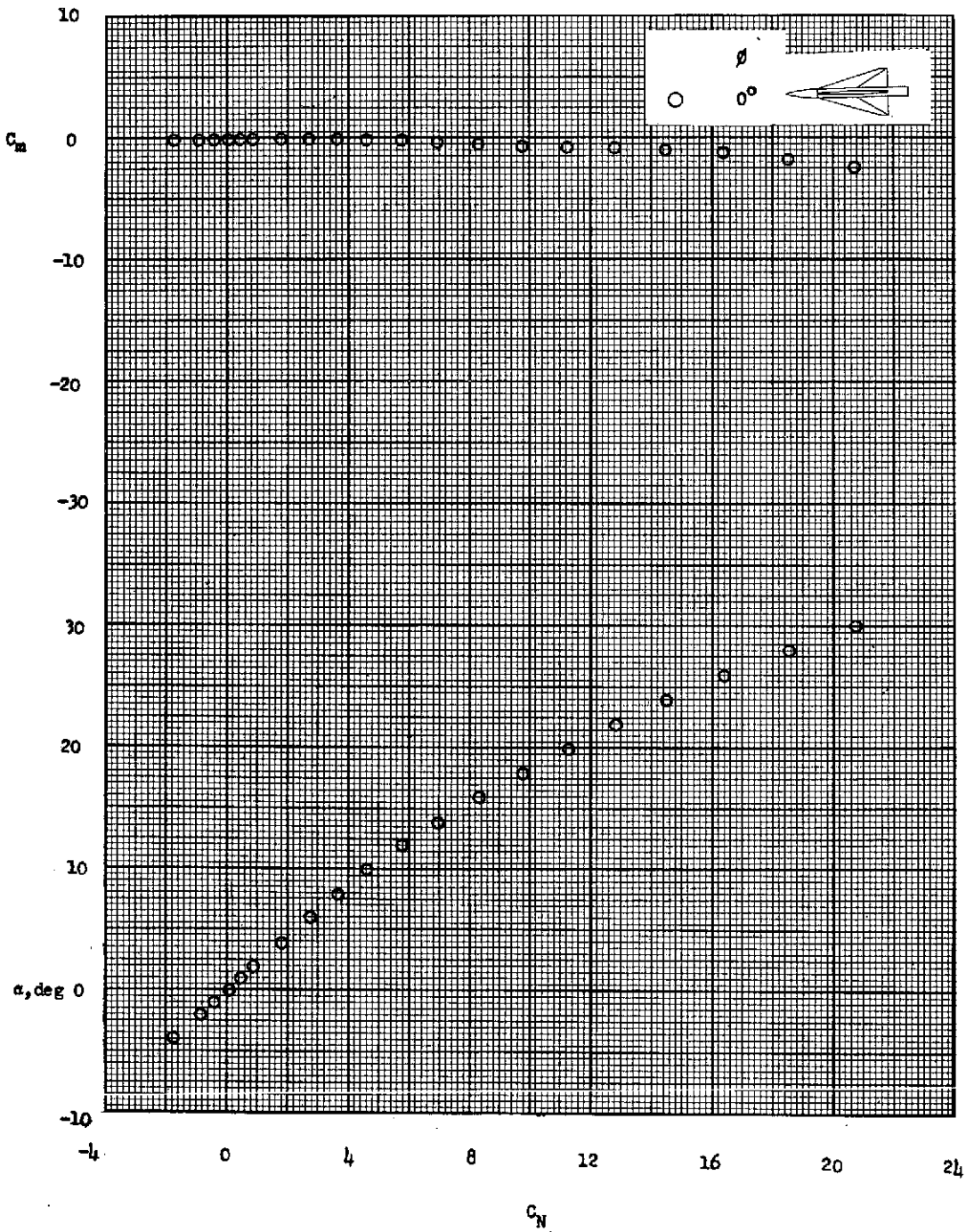

Figure 11.- Aerodynamic characteristics of configuration I-2 in pitch at a roll angle of 0° and a Mach number of 6.01. Fins are in forward position.

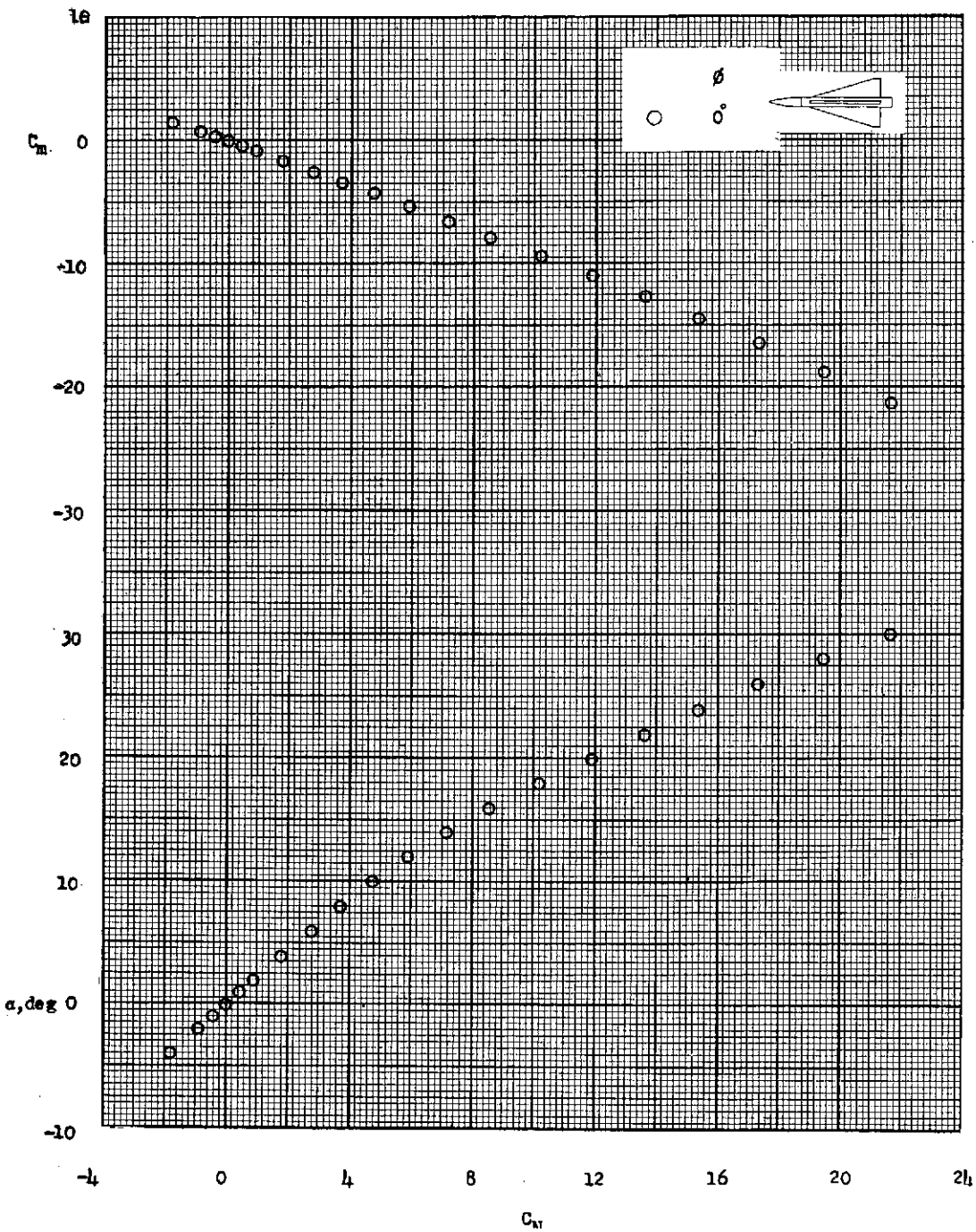

Figure 12.- Aerodynamic characteristics of configuration I-3 in pitch at a roll angle of 0° and a Mach number of 6.01. Fins are in the rear position.

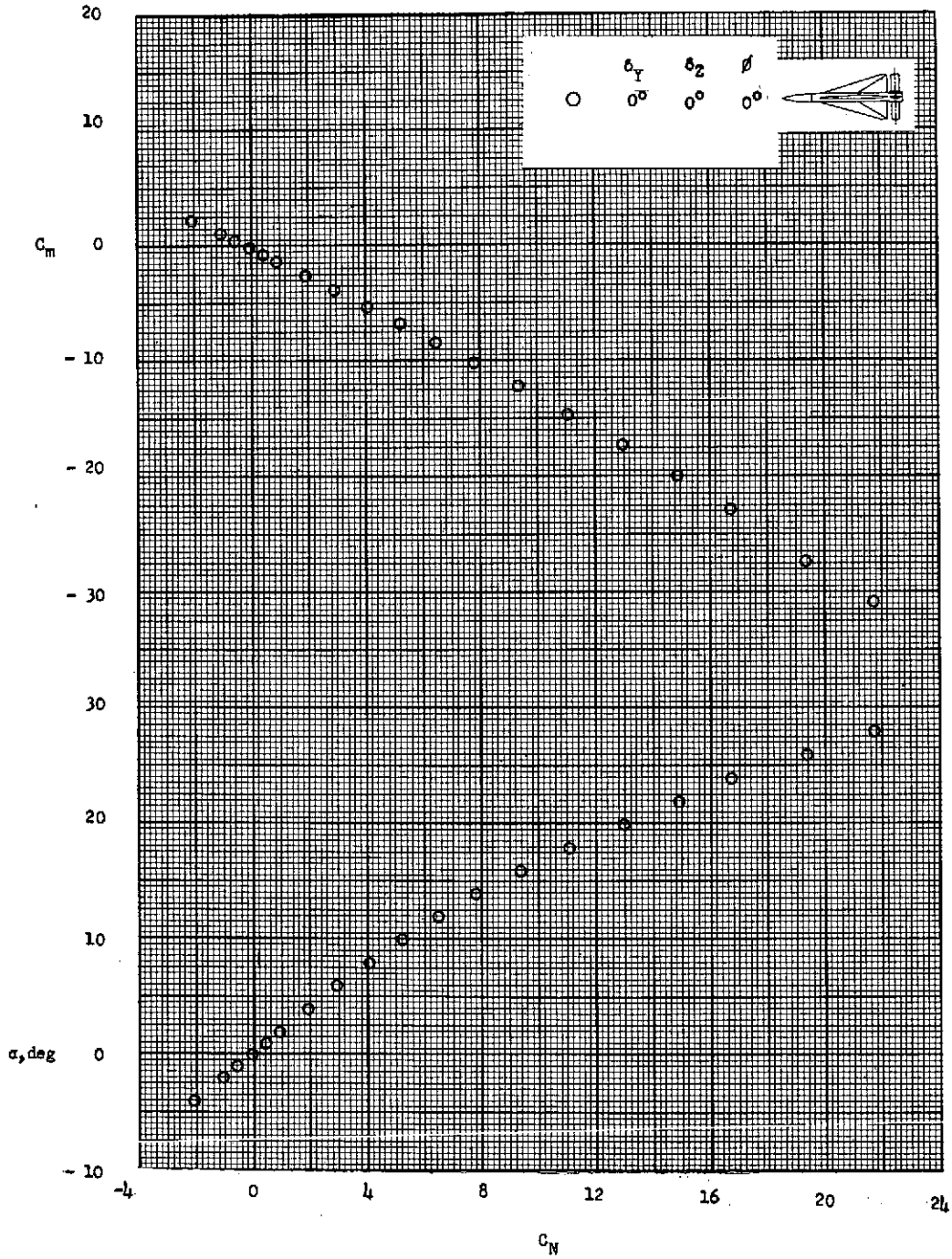

Figure 13.- Aerodynamic characteristics of configuration I-2-4 in pitch at an angle of roll of 0°, control deflection of 0°, and a Mach number of 6.01. Fins are in rear position.

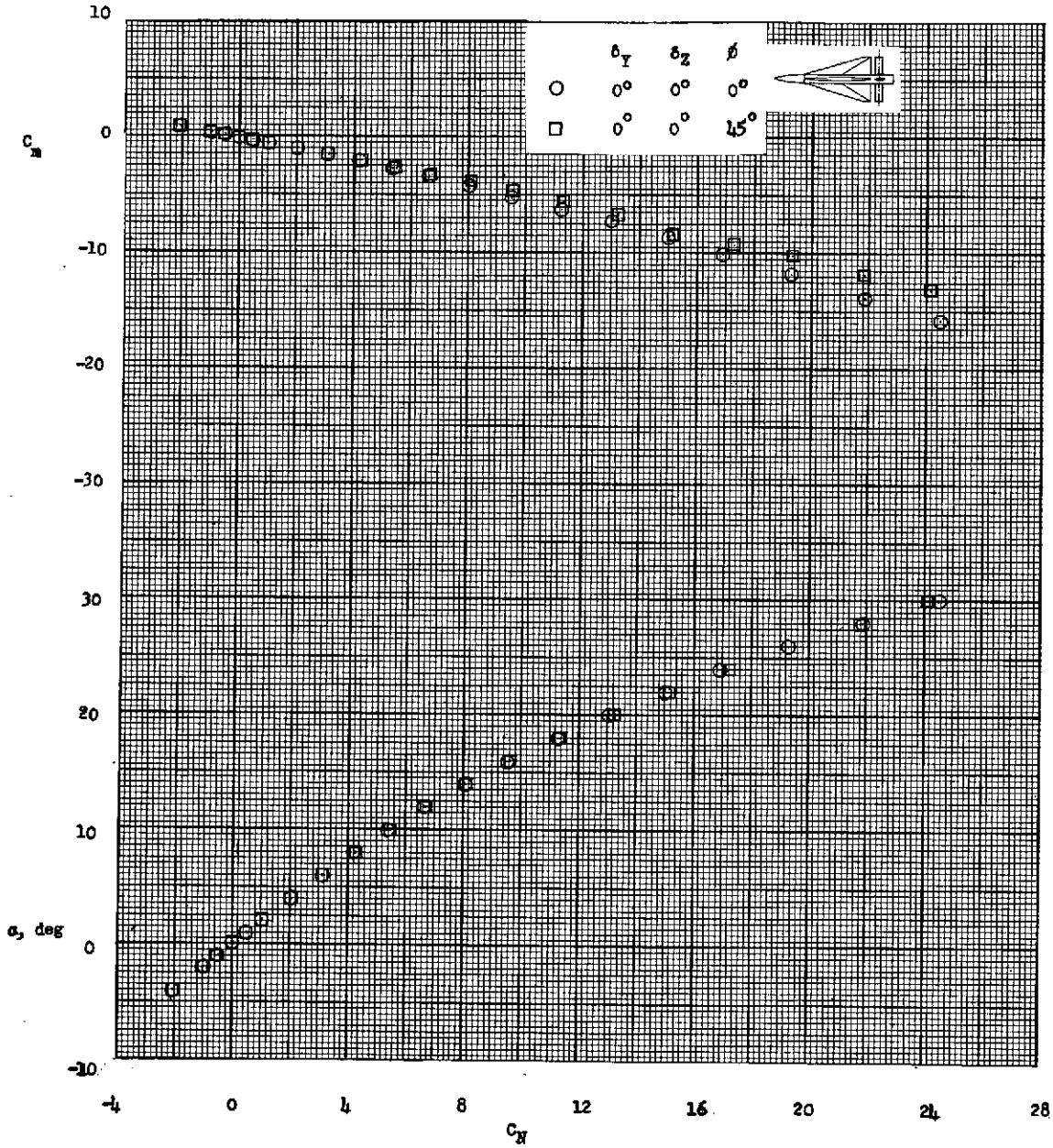

Figure 14.- Aerodynamic characteristics of configuration I-2-4 in pitch at roll angles of 0° and 45°, control deflection of 0°, and a Mach number of 6.01. Fins are in forward position.

I-857

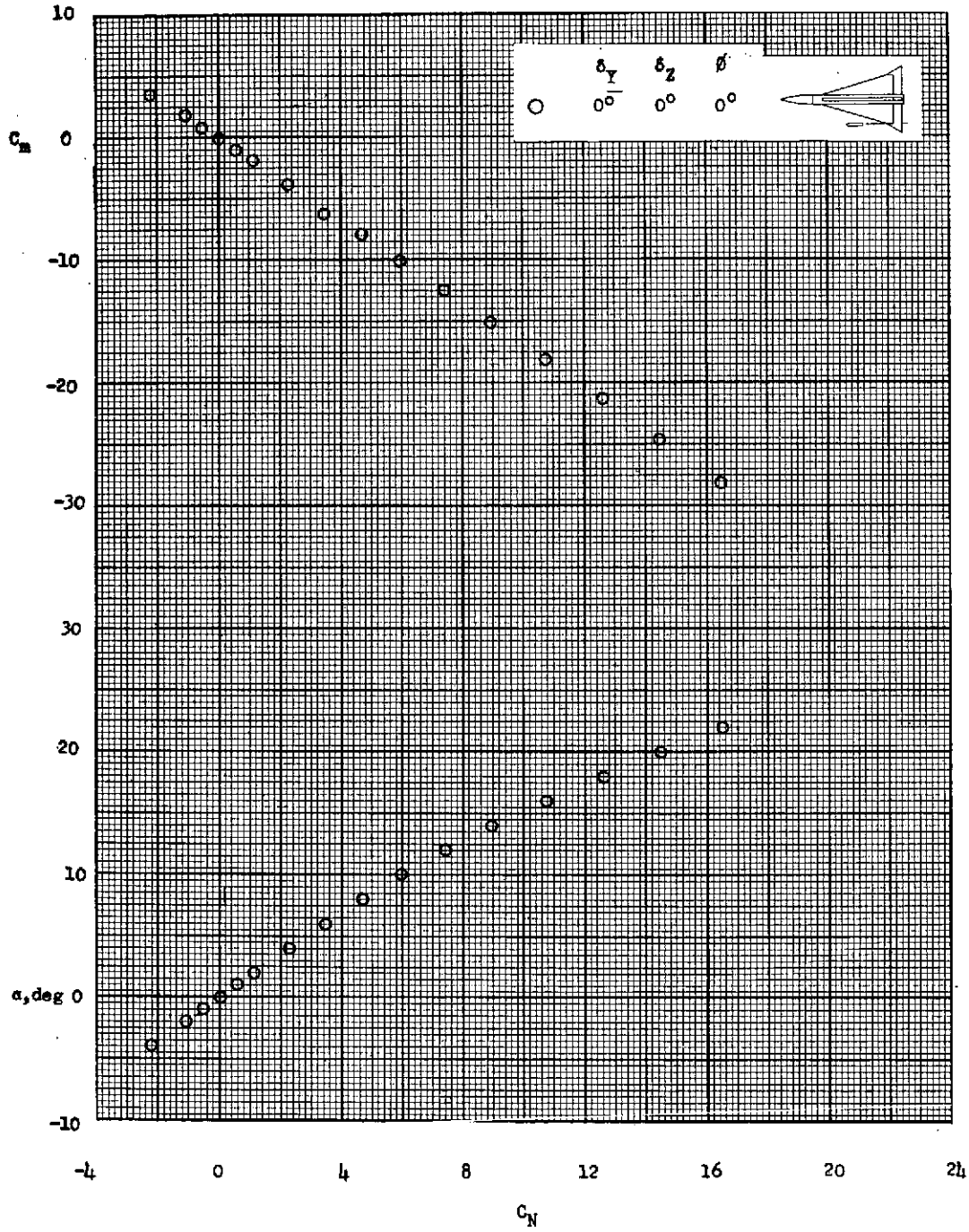

Figure 15.- Aerodynamic characteristics of configuration I-3-7 in pitch at a roll angle of 0°, a control deflection of 0°, and a Mach number of 6.01. Fins are in the rear position.

L-837

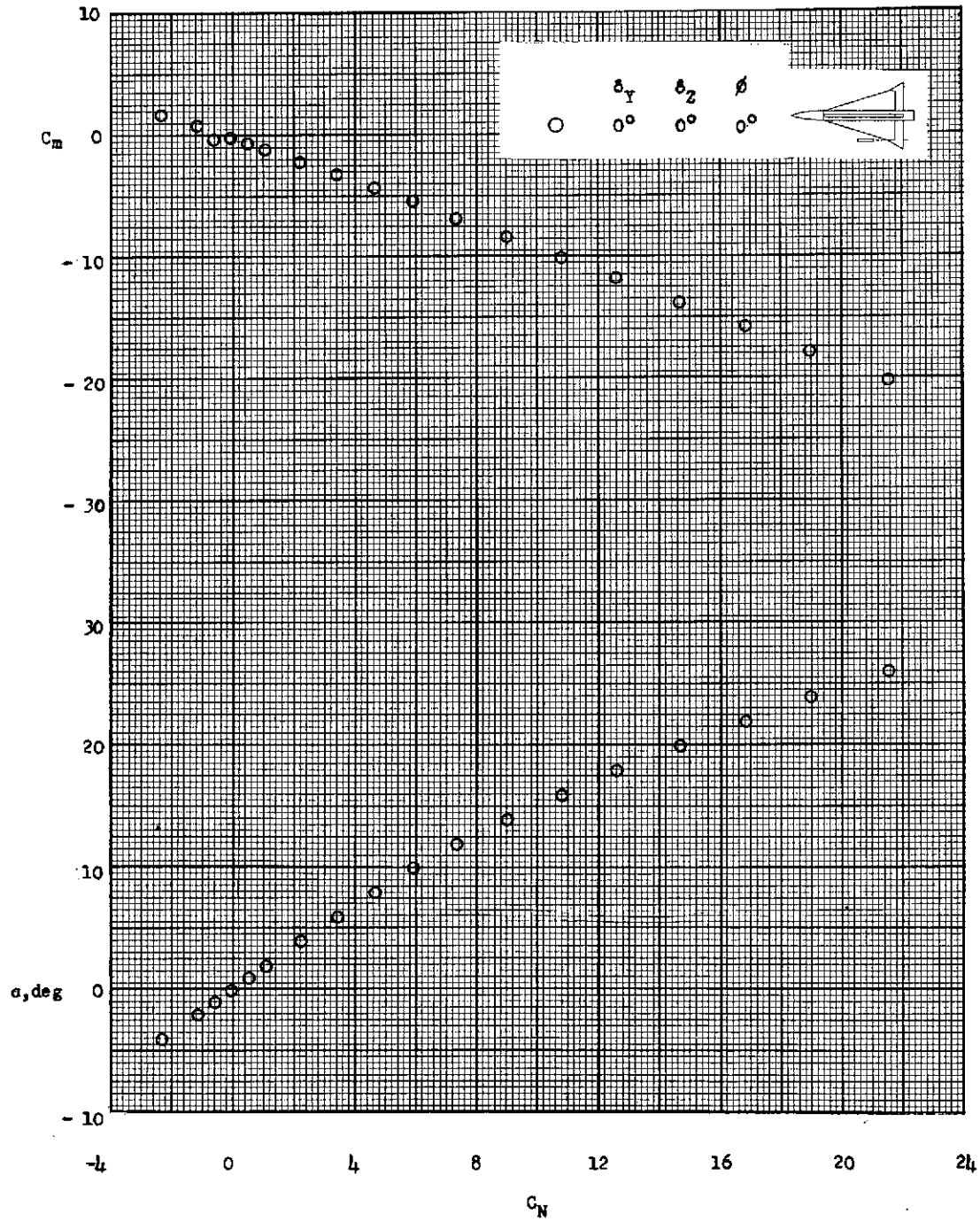

Figure 16.- Aerodynamic characteristics of configuration I-3-7 in pitch at a roll angle of 0°, control deflection of 0°, and a Mach number of 6.01. Fins are in forward position.

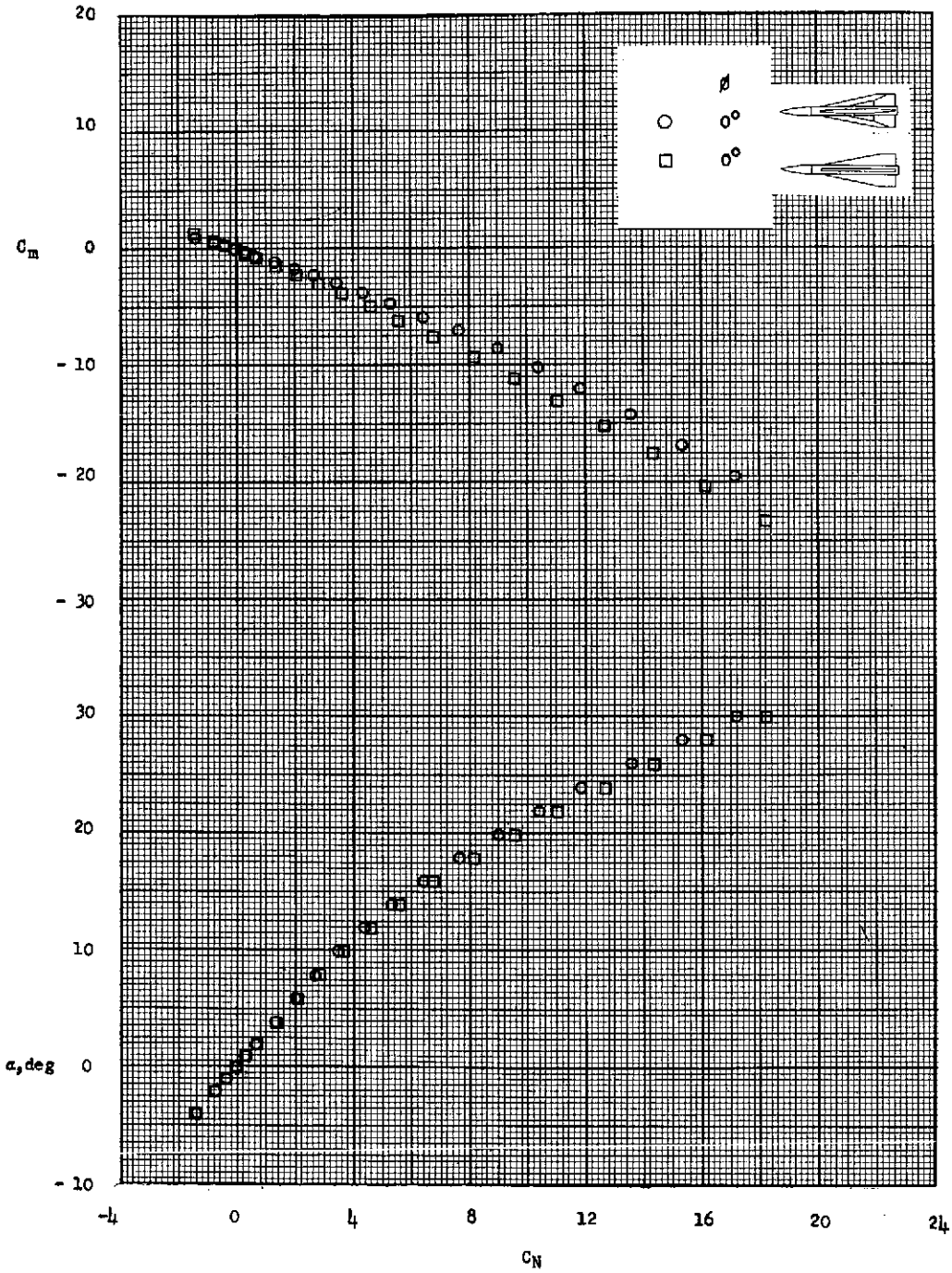

Figure 17.- Aerodynamic characteristics of configurations I-4 and I-5 in pitch at a roll angle of 0° and a Mach number of 6.01. Fins are in rear position.

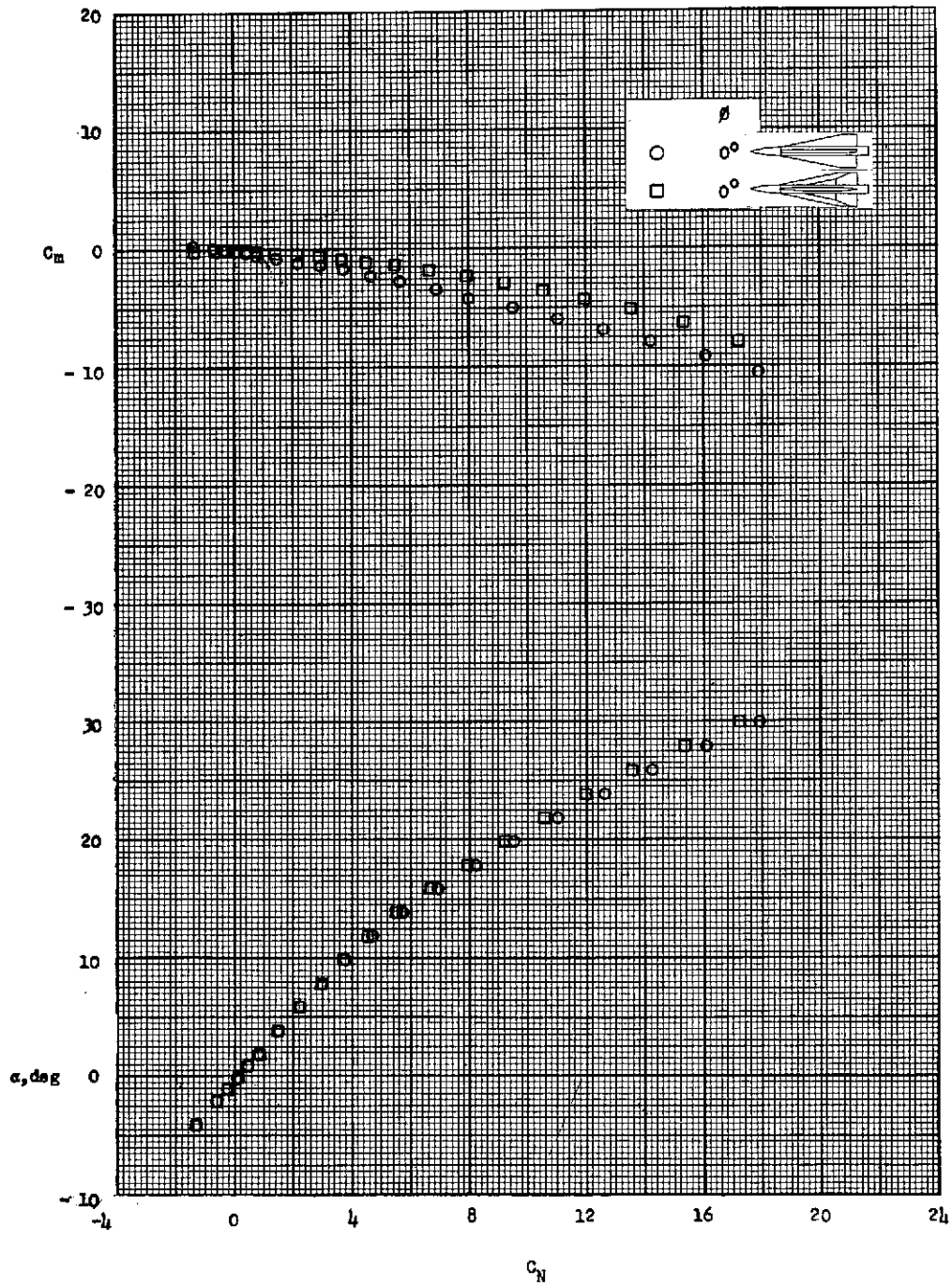

Figure 18.- Aerodynamic characteristics of configurations I-4 and I-5 in pitch at a roll angle of 0° and a Mach number of 6.01. Fins are in the forward position.

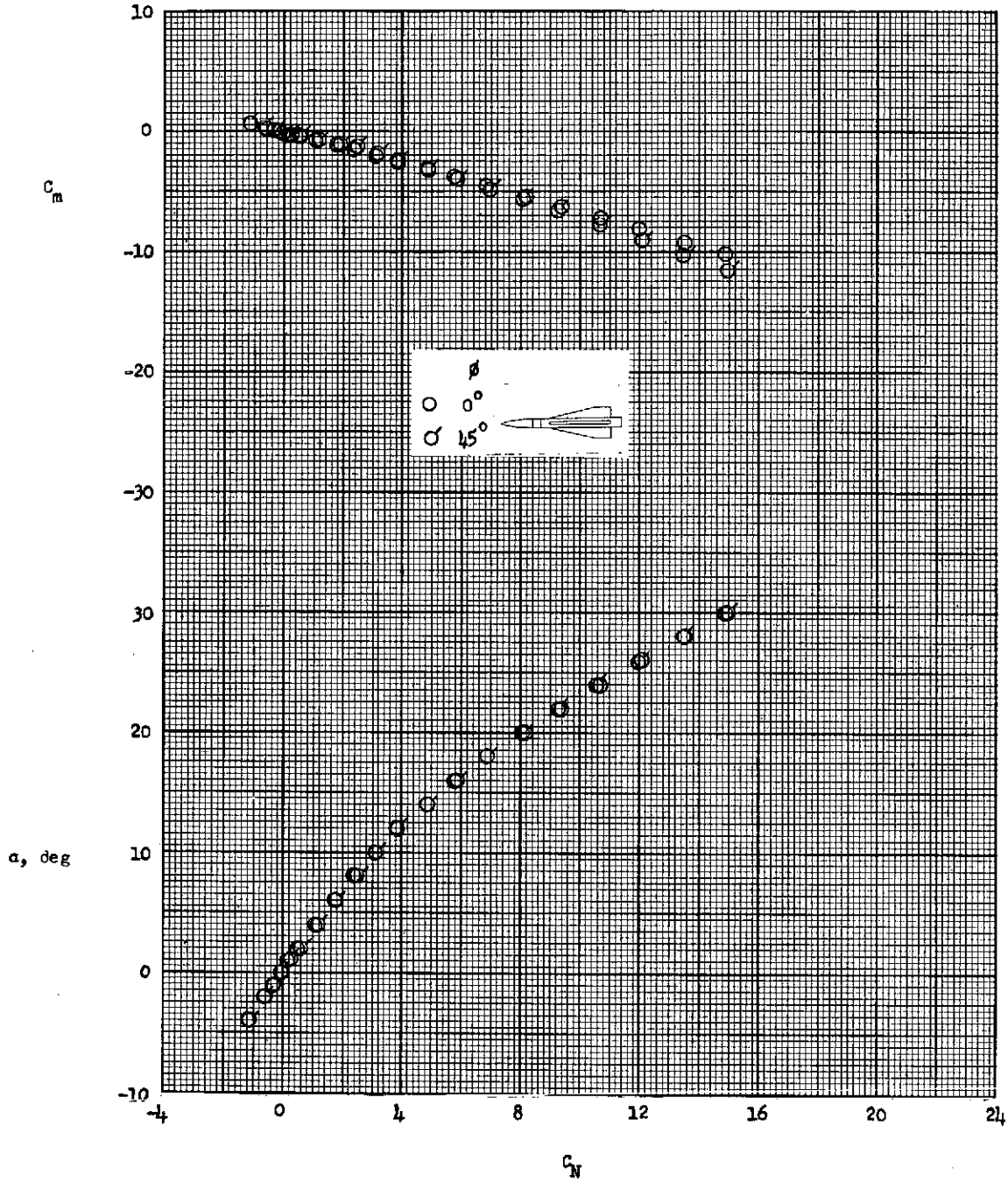

Figure 19.- Aerodynamic characteristics of configuration I-6 in pitch at roll angles of 0° and 45° and a Mach number of 6.01. Fins are in rear position.

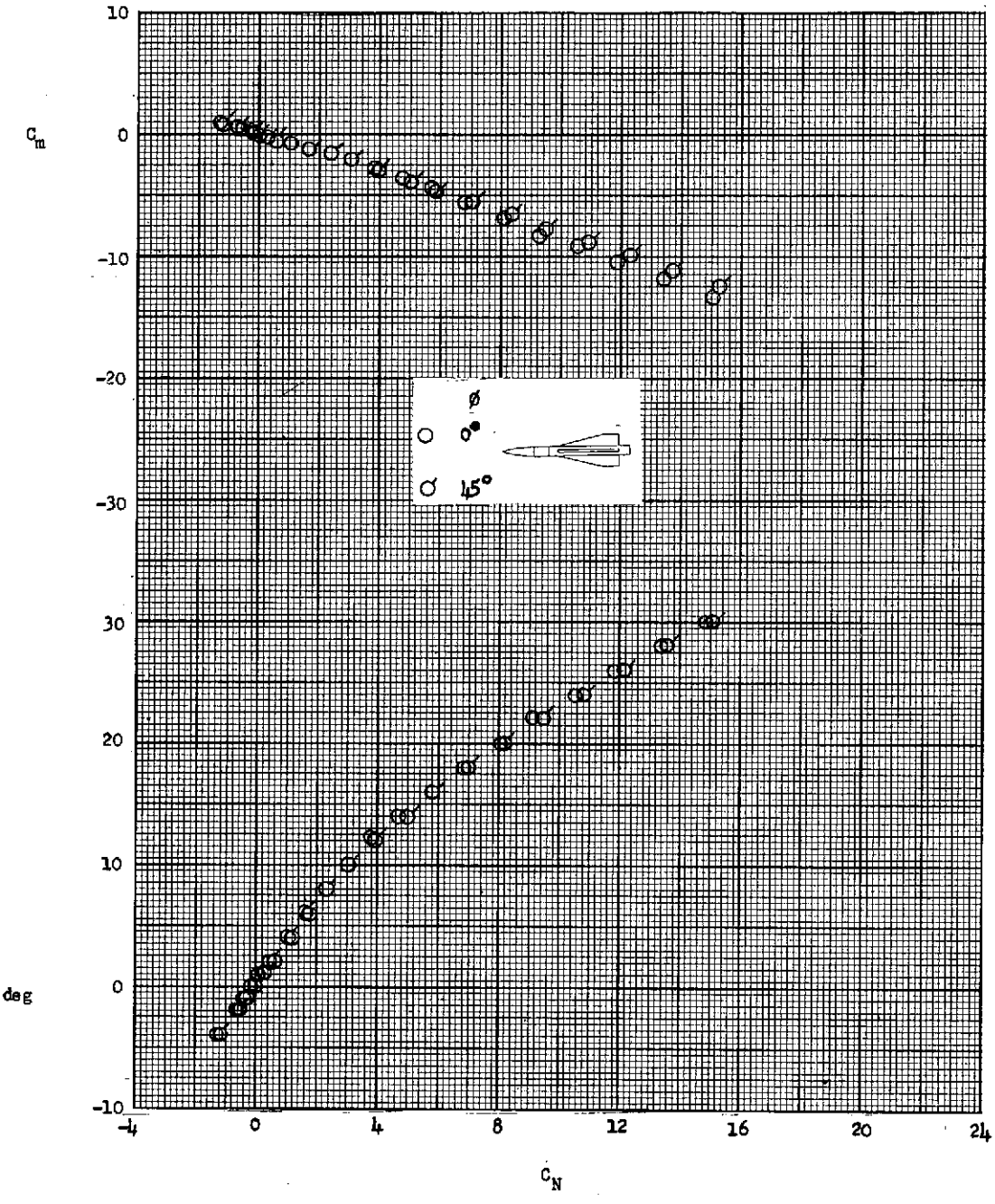

L-837

Figure 20.- Aerodynamic characteristics of configuration III-6 in pitch at a roll angle of 0° and a Mach number of 6.01. Fins are in rear position.

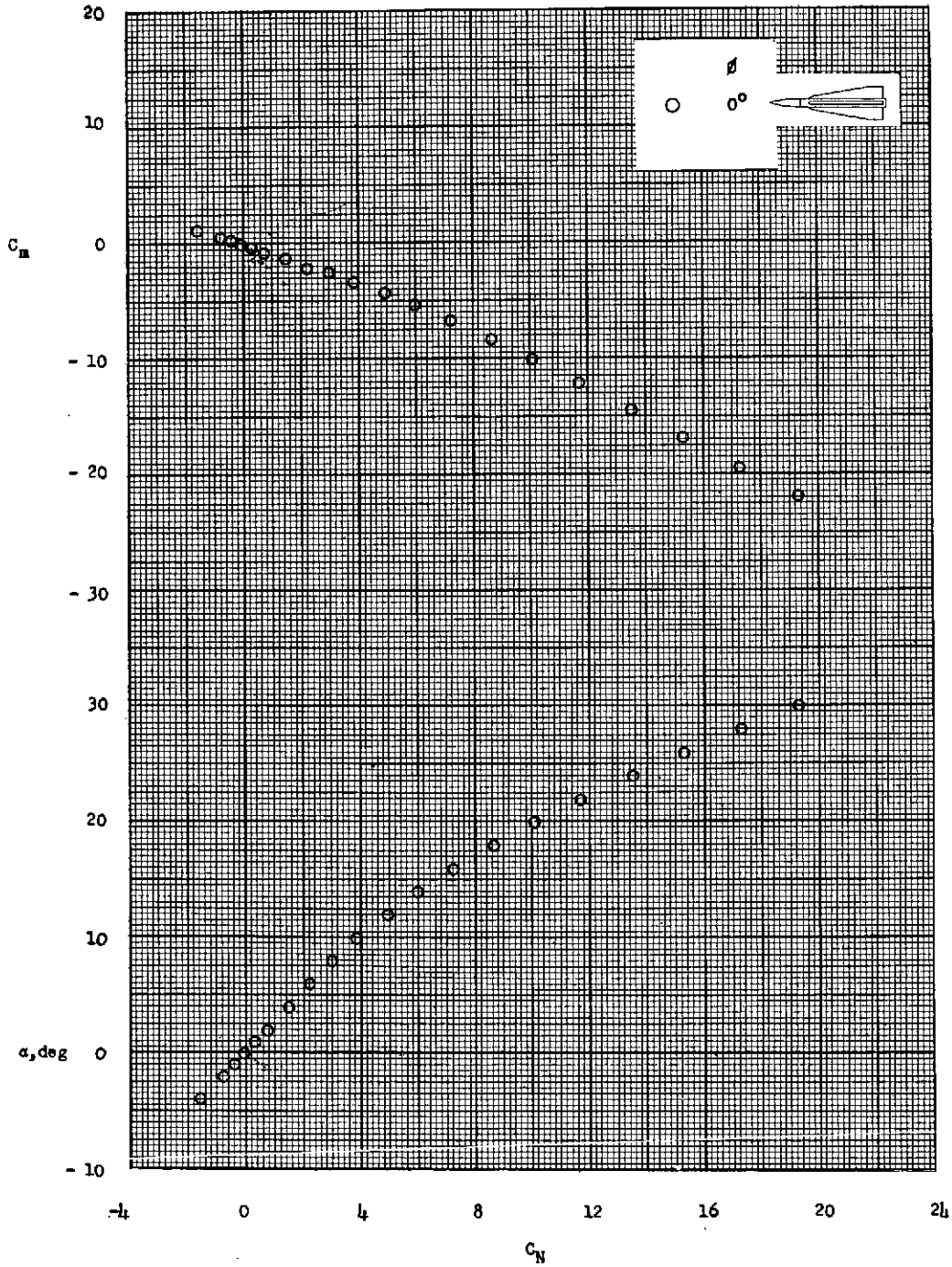

Figure 21.- Aerodynamic characteristics of configuration I-7 in pitch at a roll angle of 0° and a Mach number of 6.01. Fins are in rear position.

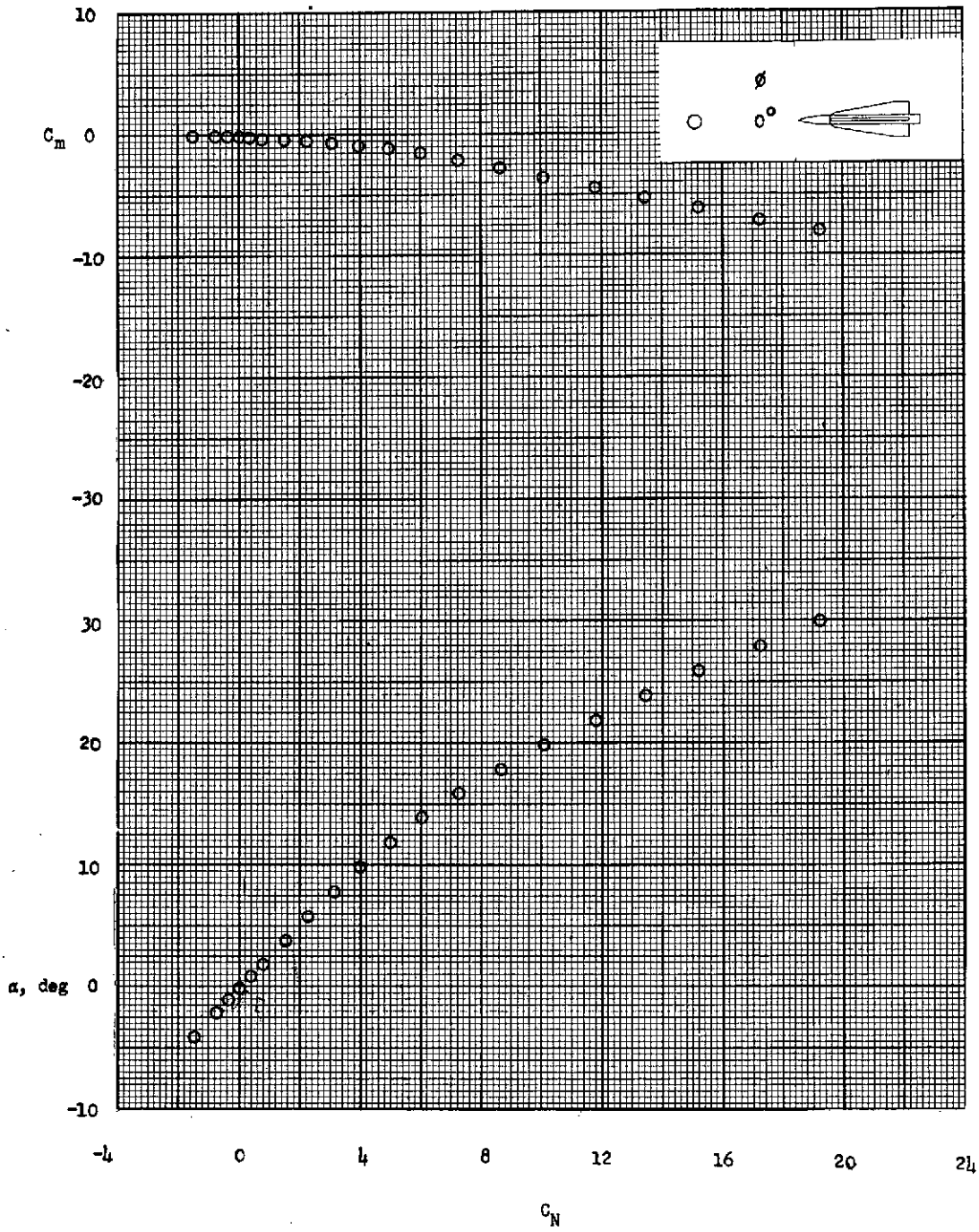

Figure 22.- Aerodynamic characteristics of configuration I-7 in pitch at roll angles of 0° and 45° and a Mach number of 6.01. Fins are in forward position.

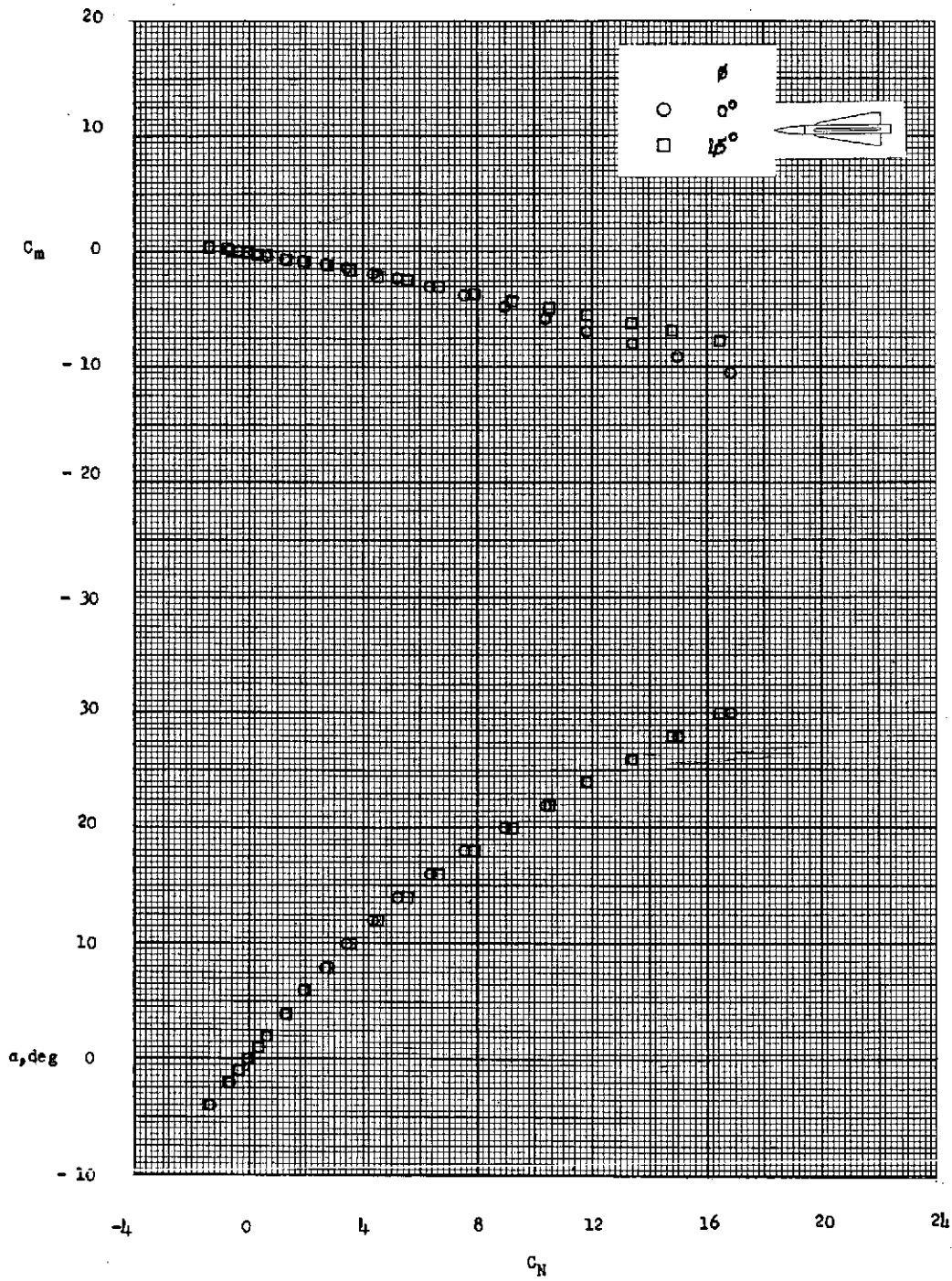

Figure 23.- Aerodynamic characteristics of configuration I-8 in pitch at roll angles of 0° and 45° and a Mach number of 6.01. Fins are in rear position.

L-837

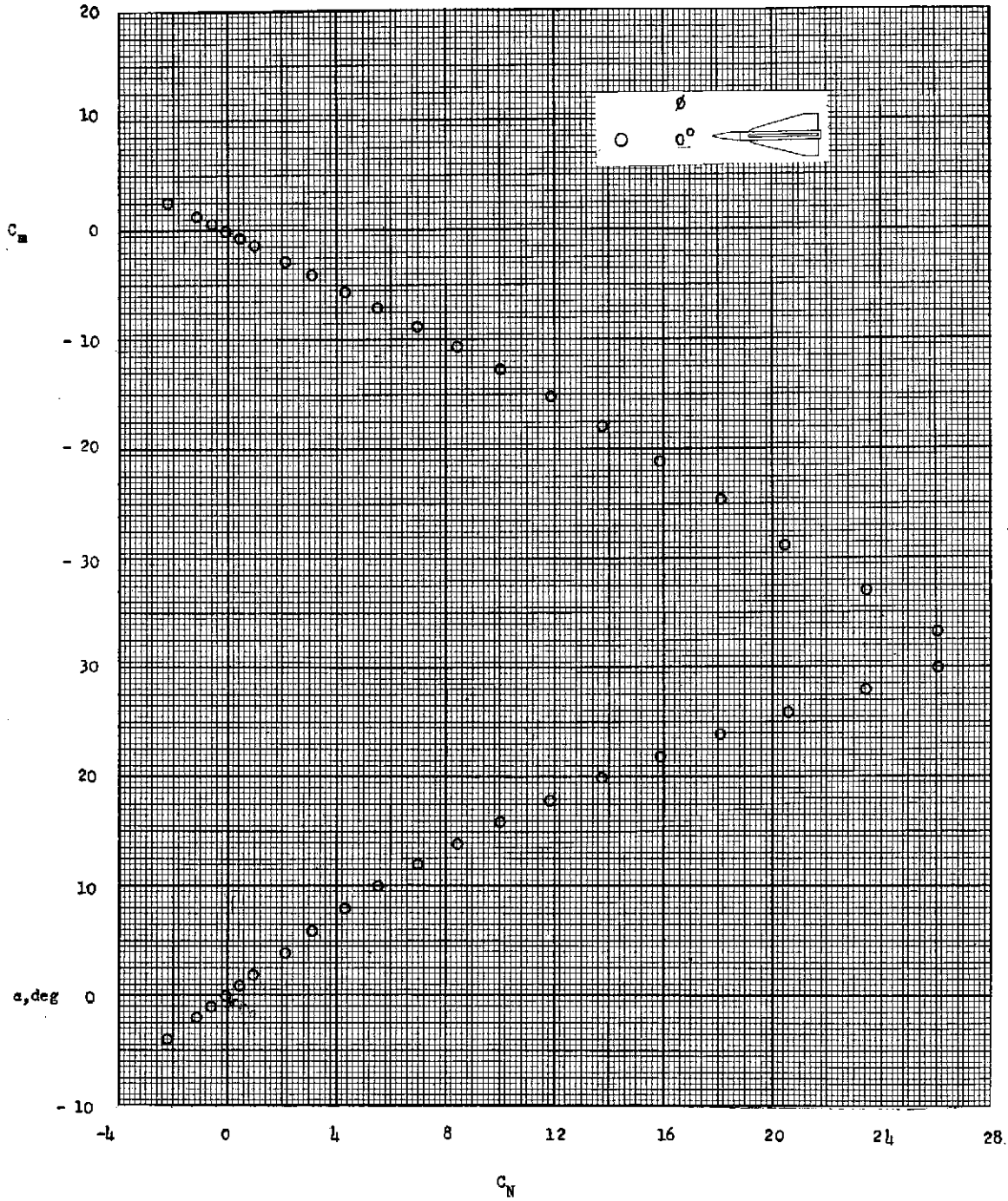

Figure 24.- Aerodynamic characteristics of configuration I-9 in pitch at a roll angle of 0° and a Mach number of 6.01. Fins are in rear position.

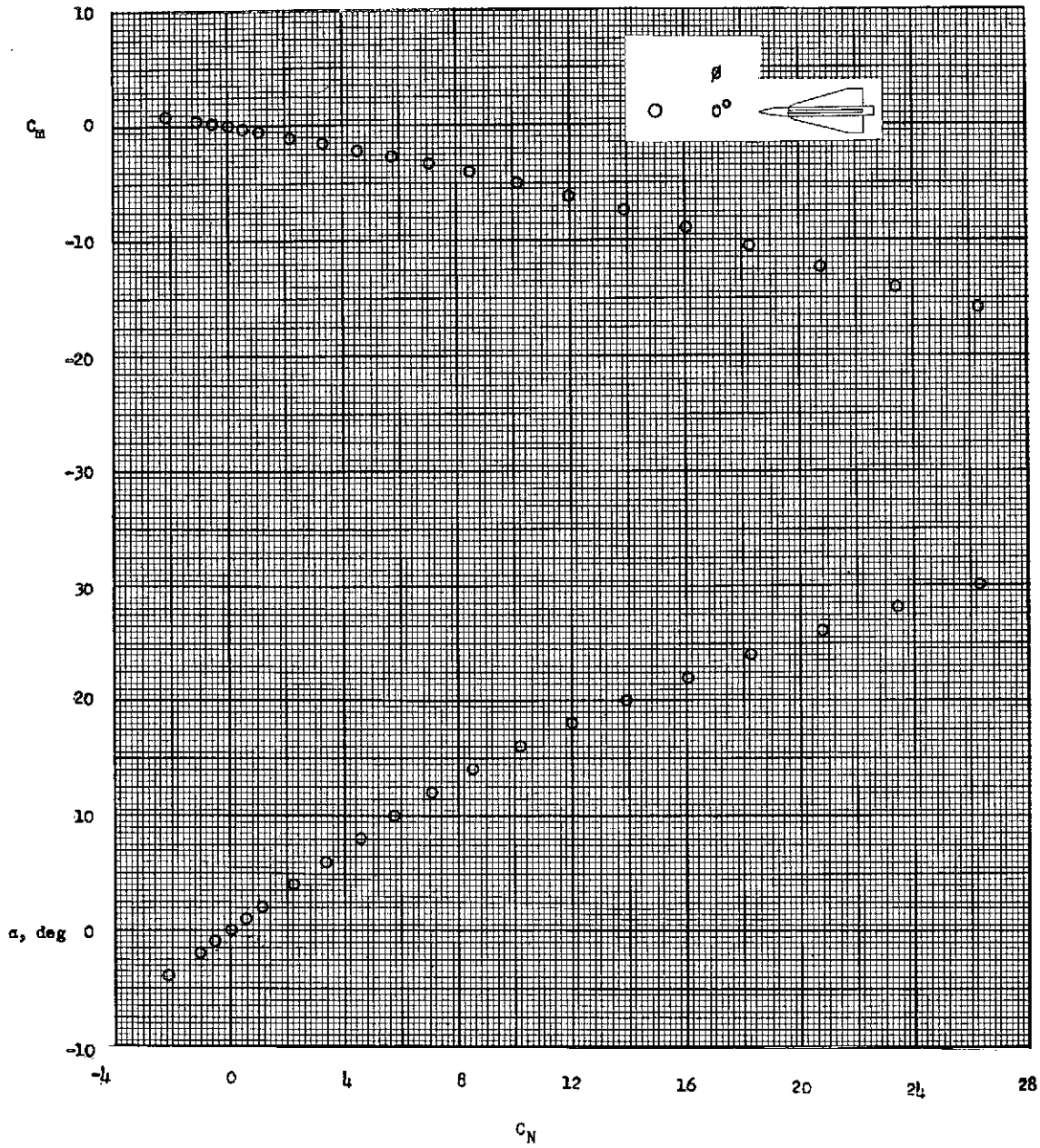

Figure 25.- Aerodynamic characteristics of configuration I-9 in pitch at a roll angle of 0° and Mach number 6.01. Fins are in forward position.

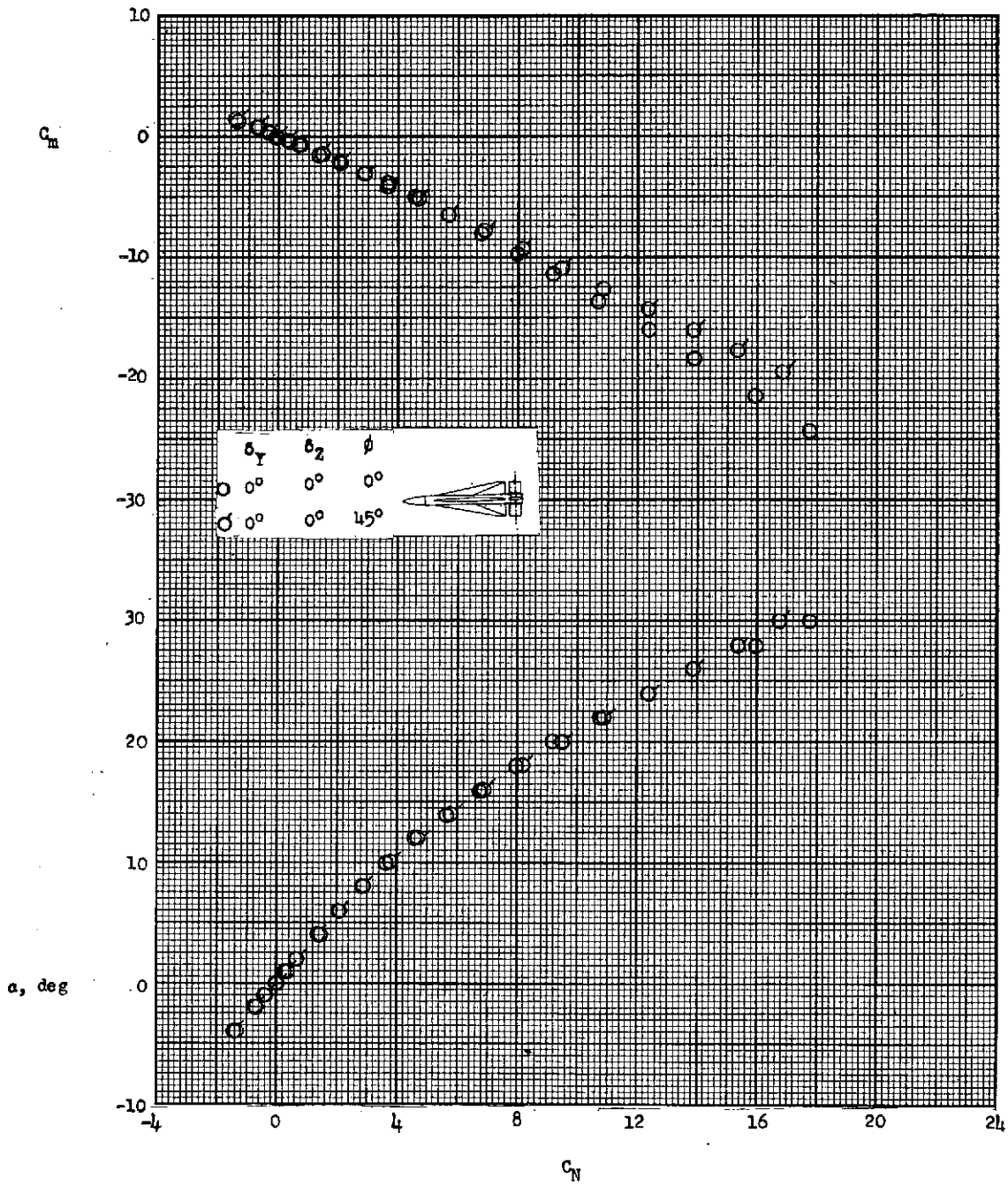

Figure 26.- Aerodynamic characteristics of configuration II-1-1 in pitch at roll angles of 0° and 45°, control deflection of 0°, and Mach number of 6.01. Fins are in rear position.

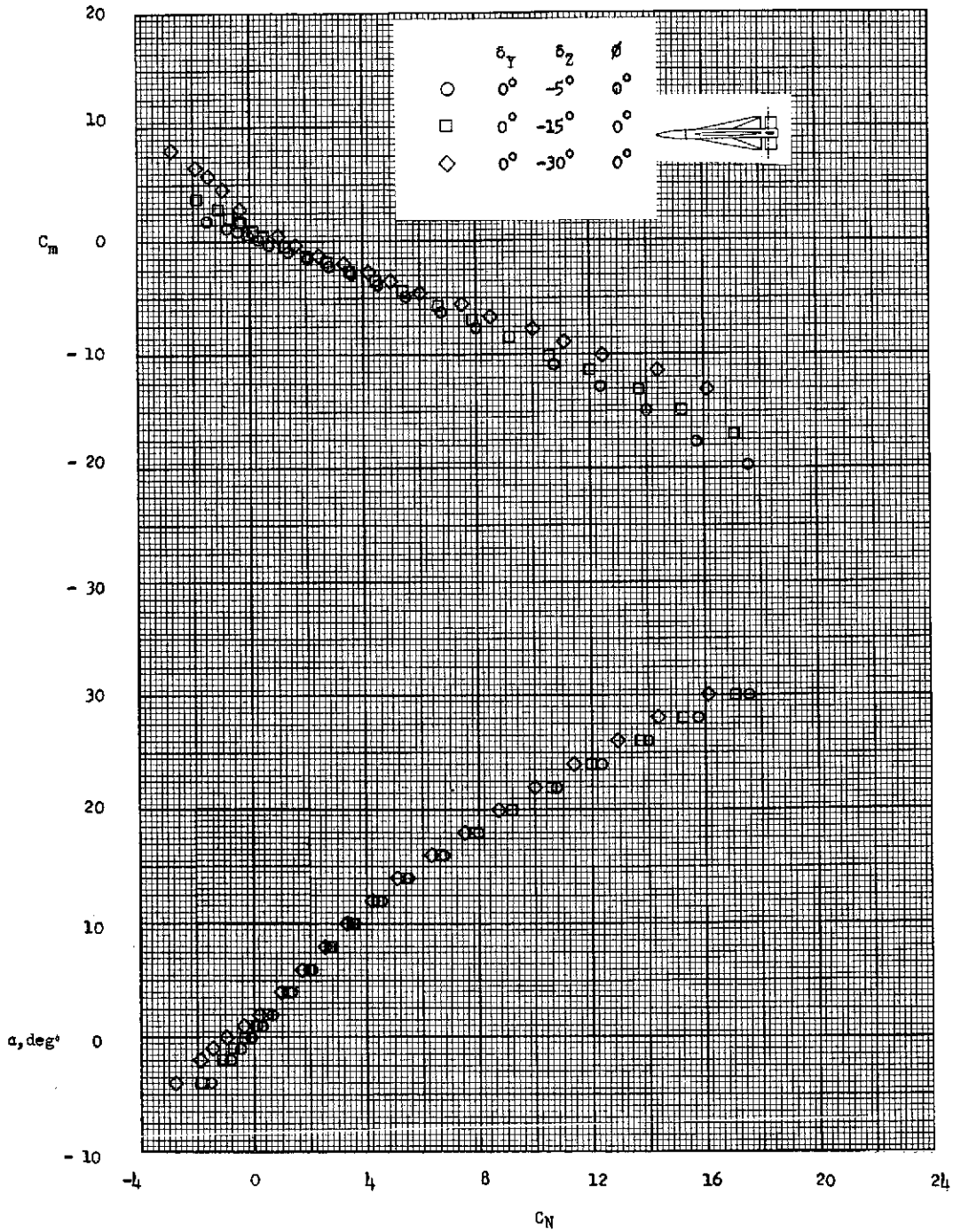

L-837

Figure 27.- Aerodynamic characteristics of configuration I-1-2 in pitch at roll angle of 0°, control-deflection angles of -5°, -15°, and -30°, and Mach number of 6.01. Fins are in rear position.

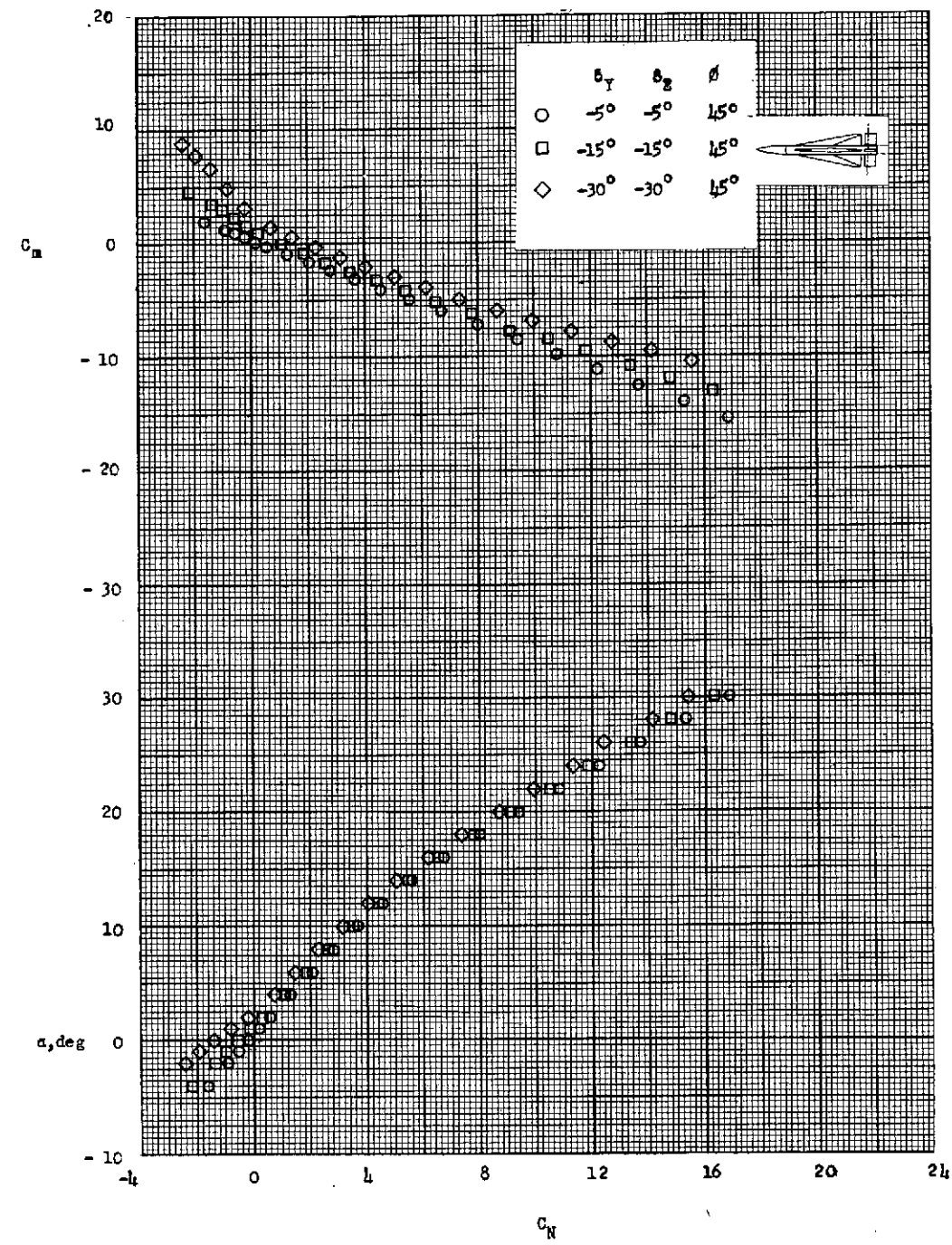

Figure 28.- Aerodynamic characteristics of configuration I-1-2 in pitch at roll angle of 45°, control-deflection angles of -5°, -15°, and -30°, and Mach number of 6.01. Fins are in rear position.

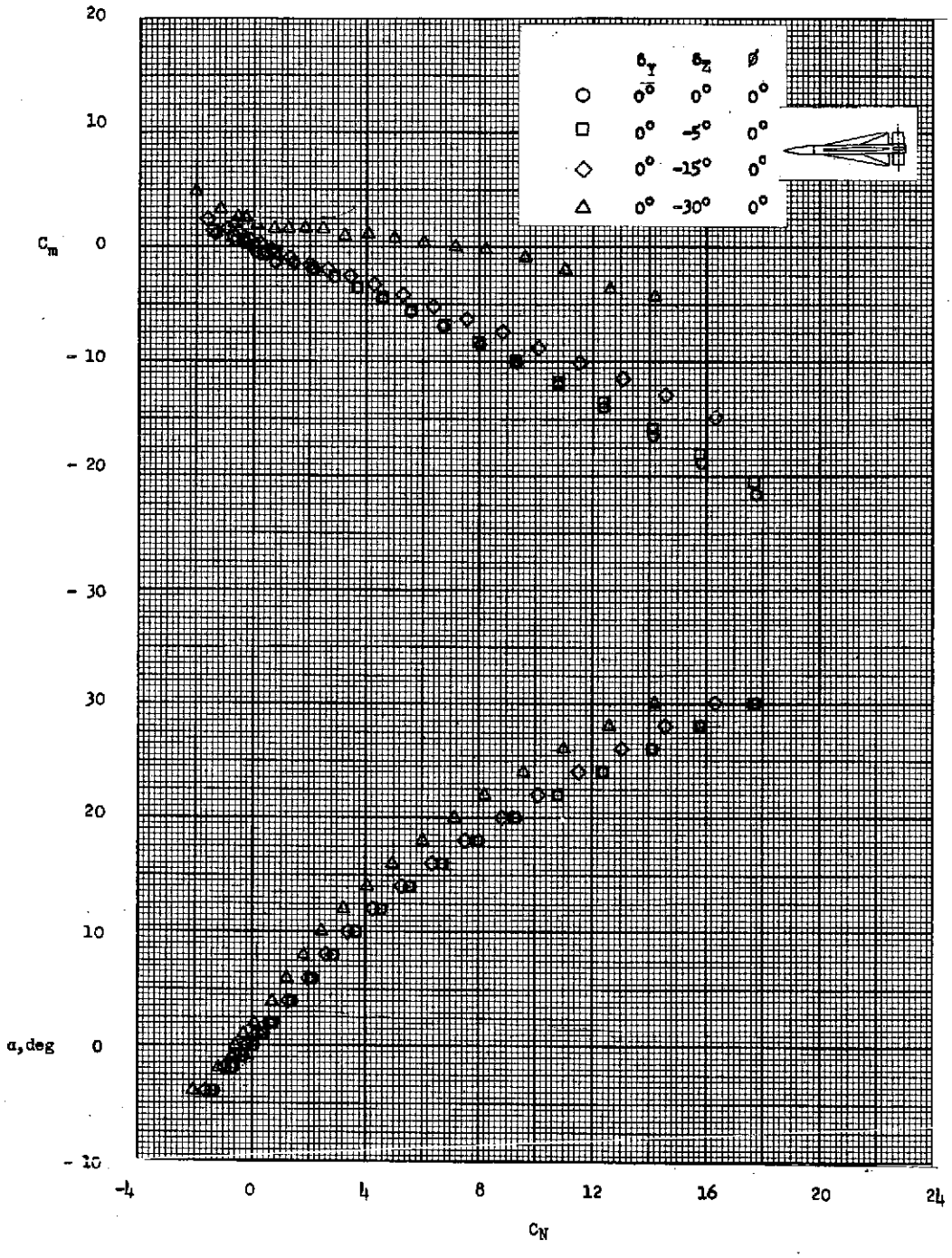

Figure 29.- Aerodynamic characteristics of configuration I-1-1 in pitch at roll angle of 0°, control-deflection angles of 0°, -5°, -15°, and -30°, and Mach number of 6.01. Fins are in rear position.

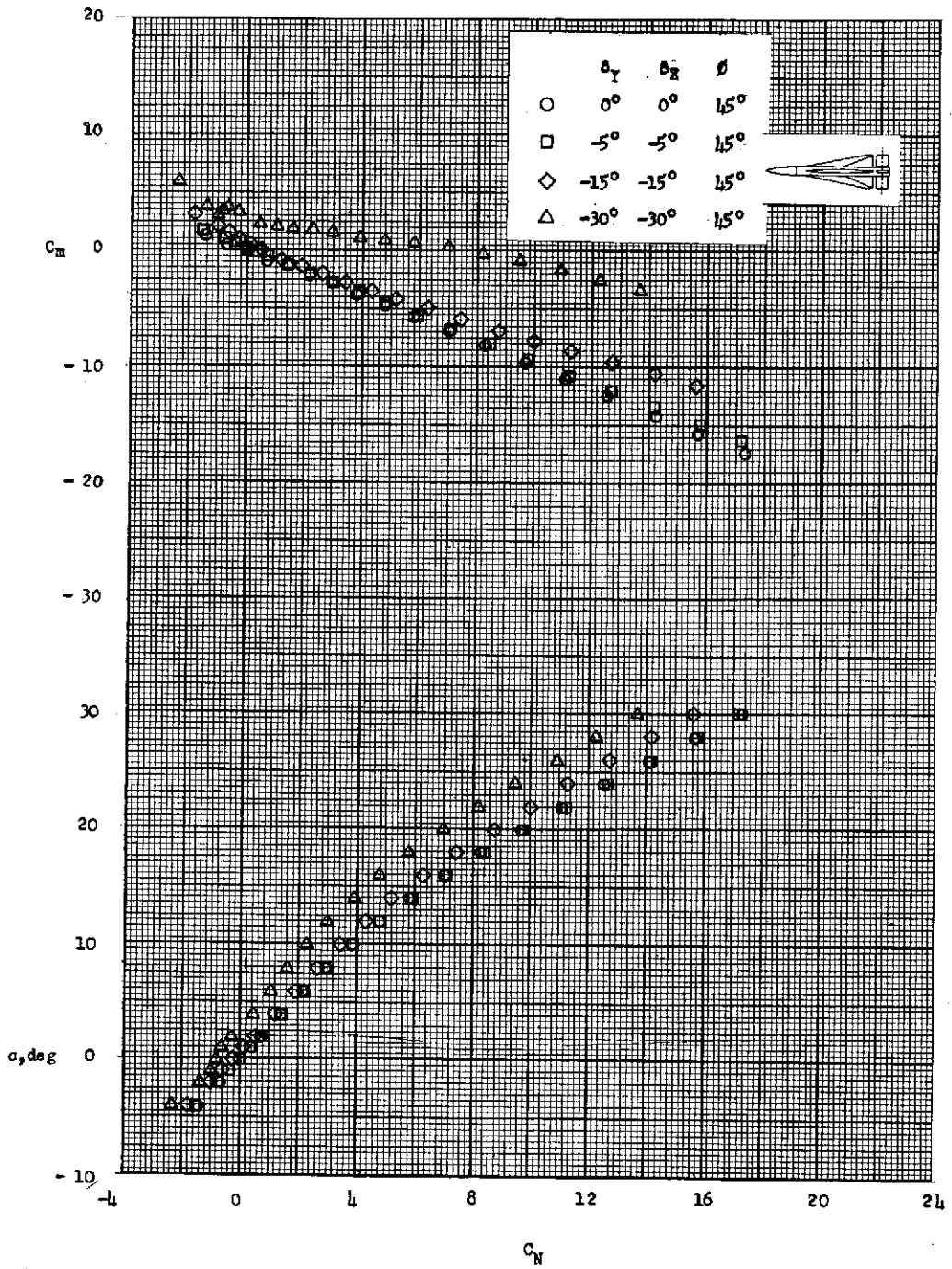

Figure 30.- Aerodynamic characteristics of configuration I-1-1 in pitch at roll angle of 45°, control-deflection angles of 0°, -5°, -15°, and -30°, and Mach number of 6.01. Fins are in rear position.

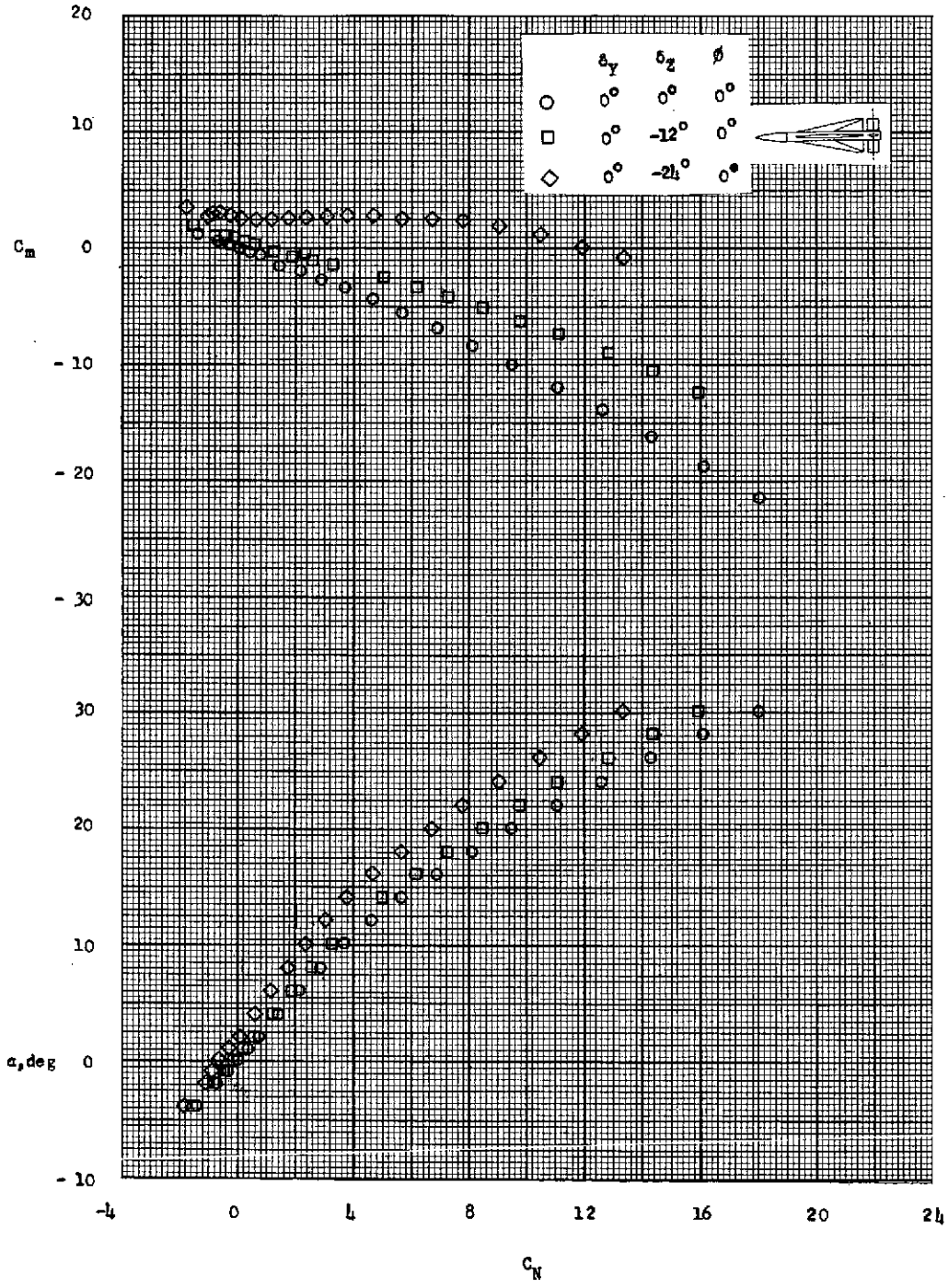

Figure 31.- Aerodynamic characteristics of configuration I-1-3 in pitch at roll angle of 0°, control-deflection angles of 0°, -12°, and -24°, and Mach number of 6.01. Fins are in rear position.

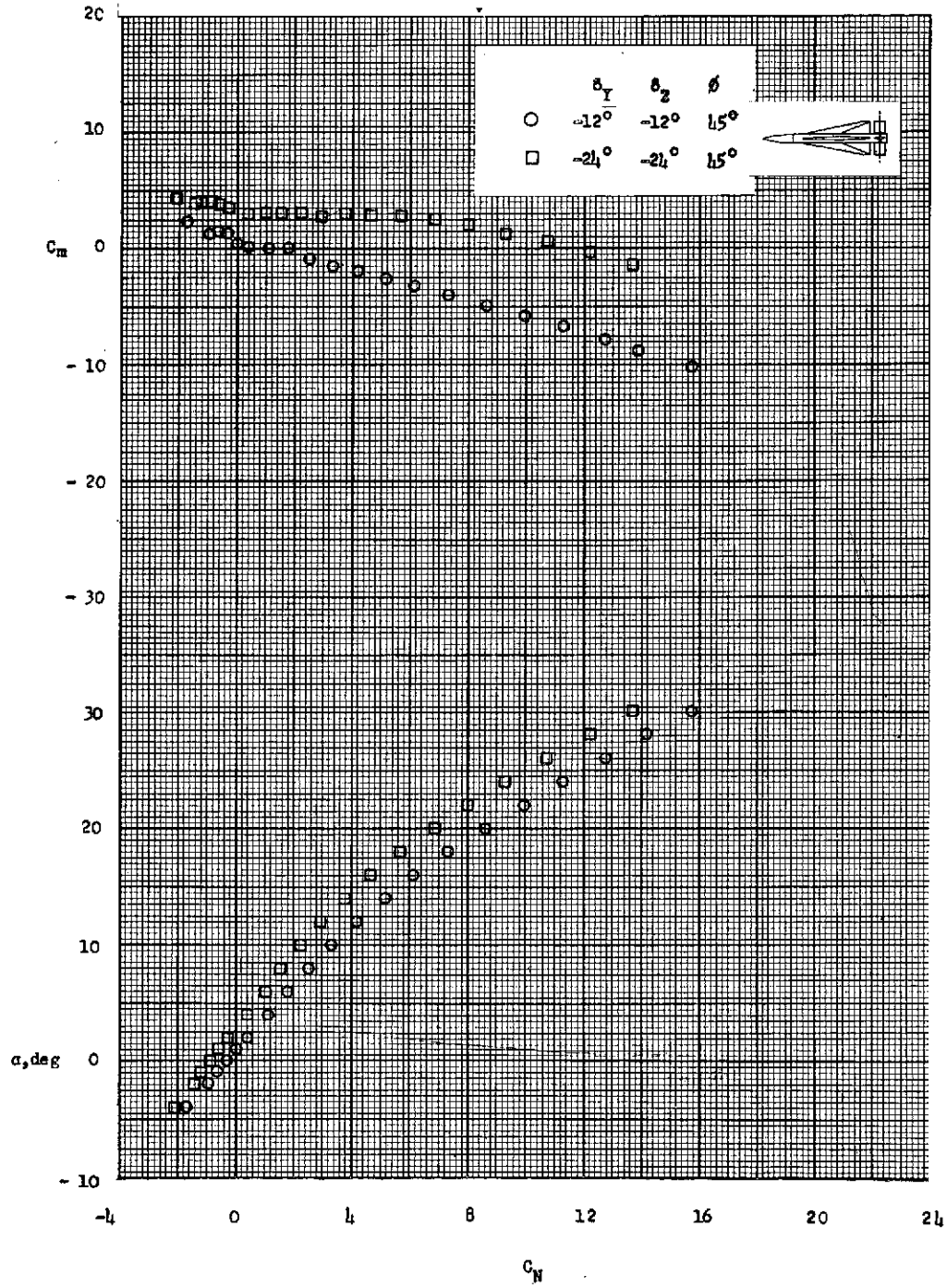

Figure 32.- Aerodynamic characteristics of configuration I-1-3 in pitch at roll angle of 45°, control-deflection angles of -12° and -24°, and Mach number of 6.01. Fins are in rear position.

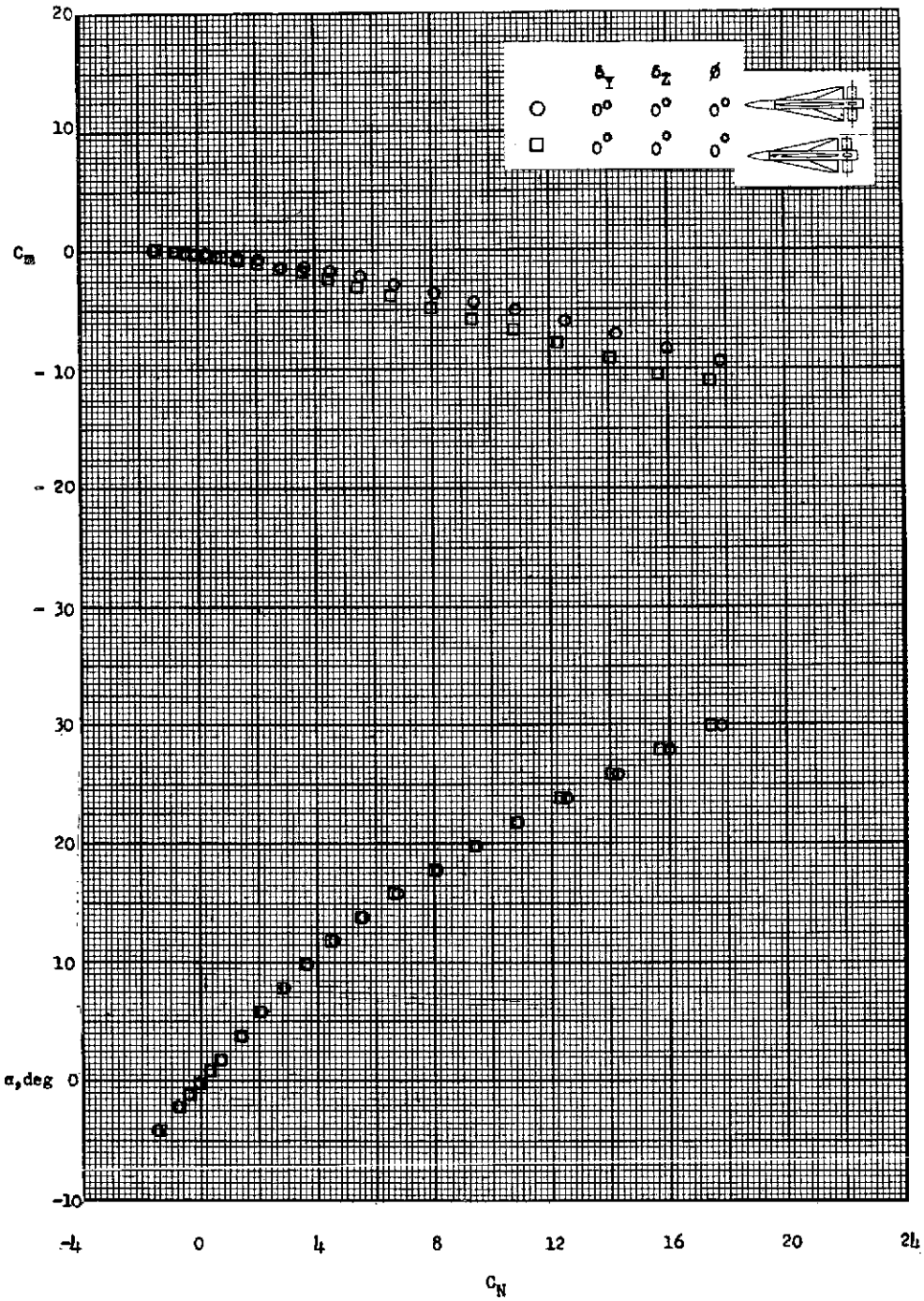

Figure 33.- Aerodynamic characteristics of configurations I-1-1 and II-1-1 in pitch at roll angle of 0°, deflection angle of 0°, and Mach number of 6.01. Fins are in the forward position.

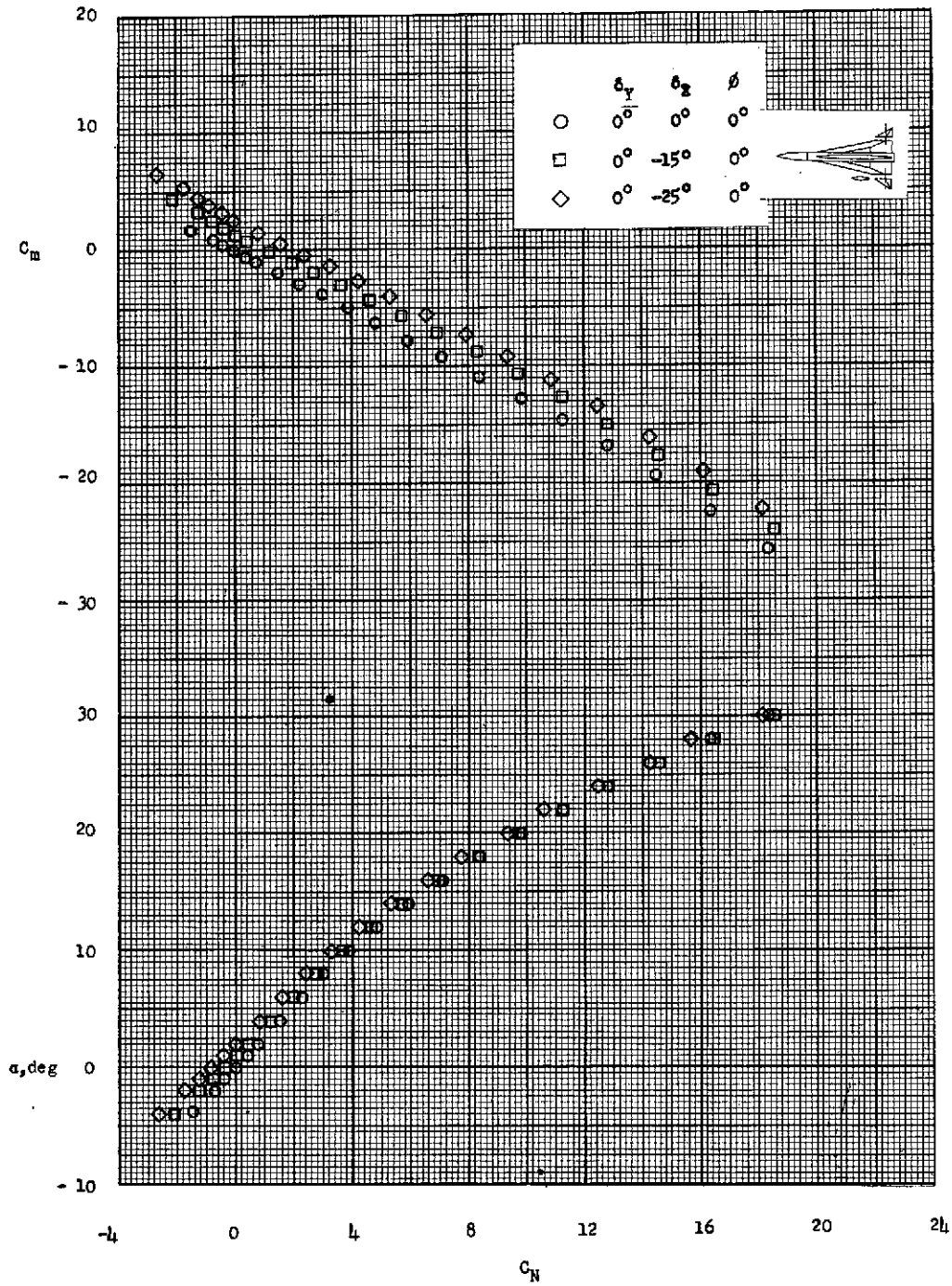

Figure 34.- Aerodynamic characteristics of configurations I-4-5 in pitch at roll angle of 0°, control-deflection angles of 0°, -15°, and -25°, and Mach number of 6.01. Fins are in the rear position.

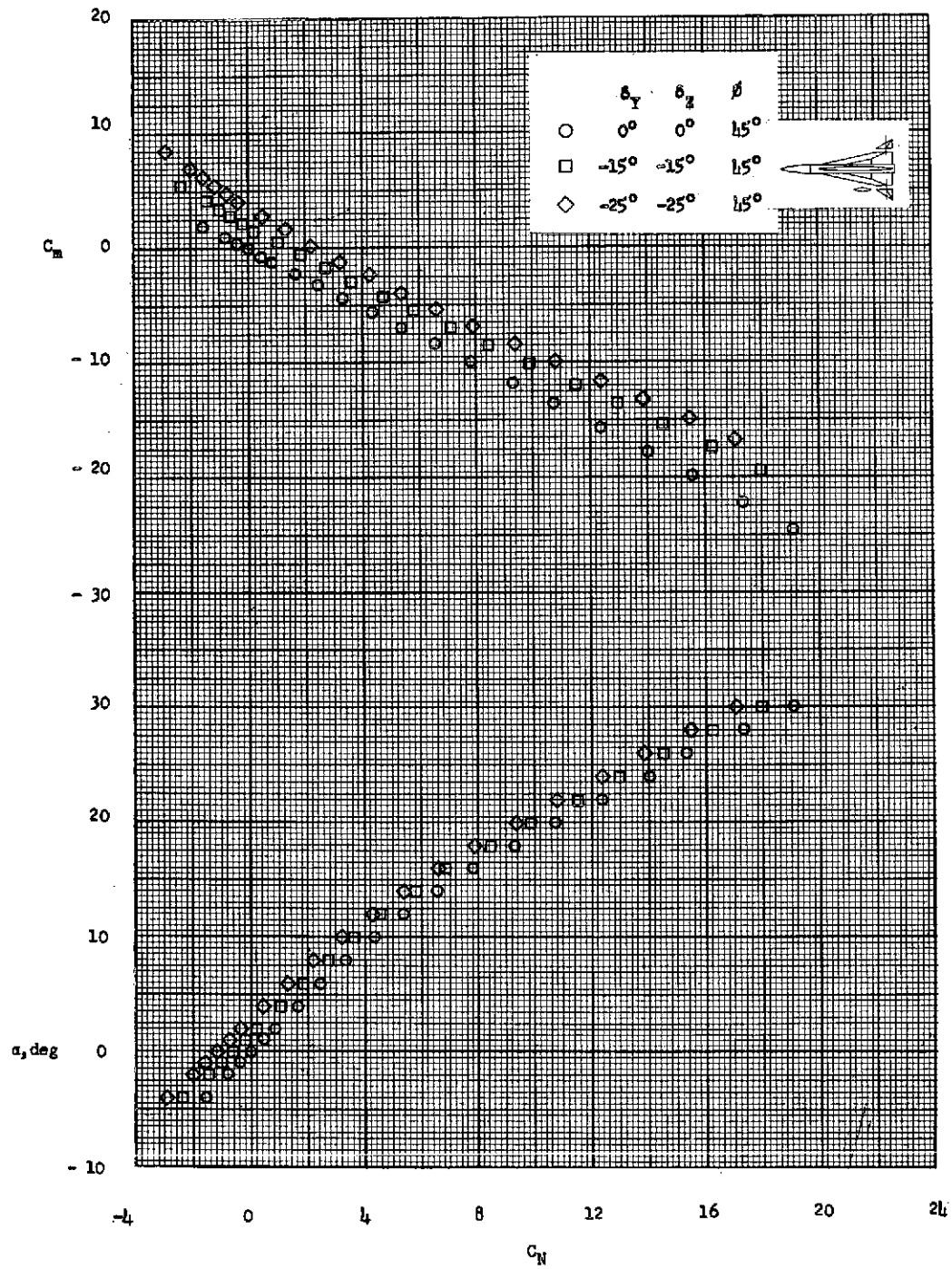

Figure 35.- Aerodynamic characteristics of configurations I-4-5 in pitch at roll angle of 45°, control-deflection angles of 0°, -15°, and -25°, and Mach number of 6.01. Fins are in the rear position.

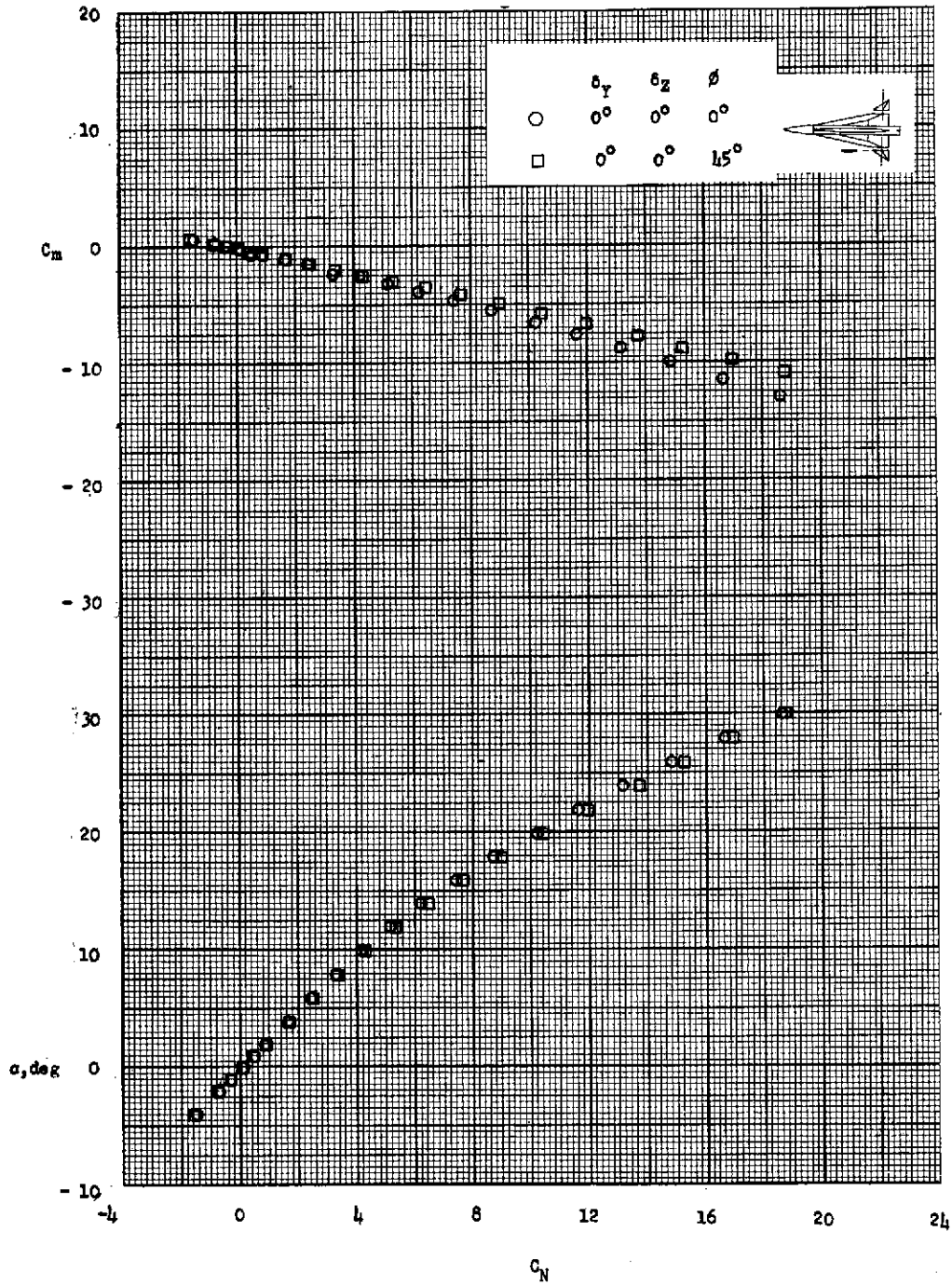

Figure 36.- Aerodynamic characteristics of configuration I-4-5 in pitch at roll angles of 0° and 45°, control-deflection angle of 0°, and Mach number of 6.01. Fins are in the forward position.

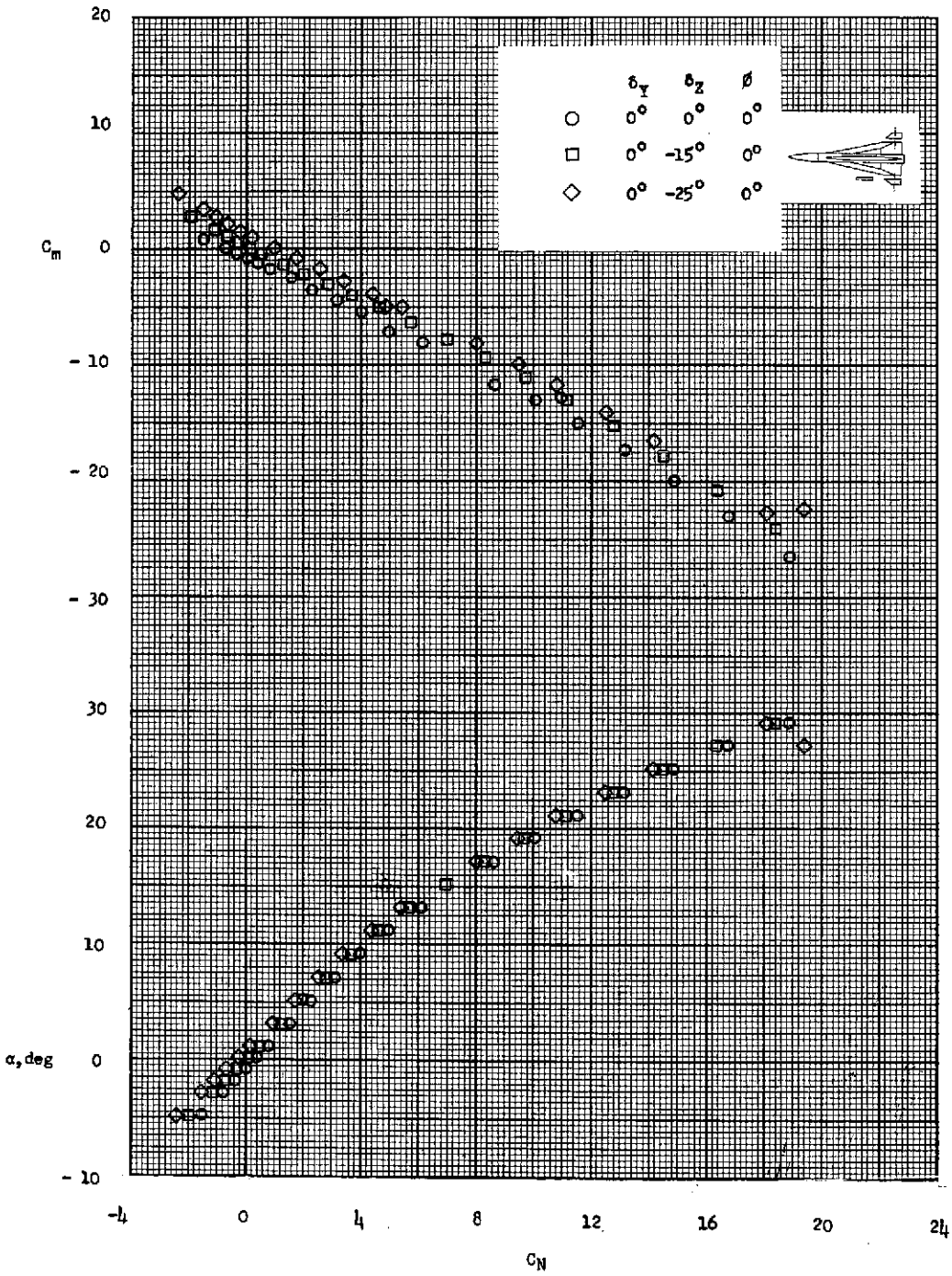

Figure 37.- Aerodynamic characteristics of configuration I-4-6 in pitch at roll angle of 0°, control-deflection angles of 0°, -15°, and -25°, and Mach number of 6.01. Fins are in rear position.

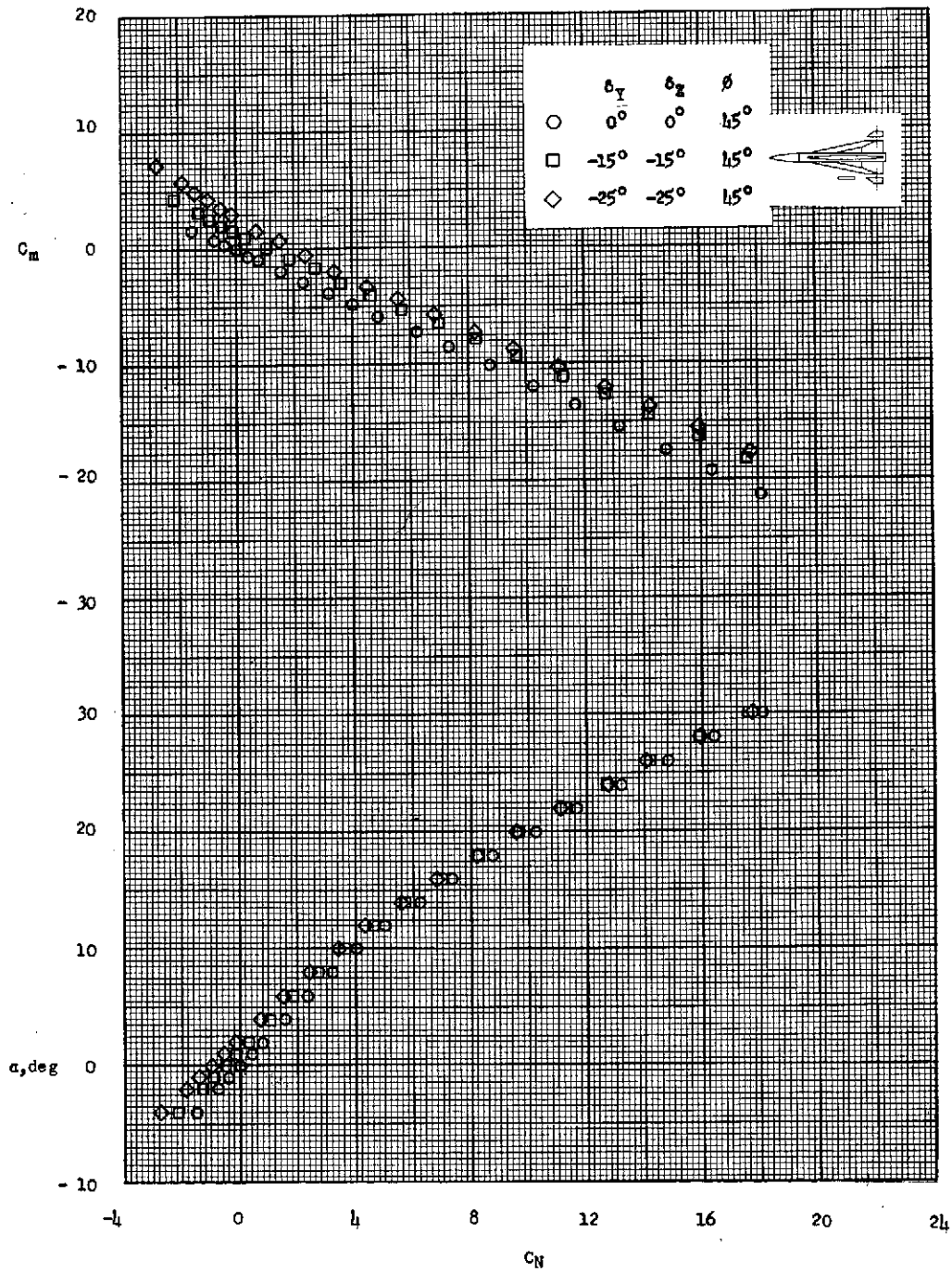

Figure 38.- Aerodynamic characteristics of configuration I-4-6 in pitch at roll angle of 45°, control-deflection angles of 0°, -15°, and -25°, and Mach number of 6.01. Fins are in rear position.

.837

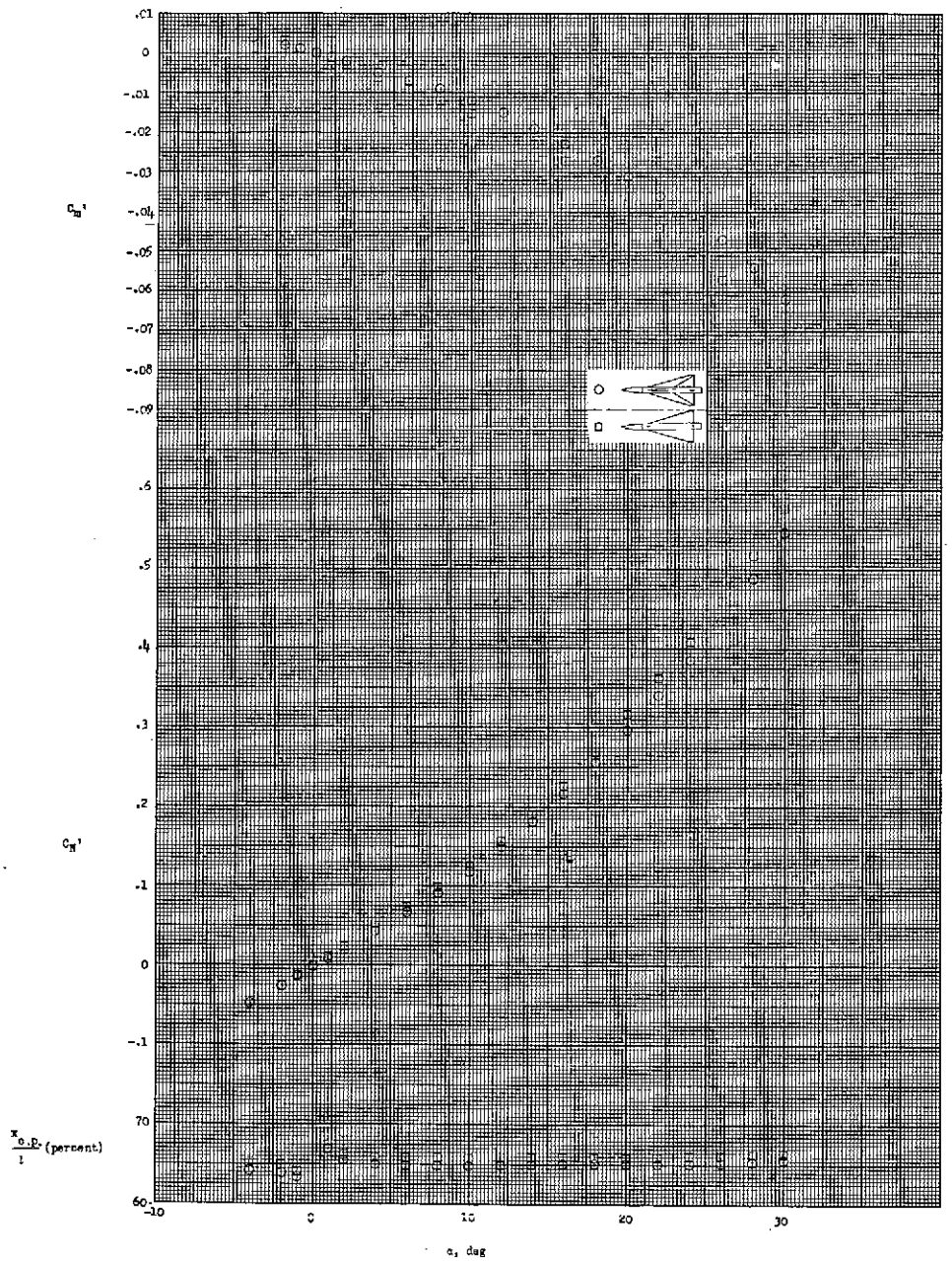

(a) Configurations I-2 and I-3.

Figure 39.- Effect of fin or fin-control profile shape on the aerodynamic characteristics of configurations in pitch having equal areas but different profile shapes. Fins are in rear position. M = 6.01; $\phi = 0^{\circ}$.

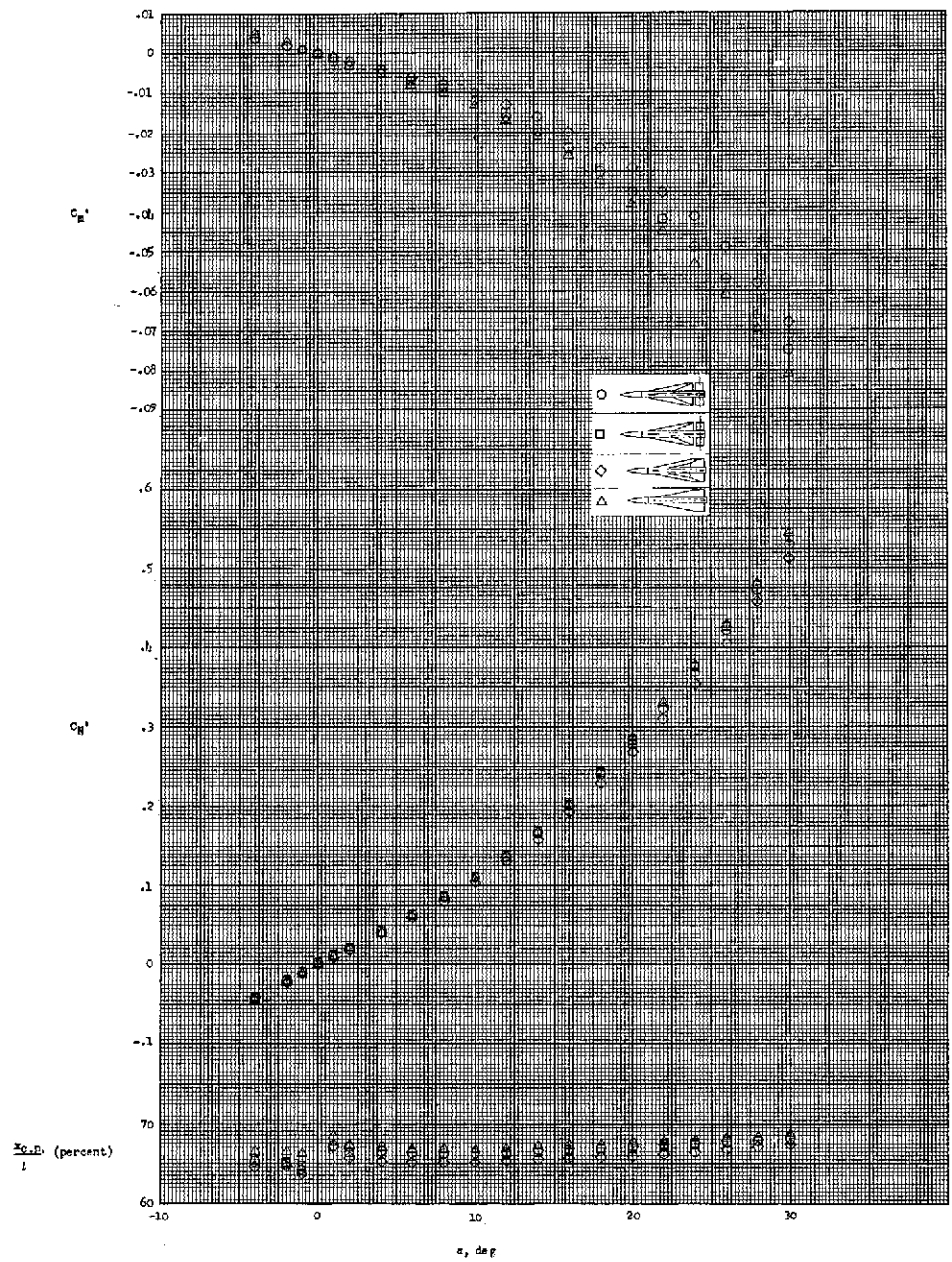

(b) Configurations I-1-1, I-1-3, I-4, and I-5.

Figure 39.- Concluded.

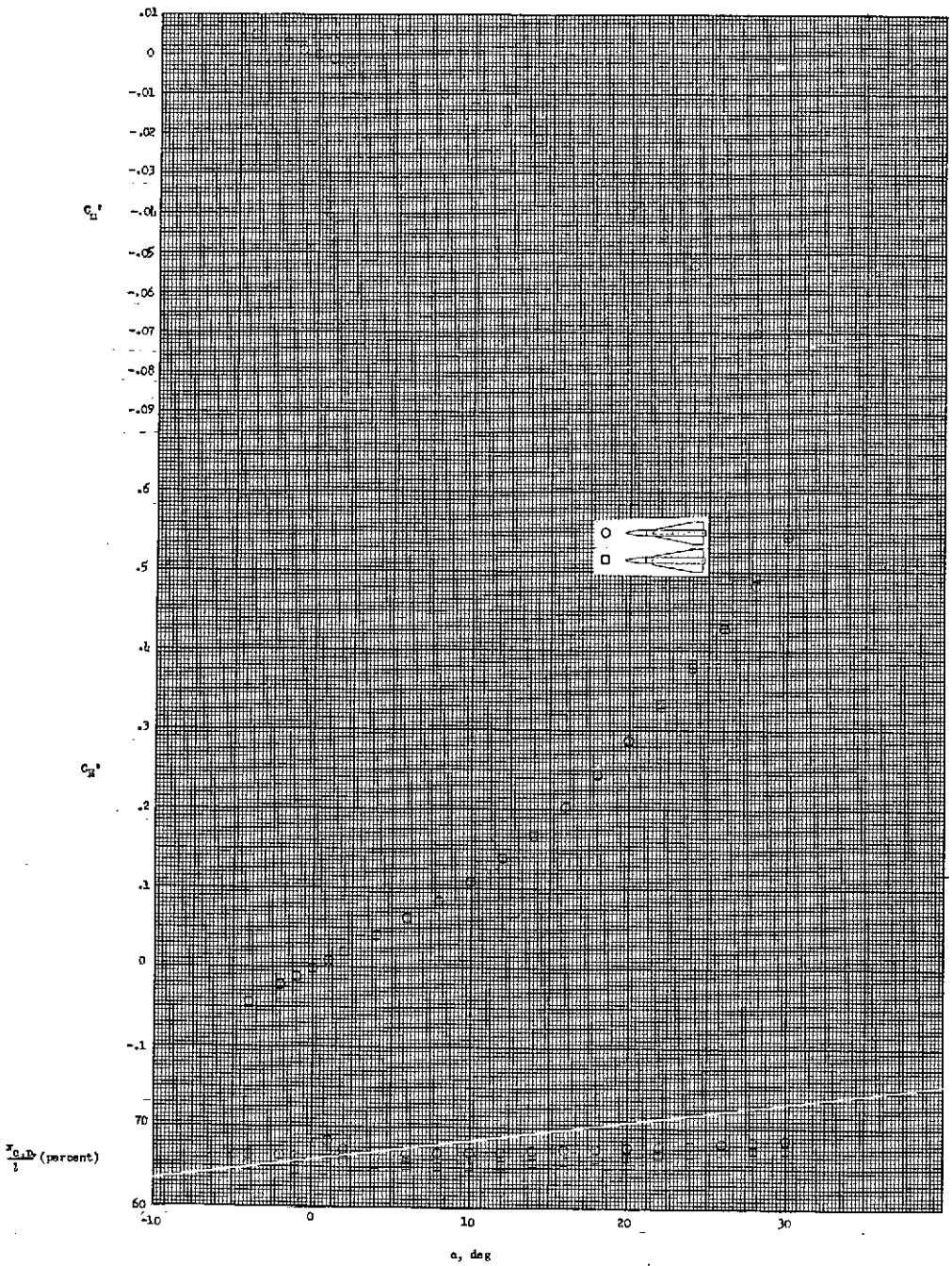

Figure 40.- Effect of planform and planform area. Comparison of the aerodynamic characteristics of configurations I-5 and I-7 in pitch at roll angle of 0°. Configuration I-7 has a cranked leading edge and a larger area. The fins are in the rear position. M = 6.01.

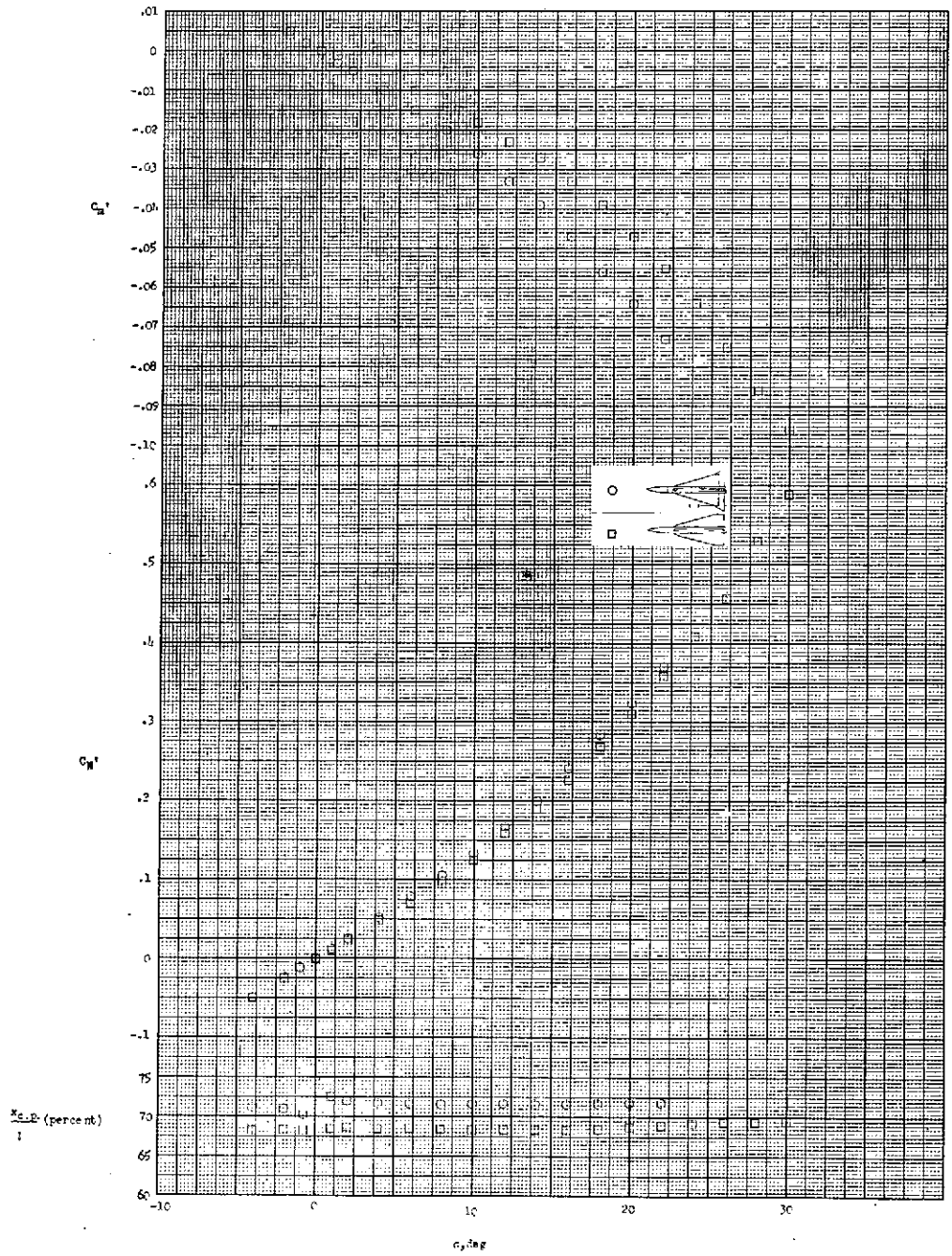

Figure 41.- Effect of planform. Comparison of the aerodynamic characteristics of configurations I-3-7 and I-9 in pitch at roll angle of 0°. The configurations have the same area and the fins are in the rear position. M = 6.01.

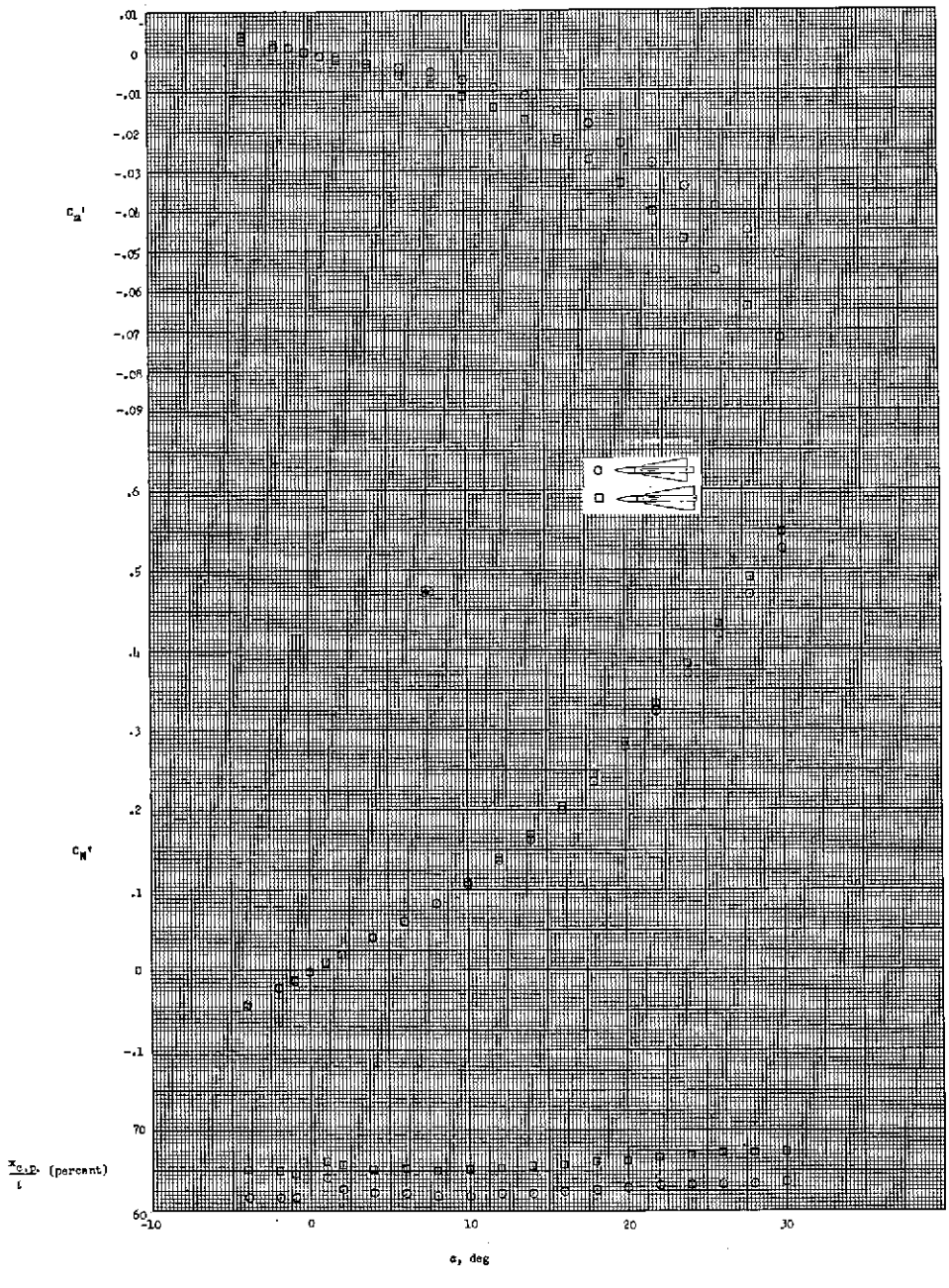

(a) Configurations I-7 and I-8.

Figure 42.- Effect of planform and planform area. Comparison of the aerodynamic characteristics of configurations, having different chords and areas, in pitch at roll angle of 0°. The fins are in the rear position. M = 6.01.

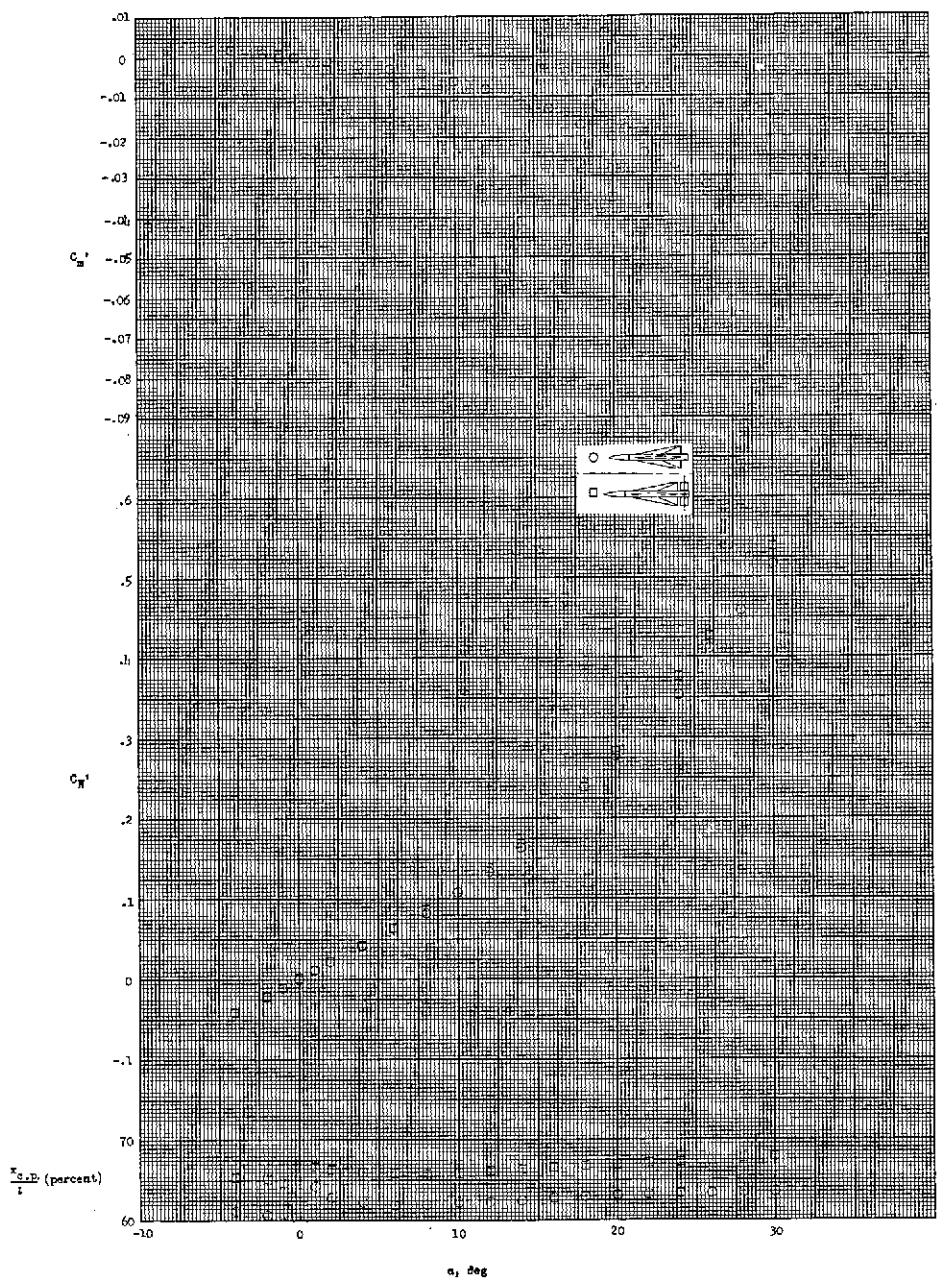

(b) Configurations I-1 and I-1-3.

Figure 42.- Concluded.

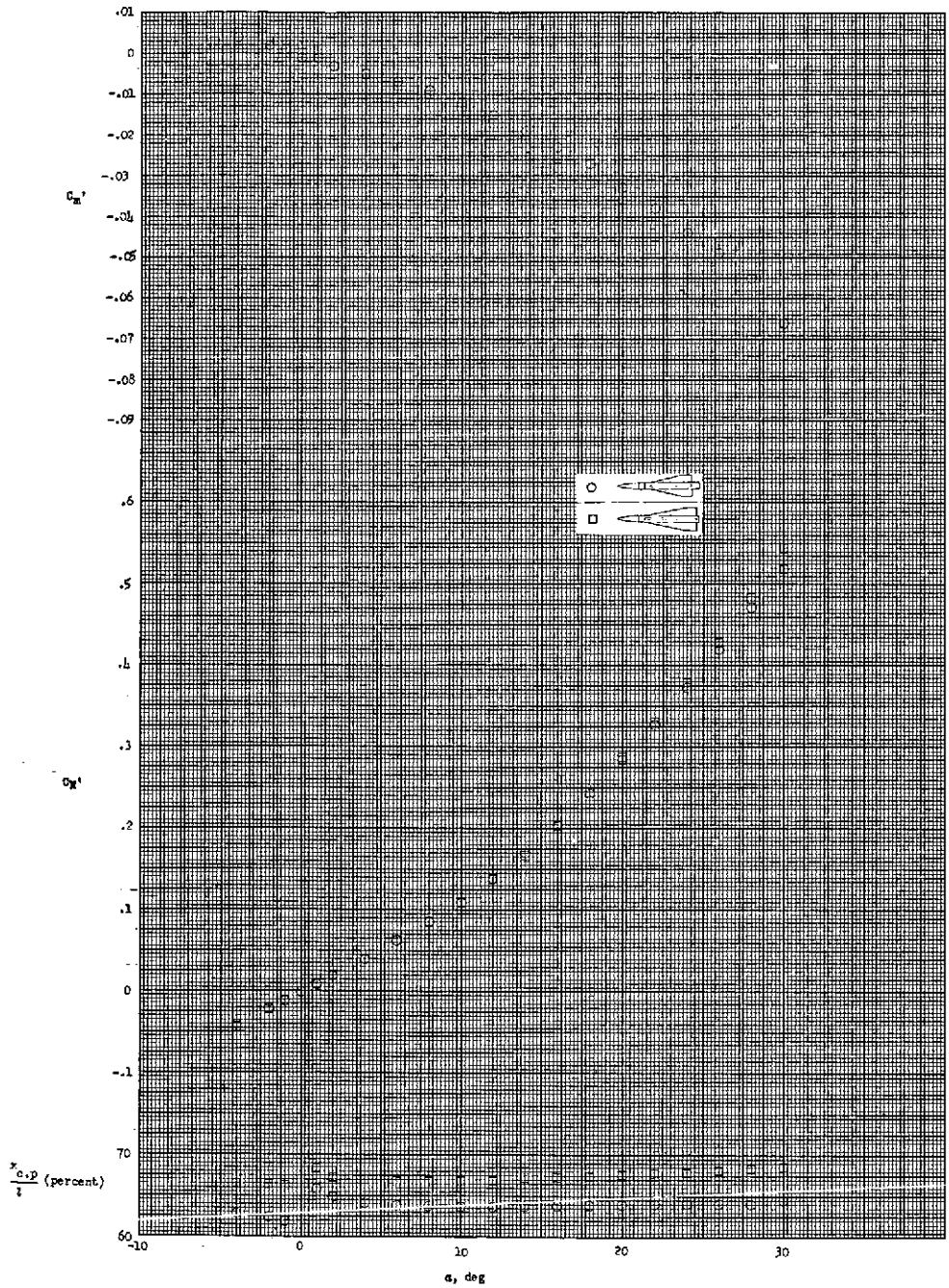

Figure 43.- Effect of planform area. Comparison of the aerodynamic characteristics of configurations I-5 and I-6 at roll angle of 0°. The fins are in the rear position. M = 6.01.

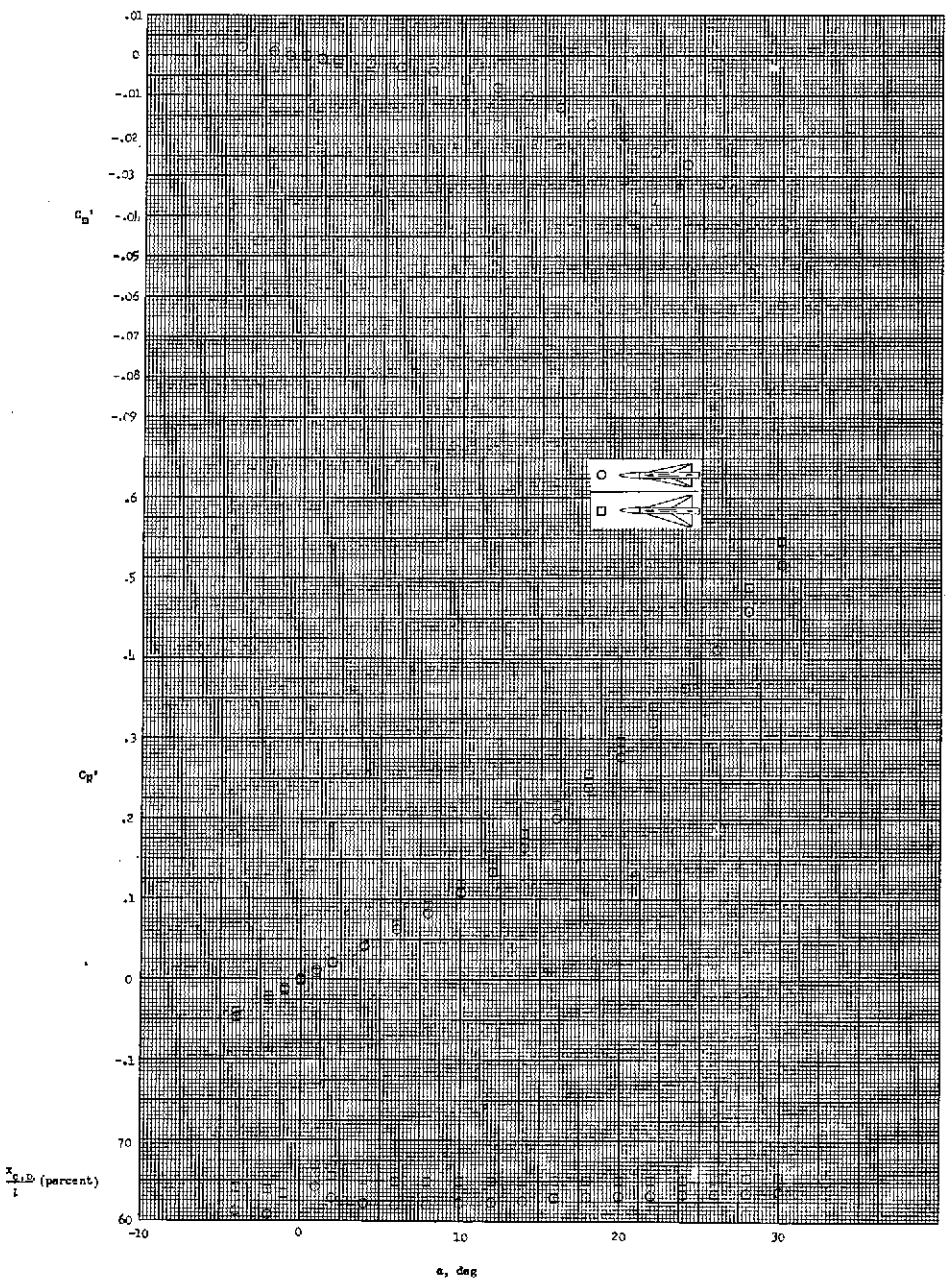

(a) Configurations I-1 and I-2.

Figure 44.- Effect of planform and planform area. Comparison of the aerodynamic characteristics of configurations having different spans and area in pitch at roll angle of 0°. The fins are in the rear position. M = 6.01.

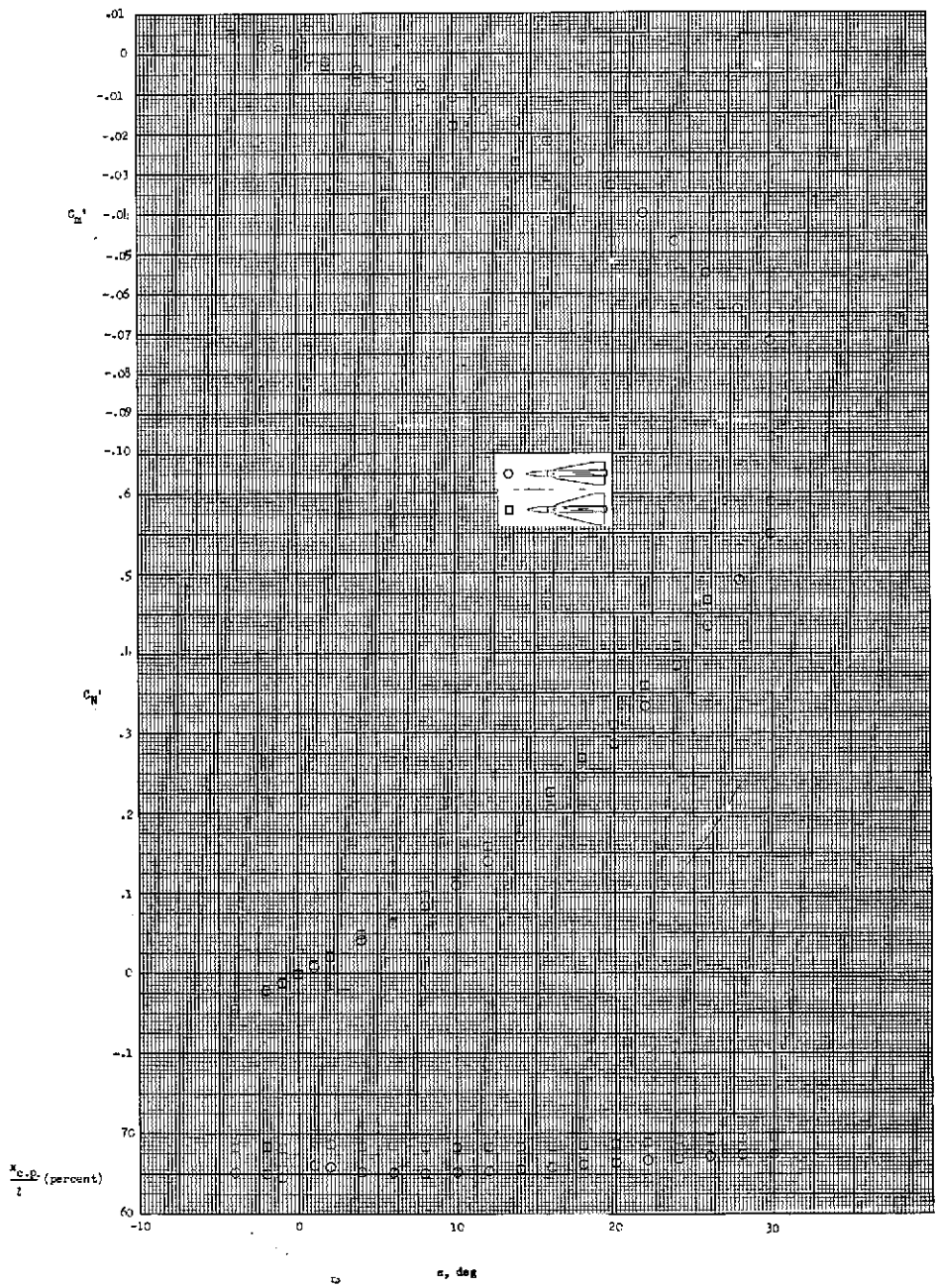

(b) Configurations I-4 and I-6.

Figure 44.- Continued.

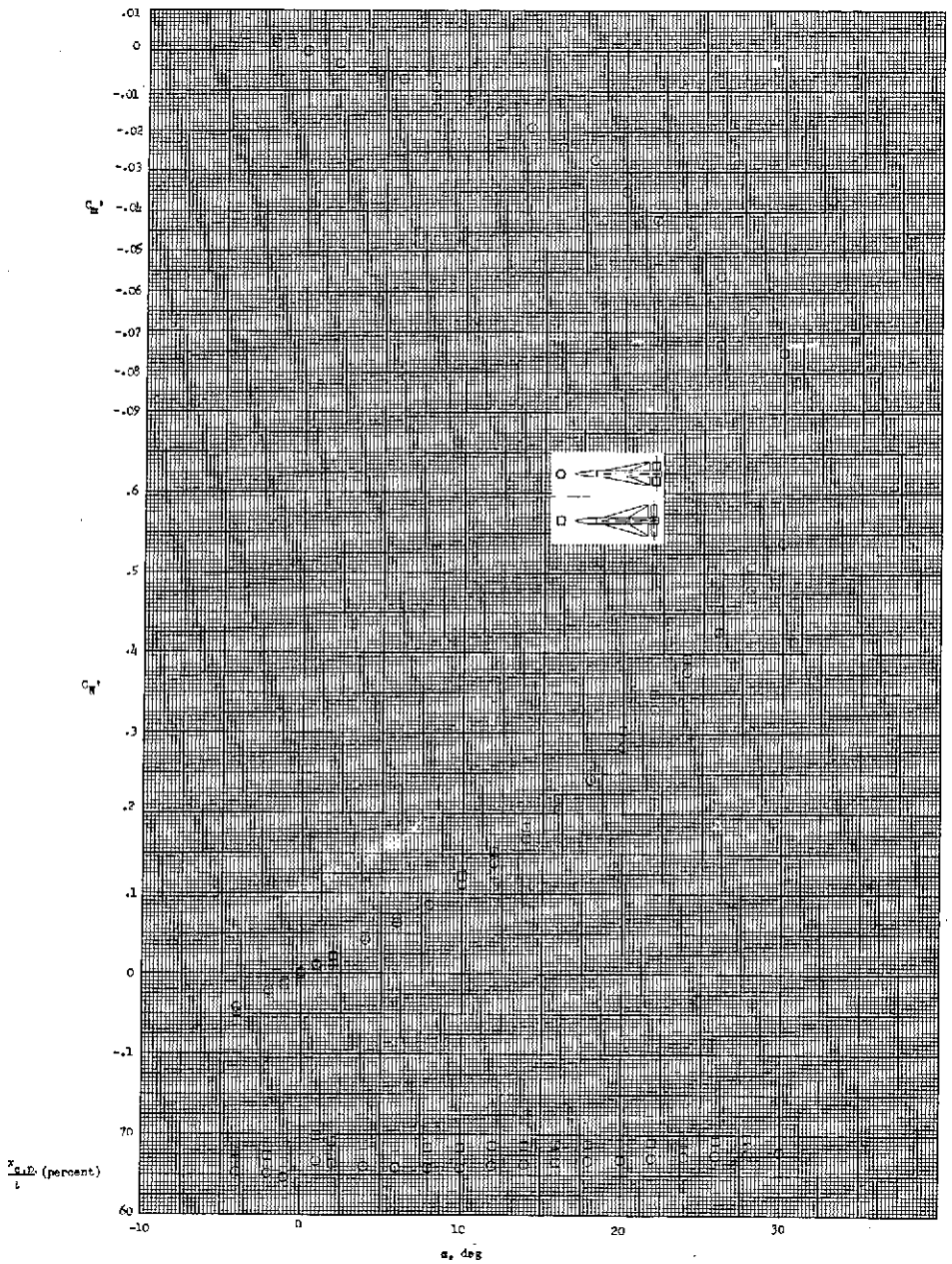

(c) Configurations I-1-3 and I-2-4.

Figure 44.- Concluded.

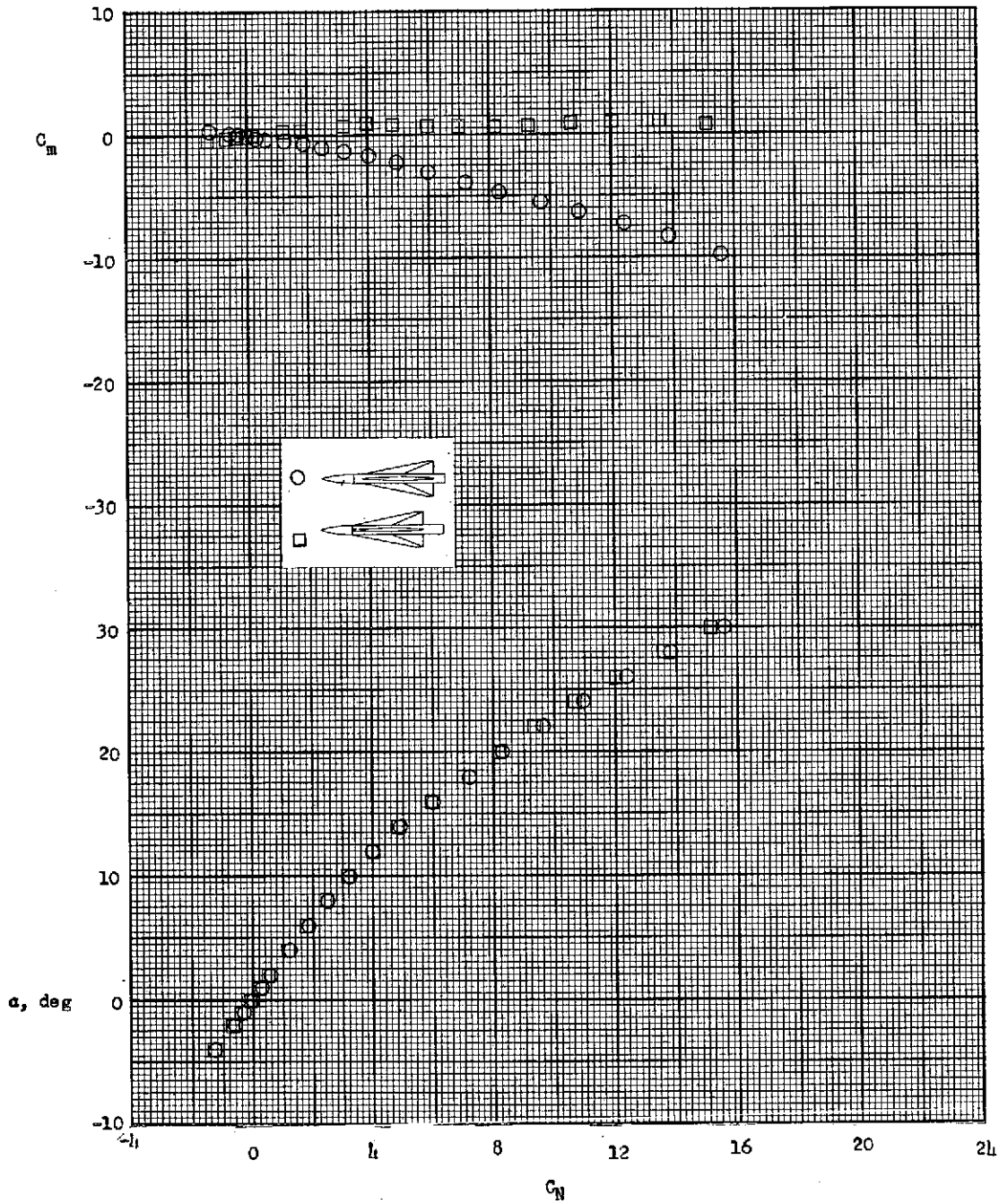

(a) Configuration I-1.

Figure 45.- Effect of fin longitudinal location. Comparison of the aerodynamic characteristics of a configuration in pitch at roll angle of 0° and Mach number of 6.01 for two longitudinal locations of the fins on the body.

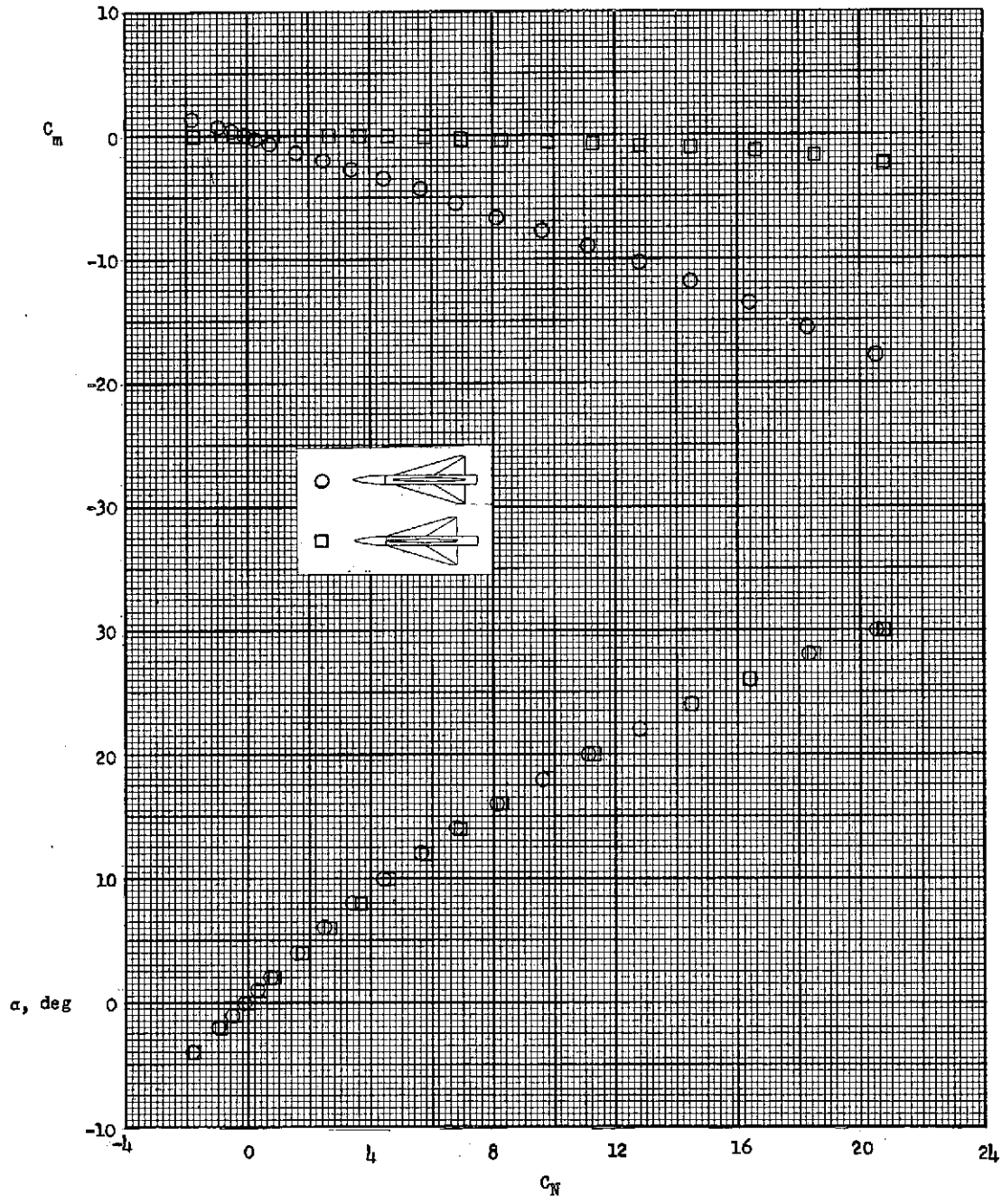

(b) Configuration I-2.

Figure 45.- Continued.

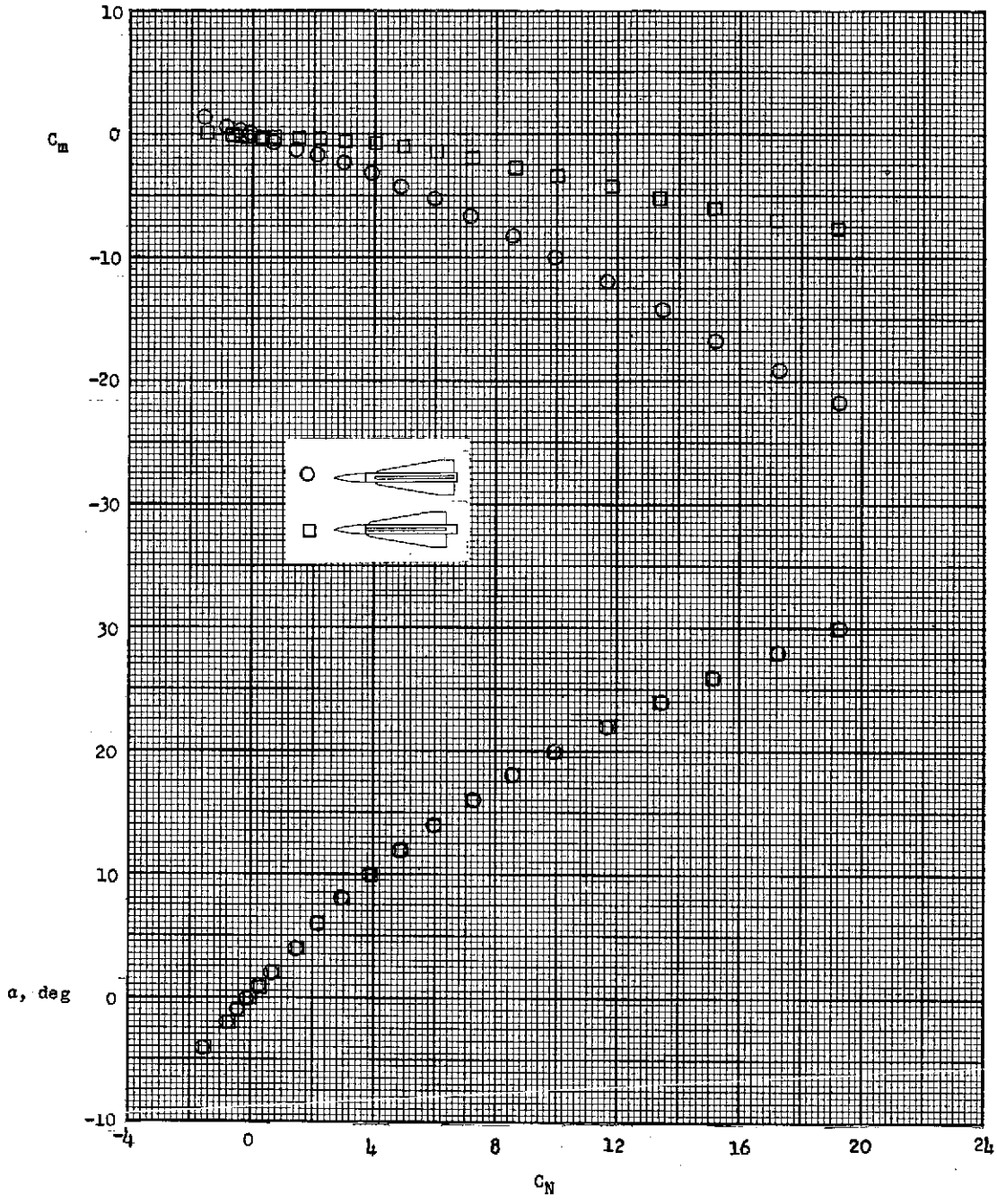

(c) Configuration I-7.

Figure 45.- Continued.

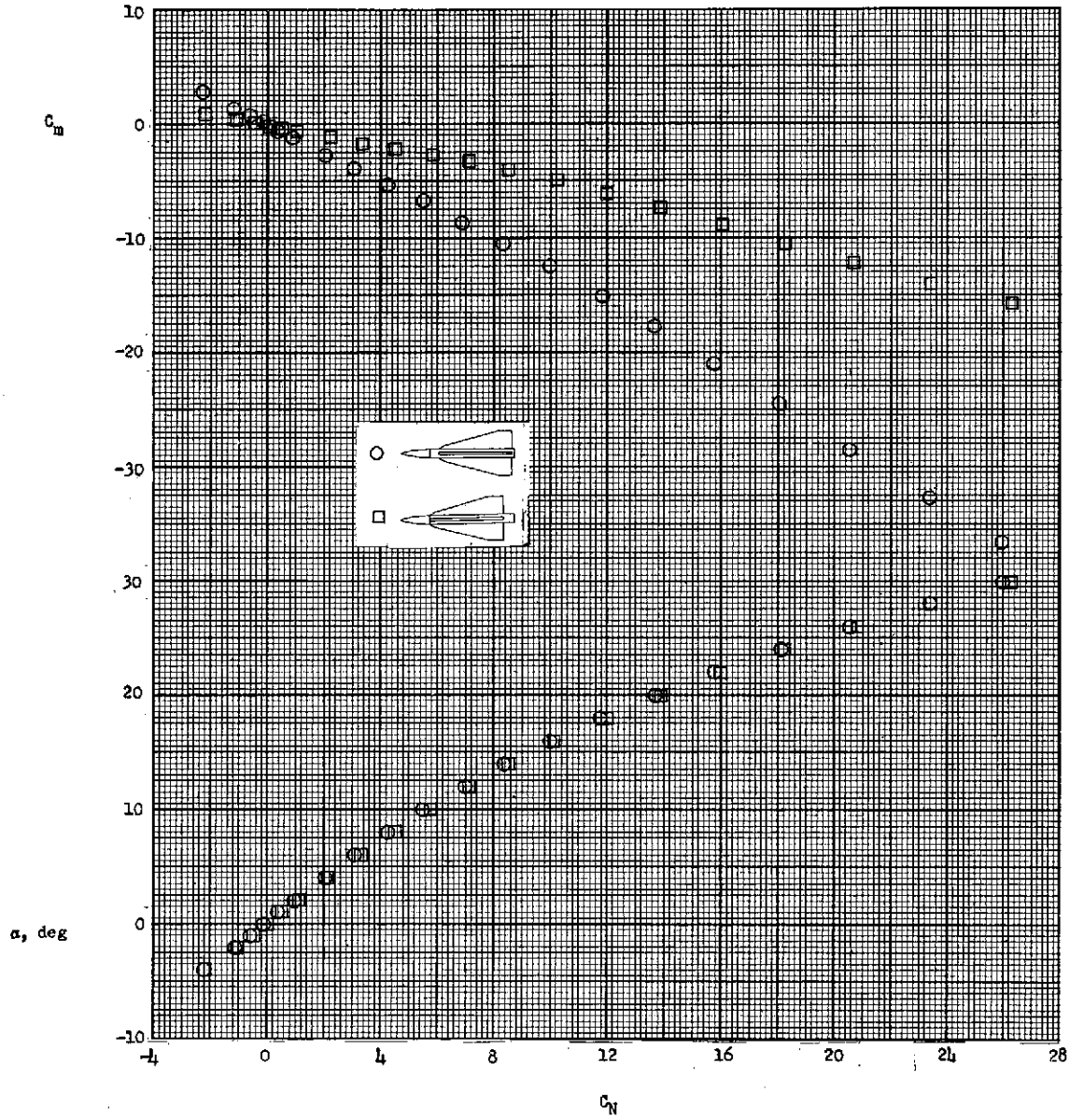

(d) Configuration I-9.

Figure 45.- Continued.

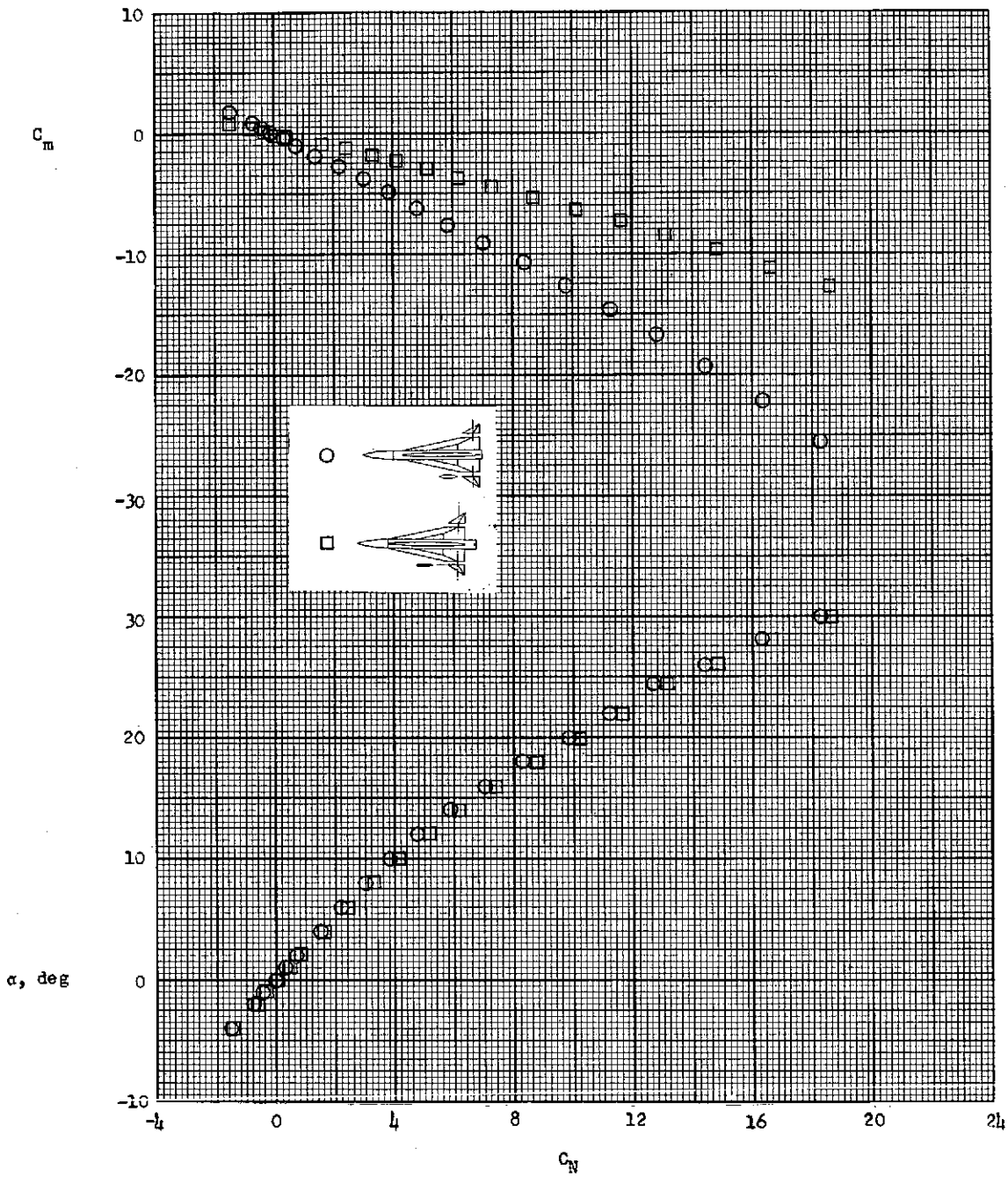

(e) Configuration I-4-5.

Figure 45.- Concluded.

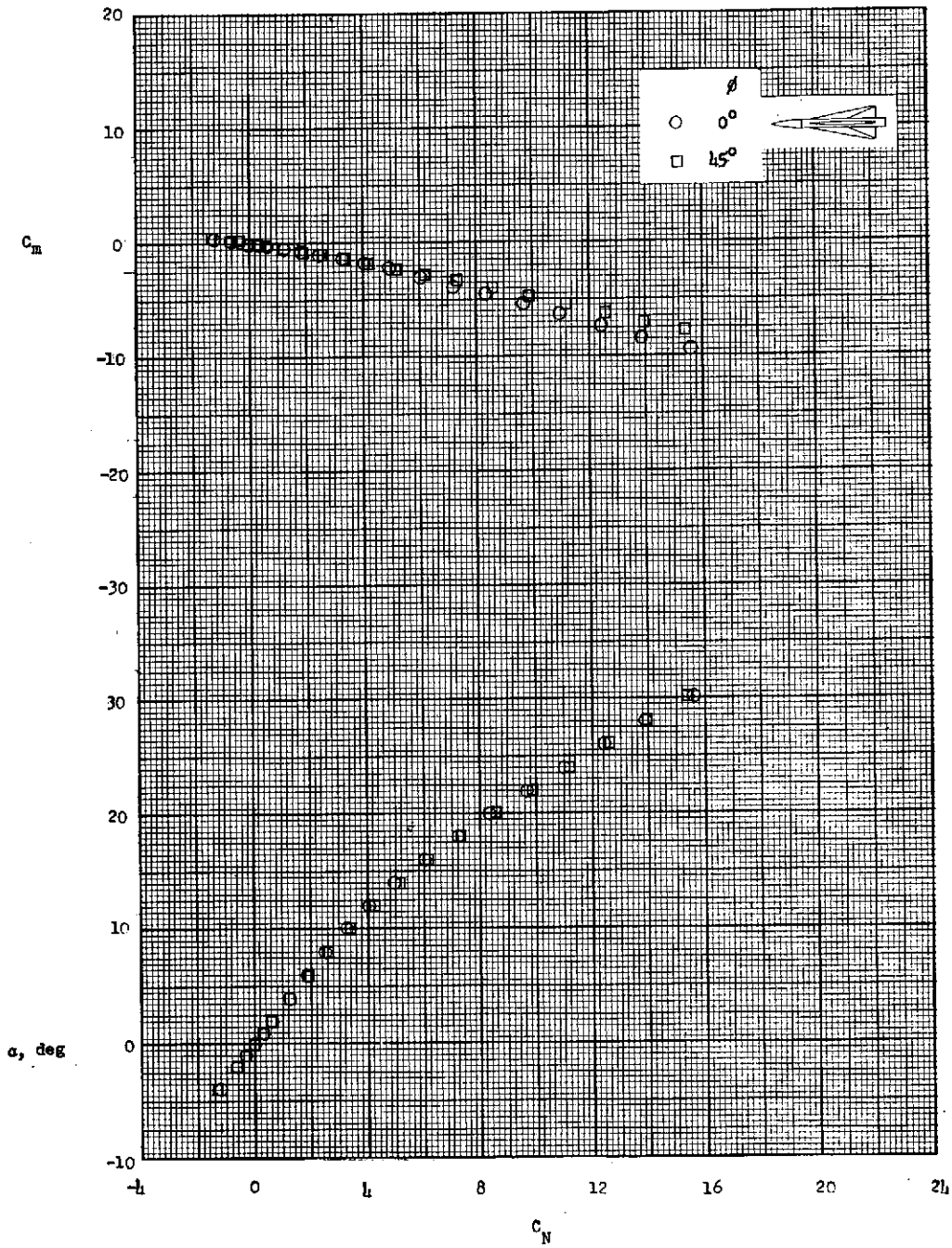

(a) Configuration I-1 with fins in rear position.

Figure 46.- Effect of roll angle. Comparison of the aerodynamic characteristics of a configuration in pitch at roll angles of 0° and 45°. M = 6.01.

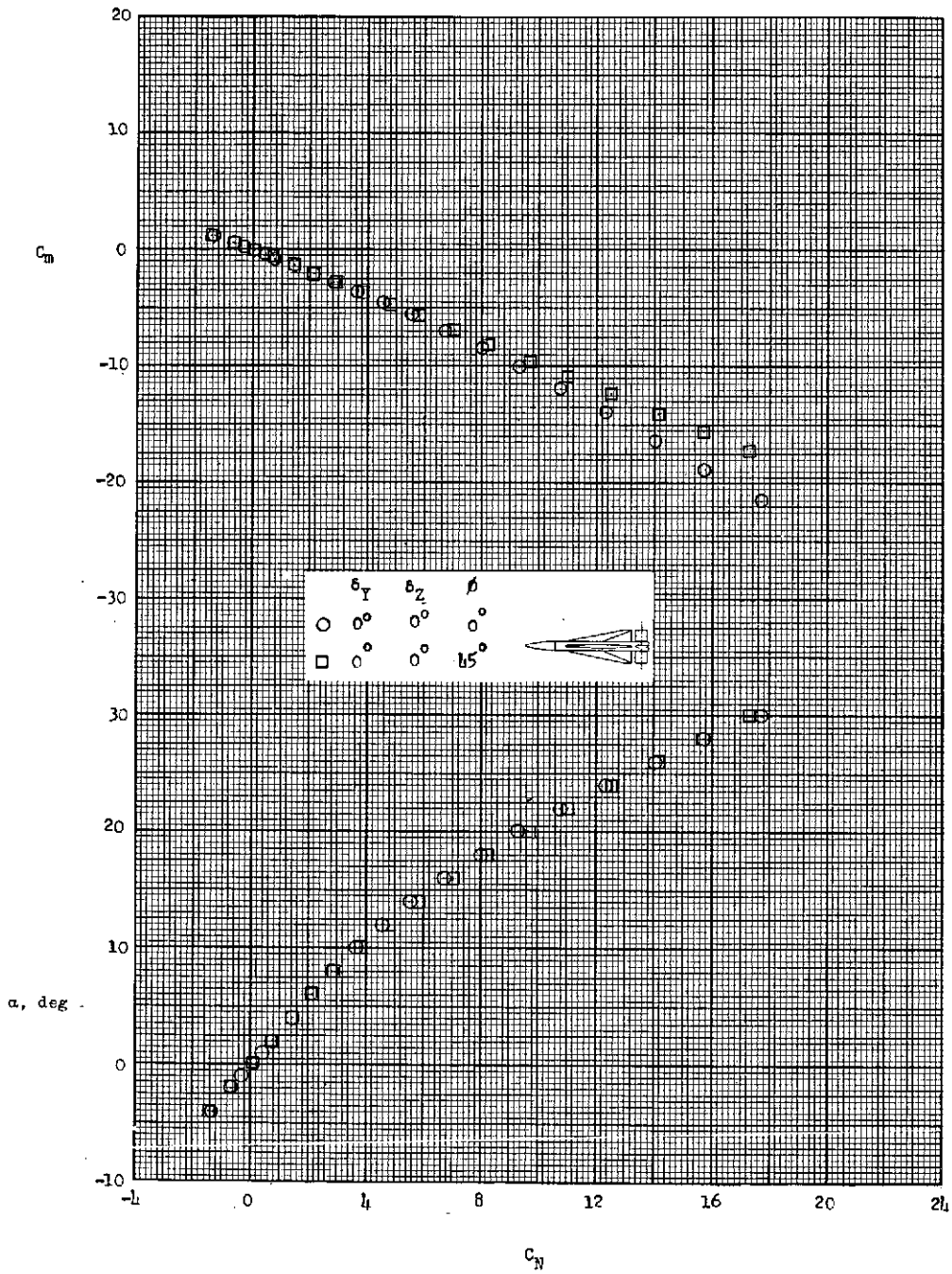

(b) Configuration I-1-1 with fins in rear position.

Figure 46.- Continued.

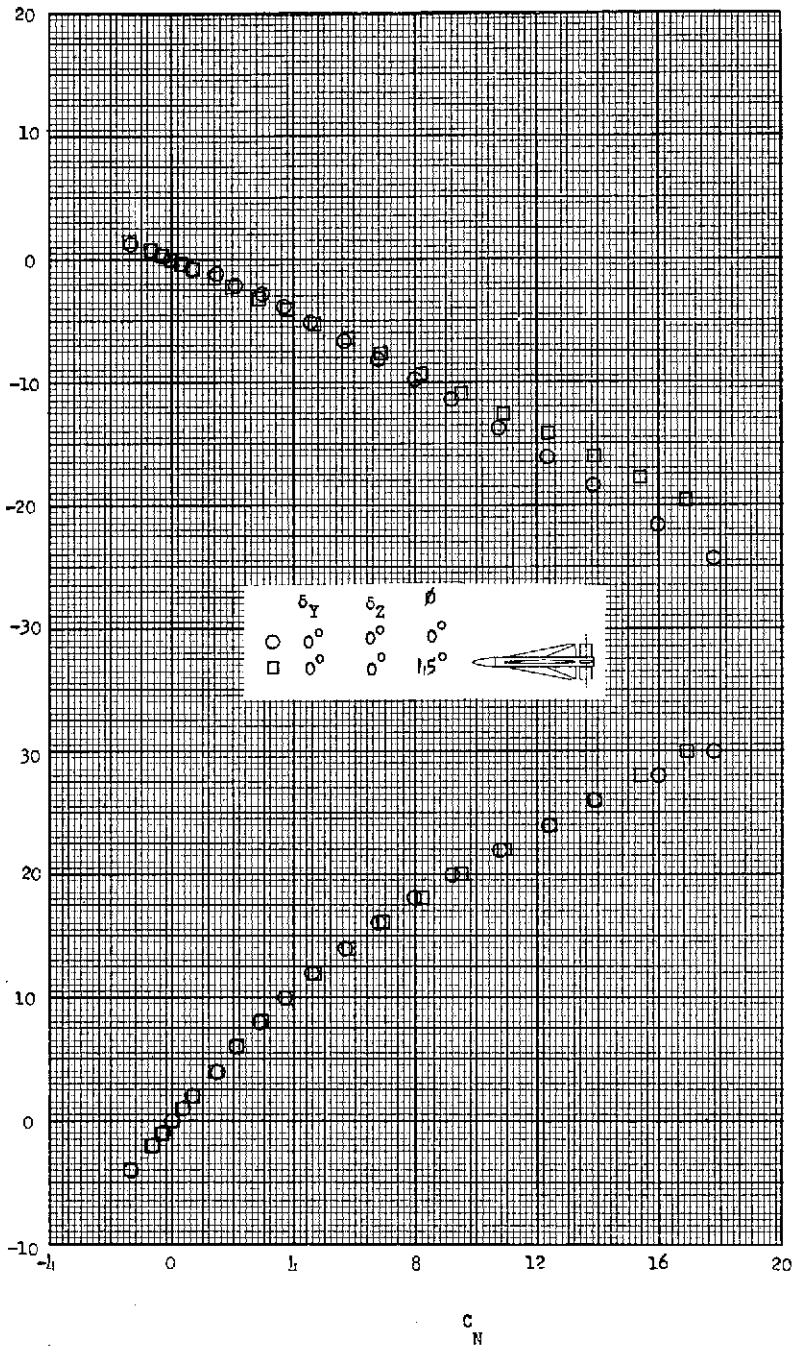

(c) Configuration II-1-1 with fins in rear position.

Figure 46.- Continued.

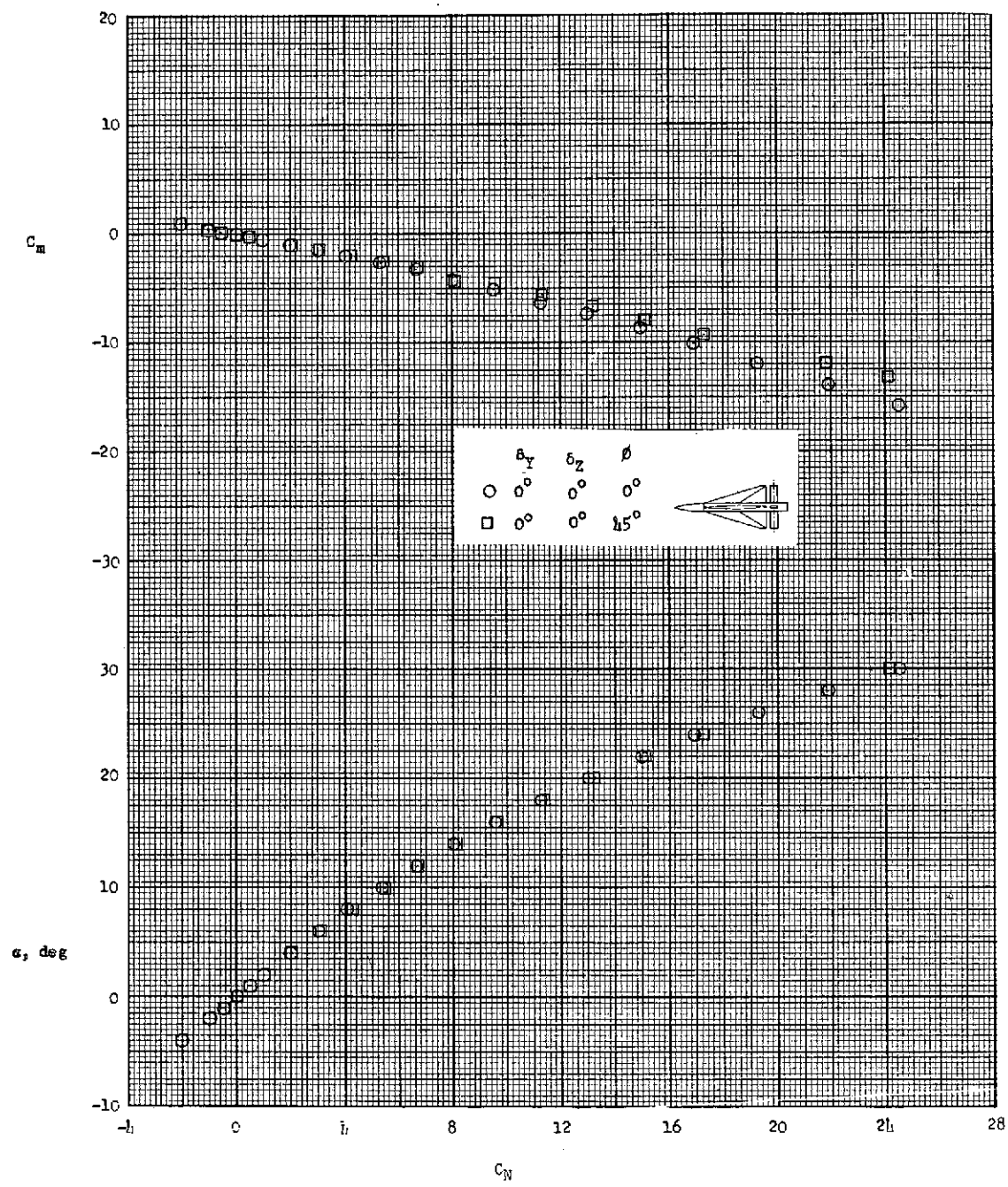

(d) Configuration I-2-4 with fins in forward position.

Figure 46.- Continued.

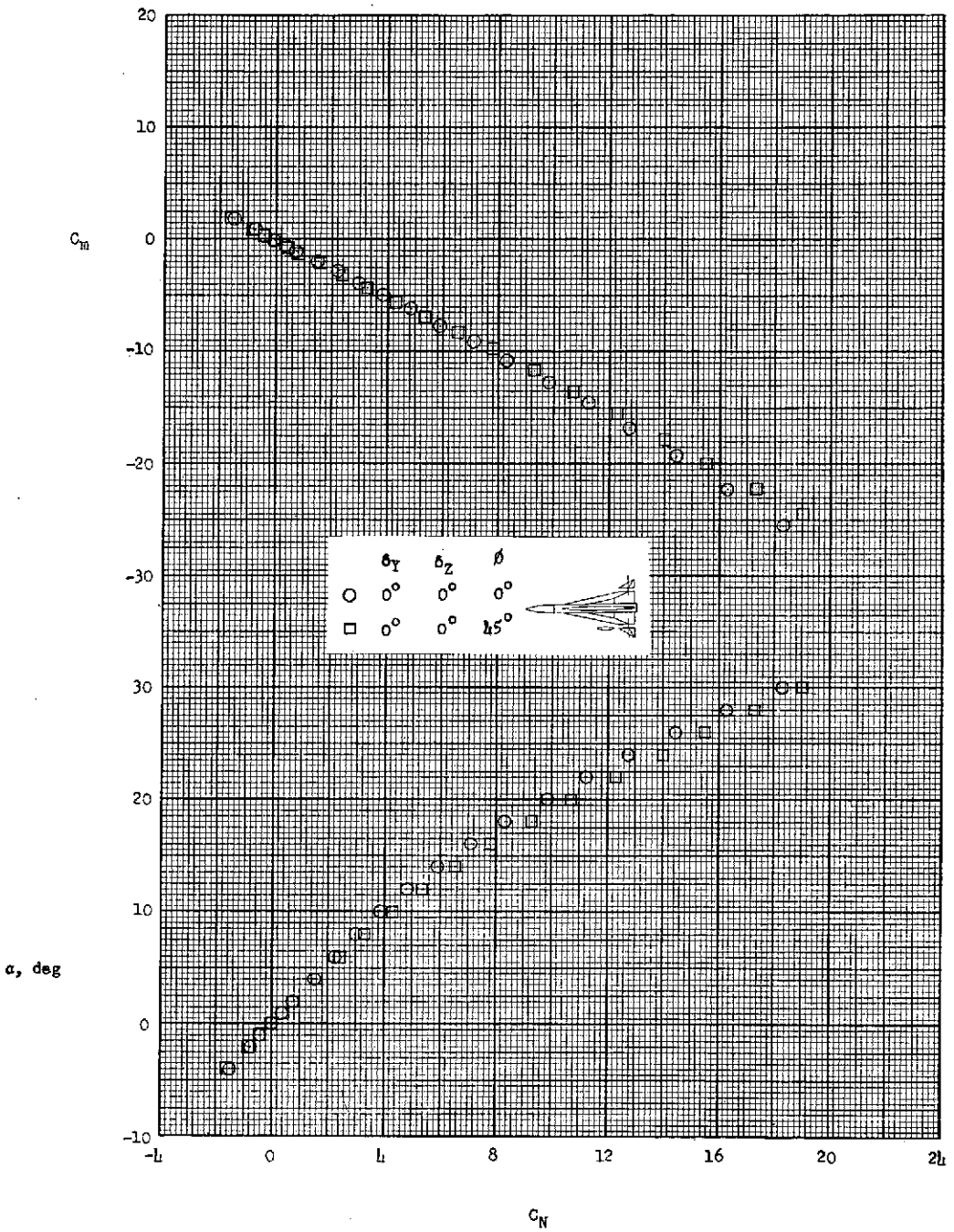

(e) Configuration I-4-5 with fins in rear position.

Figure 46.- Continued.

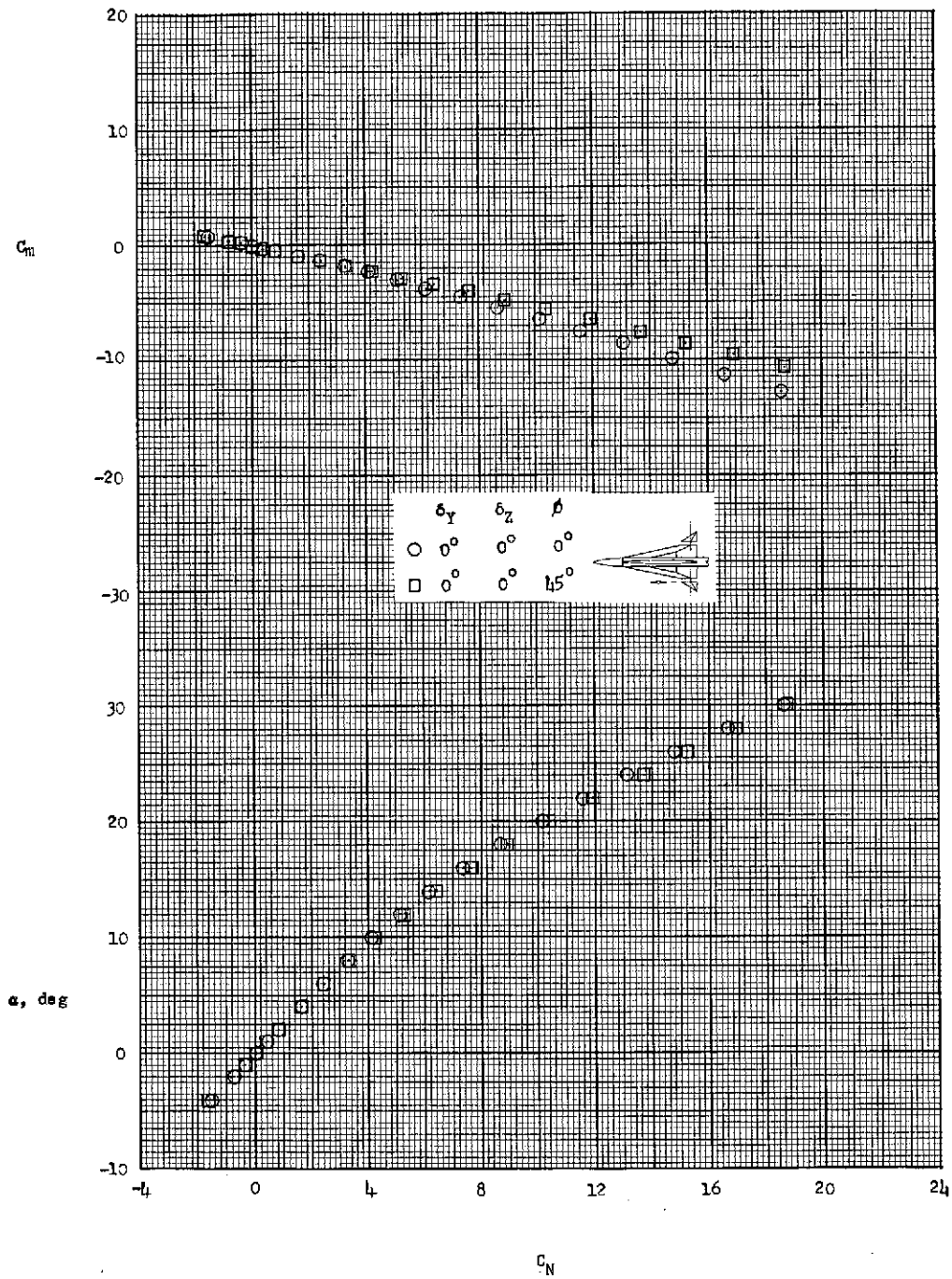

(f) Configuration I-4-5 with fins in forward position.

Figure 46.- Continued.

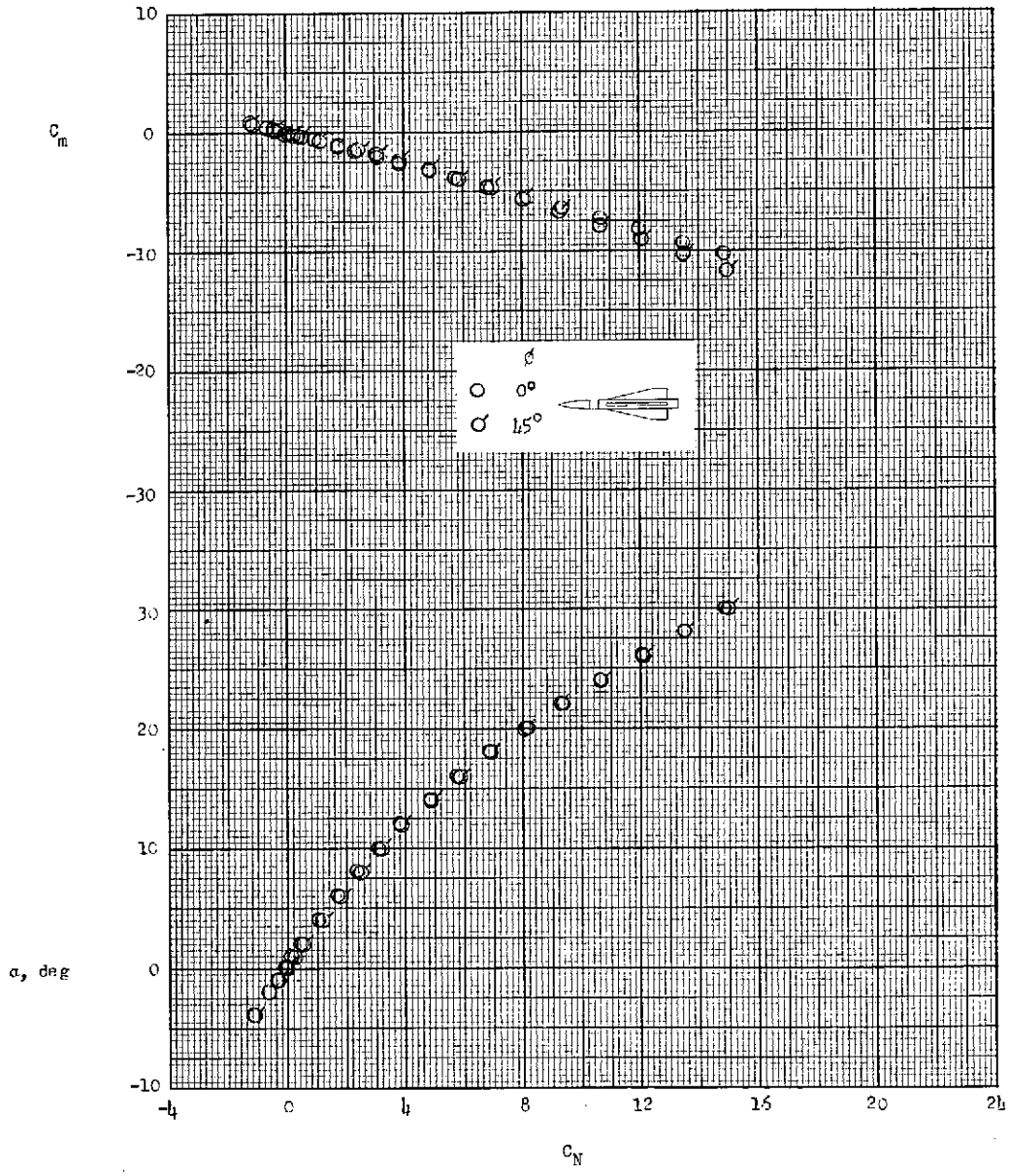

(g) Configuration I-6 with fins in rear position.

Figure 46.- Continued.

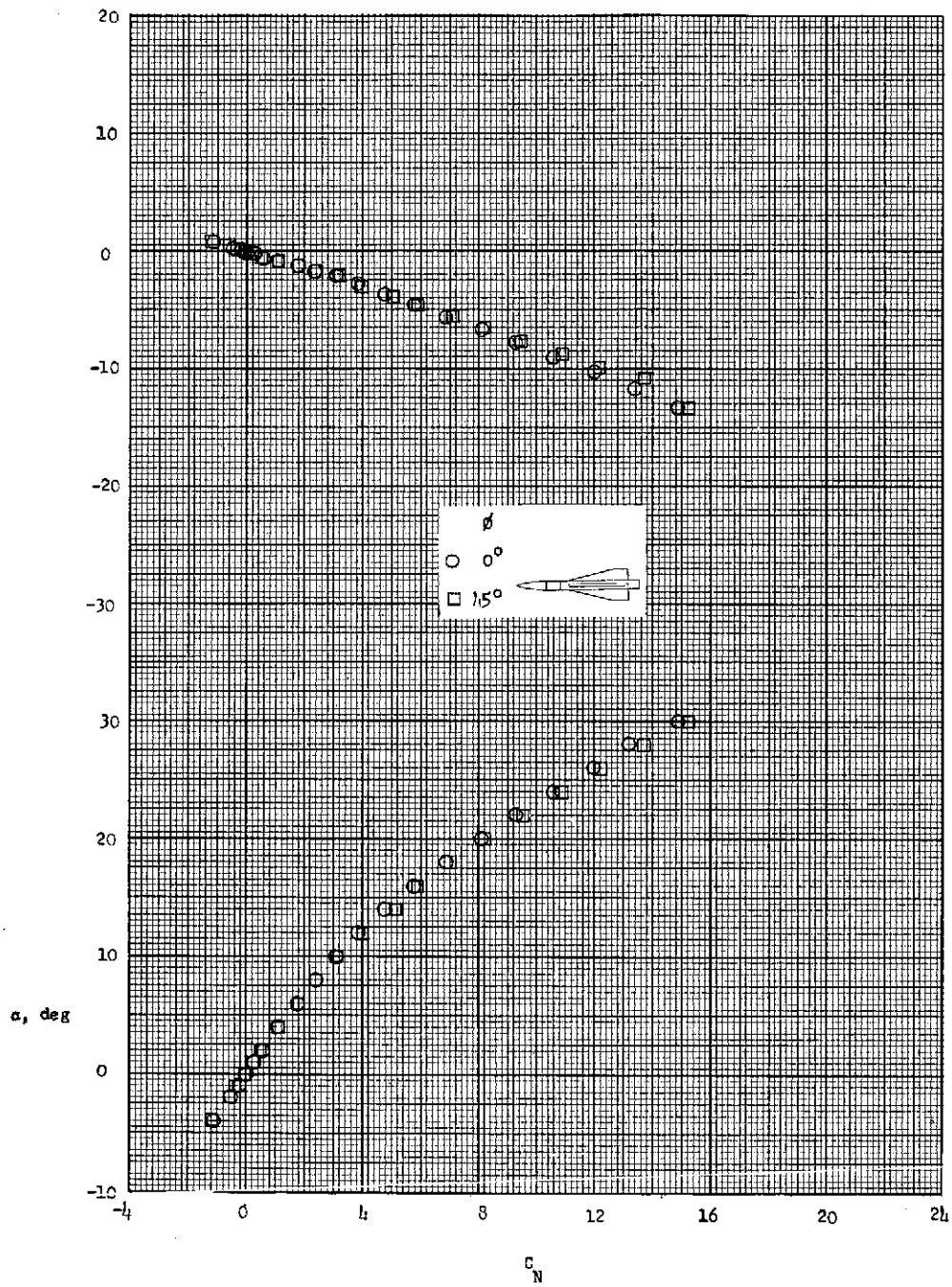

(h) Configuration III-6 with fins in rear position.

Figure 46.- Continued.

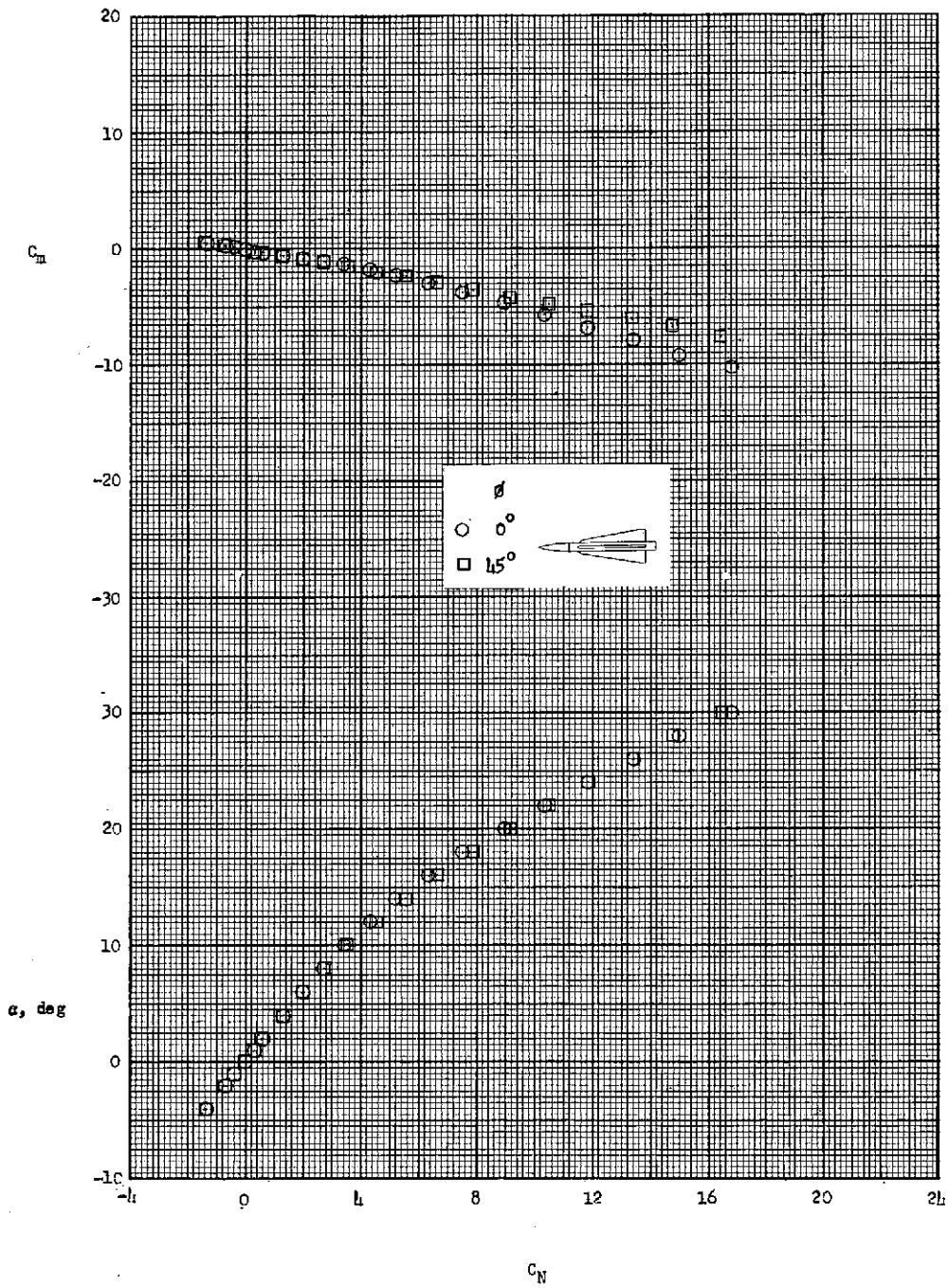

(i) Configuration I-8 with fins in rear position.

Figure 46.- Concluded.

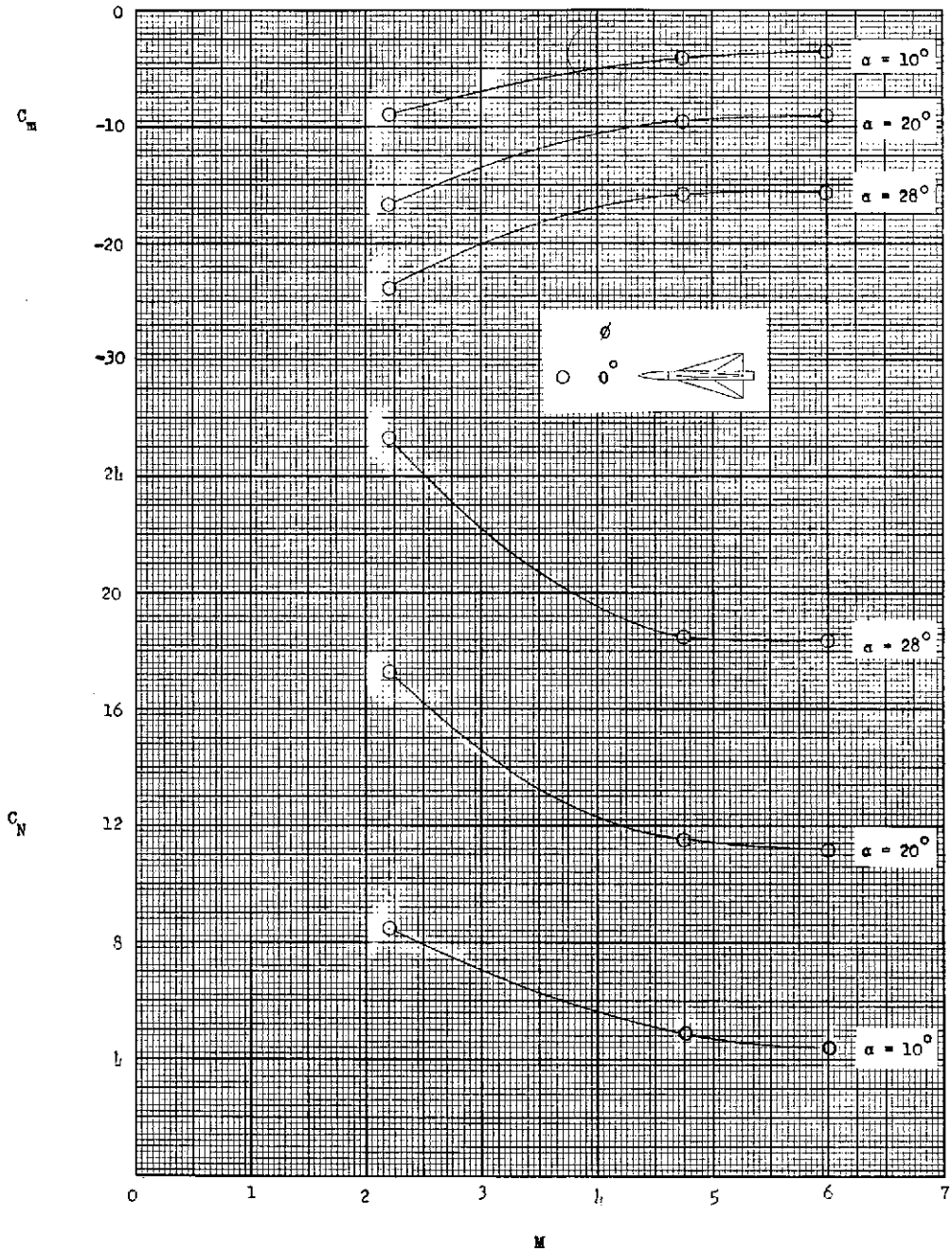

(a) Fins in rear position.

Figure 47.- Effect of Mach number. Variation of the aerodynamic characteristics of configuration I-2 with Mach number at roll angle of 0° and angles of attack of 10°, 20°, and 28°. Data at Mach numbers 2.21 and 4.76 are from unpublished Jet Propulsion Laboratory tests.

L-65-1

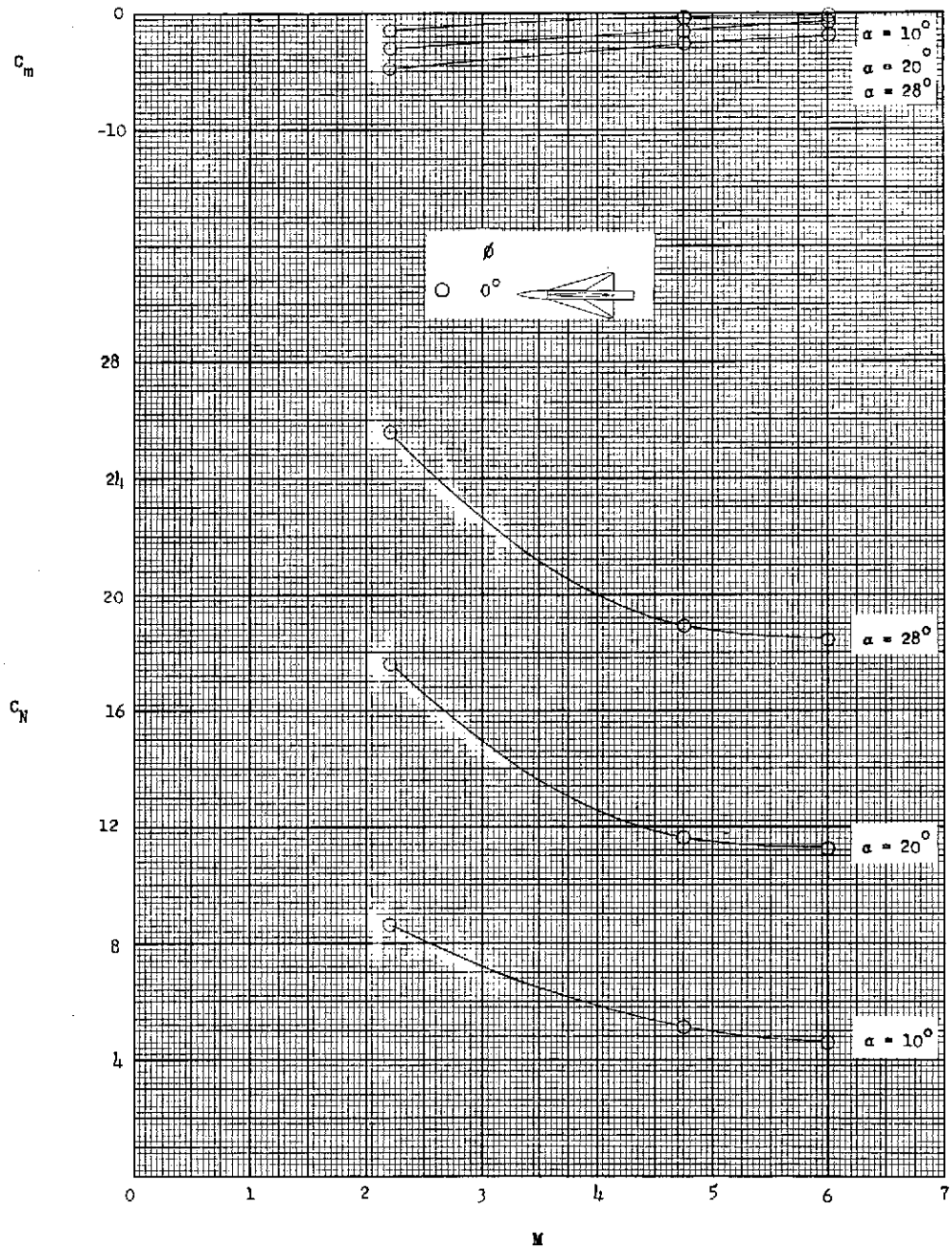

(b) Fins in forward position.

Figure 47.- Concluded.

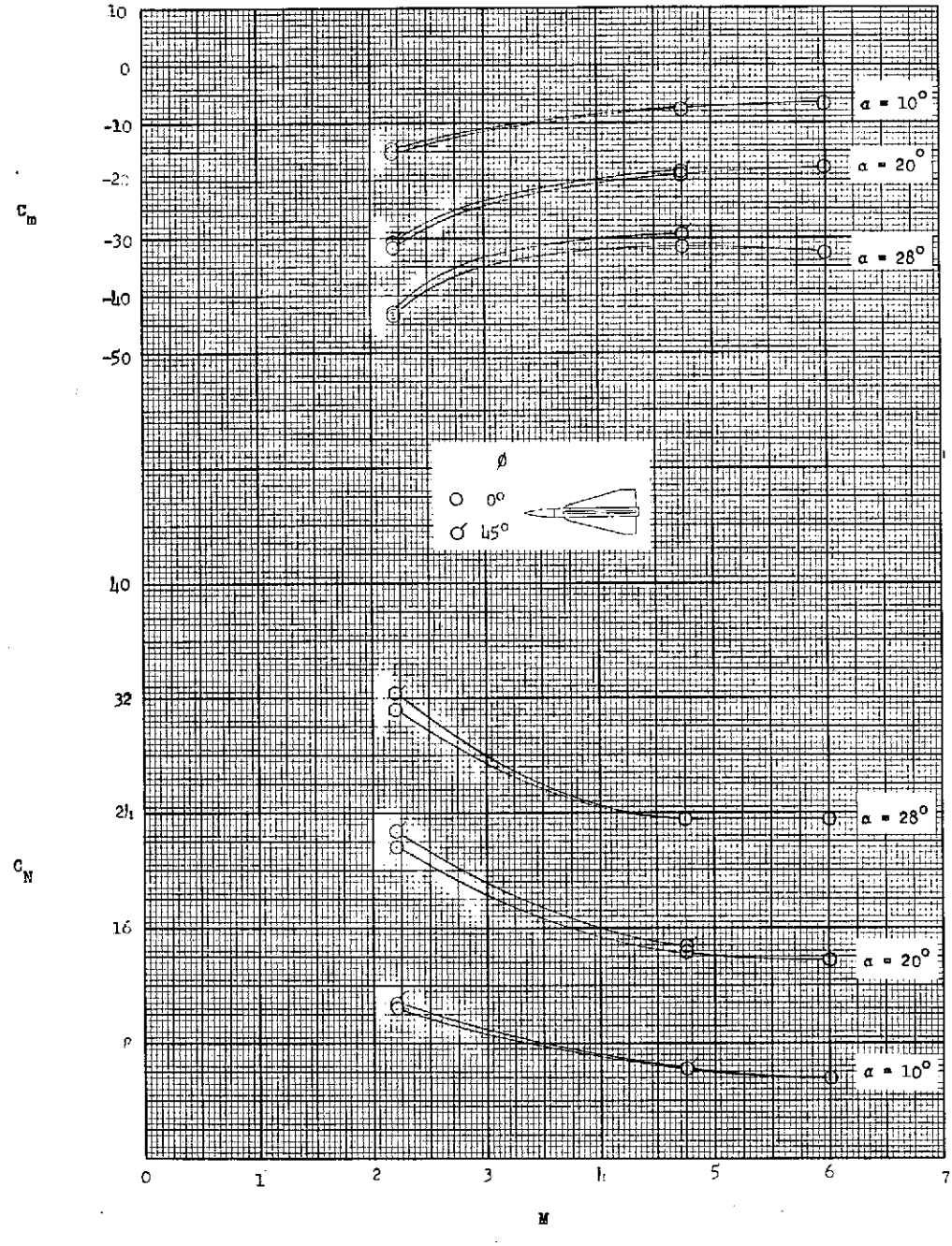

(a) Fins in rear position.

Figure 48.- Effect of Mach number. Variation of the aerodynamic characteristics of configuration I-9 with Mach number at roll angles of 0° and 45° and angles of attack of 10°, 20°, and 28°. Data at Mach numbers 2.21 and 4.76 are from unpublished Jet Propulsion Laboratory tests.

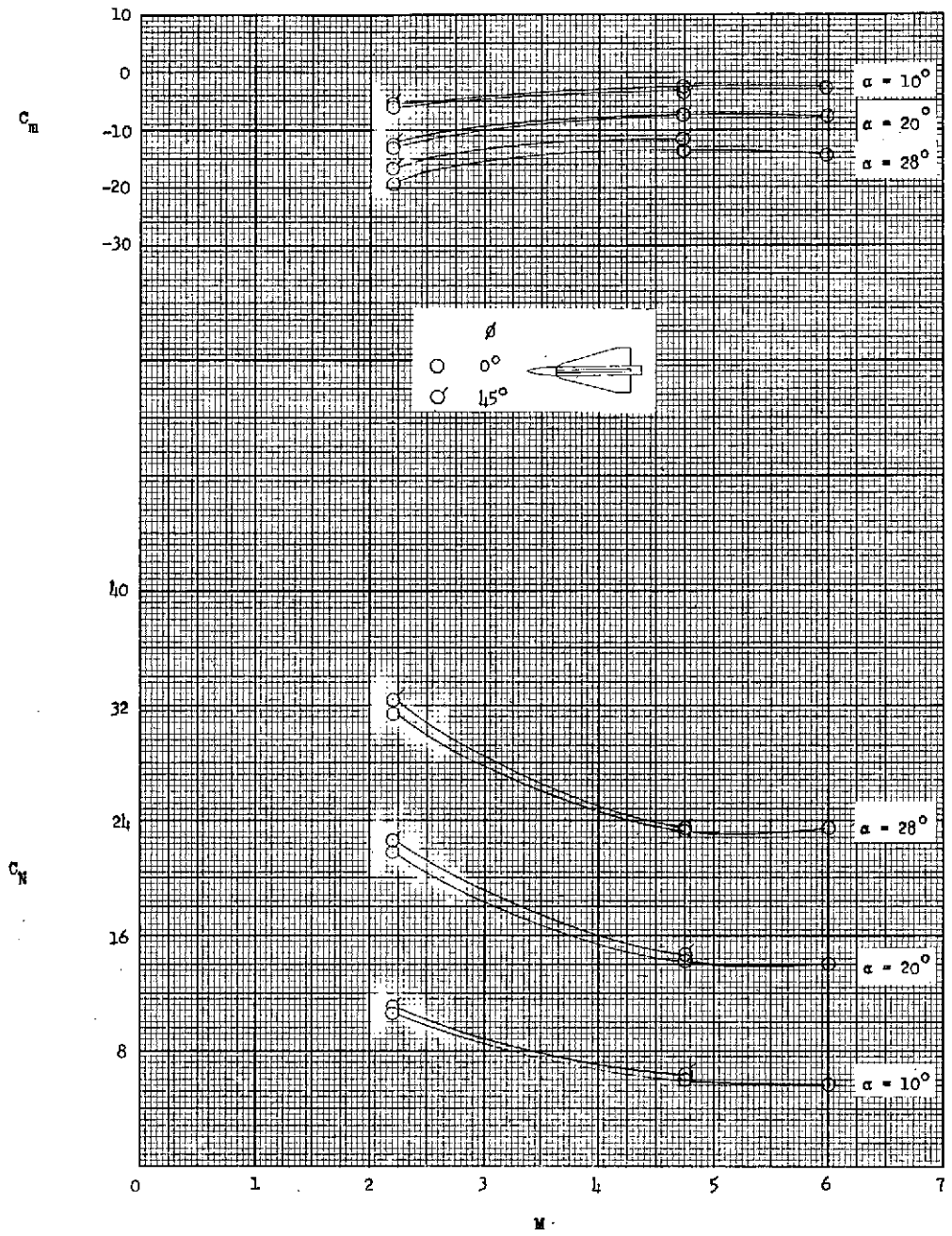

(b) Fins in forward position.

Figure 48.- Concluded.

L-837

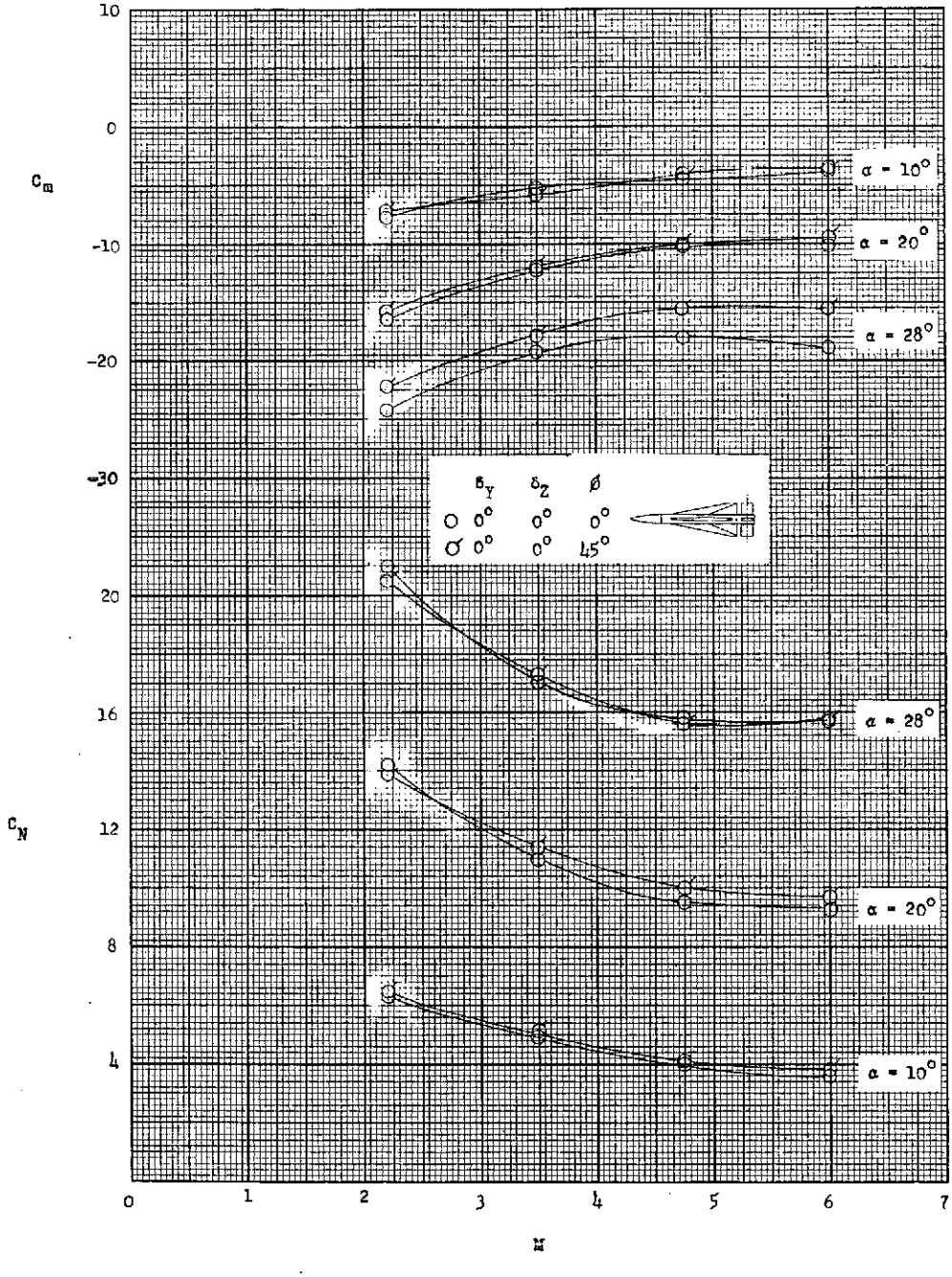

(a) Fins in rear position.

Figure 49.- Effect of Mach number. Variation of the aerodynamic characteristics of configuration I-1-1 with Mach number at roll angles of 0° and 45° and angles of attack of 10°, 20°, and 28°. Data at Mach numbers 2.21, 3.50, and 4.76 are from unpublished Jet Propulsion Laboratory tests.

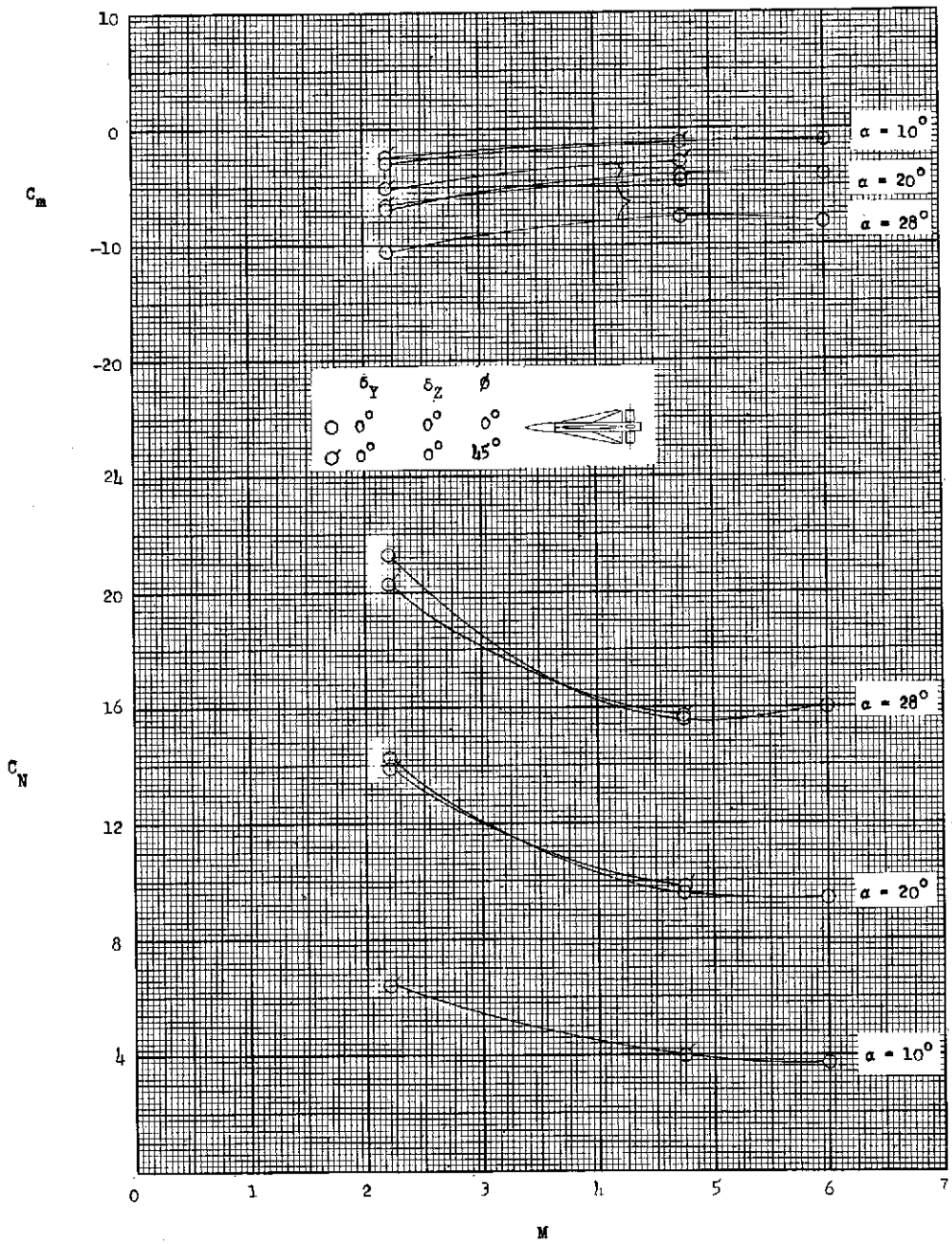

(b) Fins in forward position.

Figure 49.- Concluded.

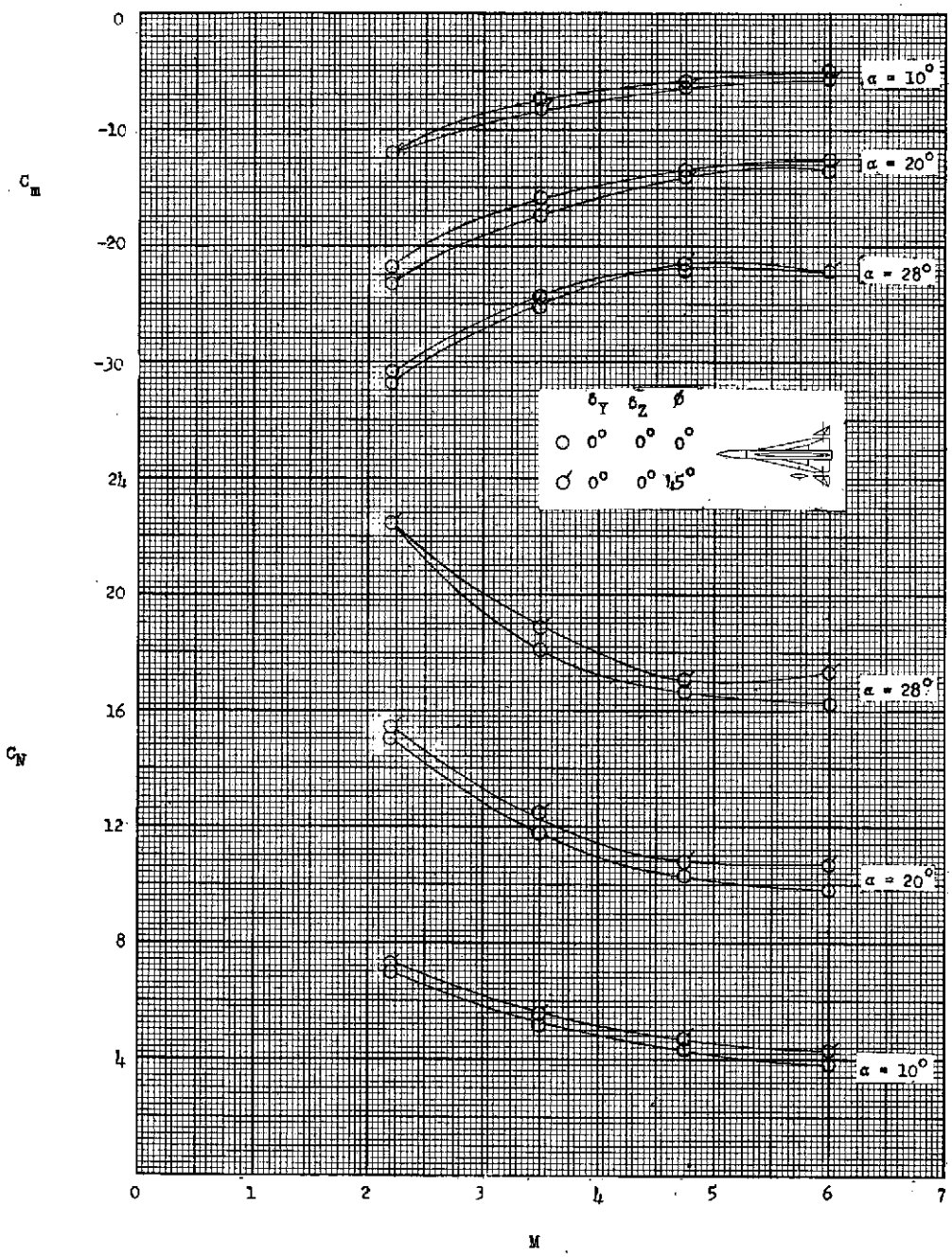

(a) Fins in rear position.

Figure 50.- Effect of Mach number. Variation of the aerodynamic characteristics of configuration I-4-5 with Mach number at roll angles of 0° and 45° and angles of attack of 10°, 20°, and 28°. Data at Mach numbers 2.21, 3.50, and 4.76 are from unpublished Jet Propulsion Laboratory tests.

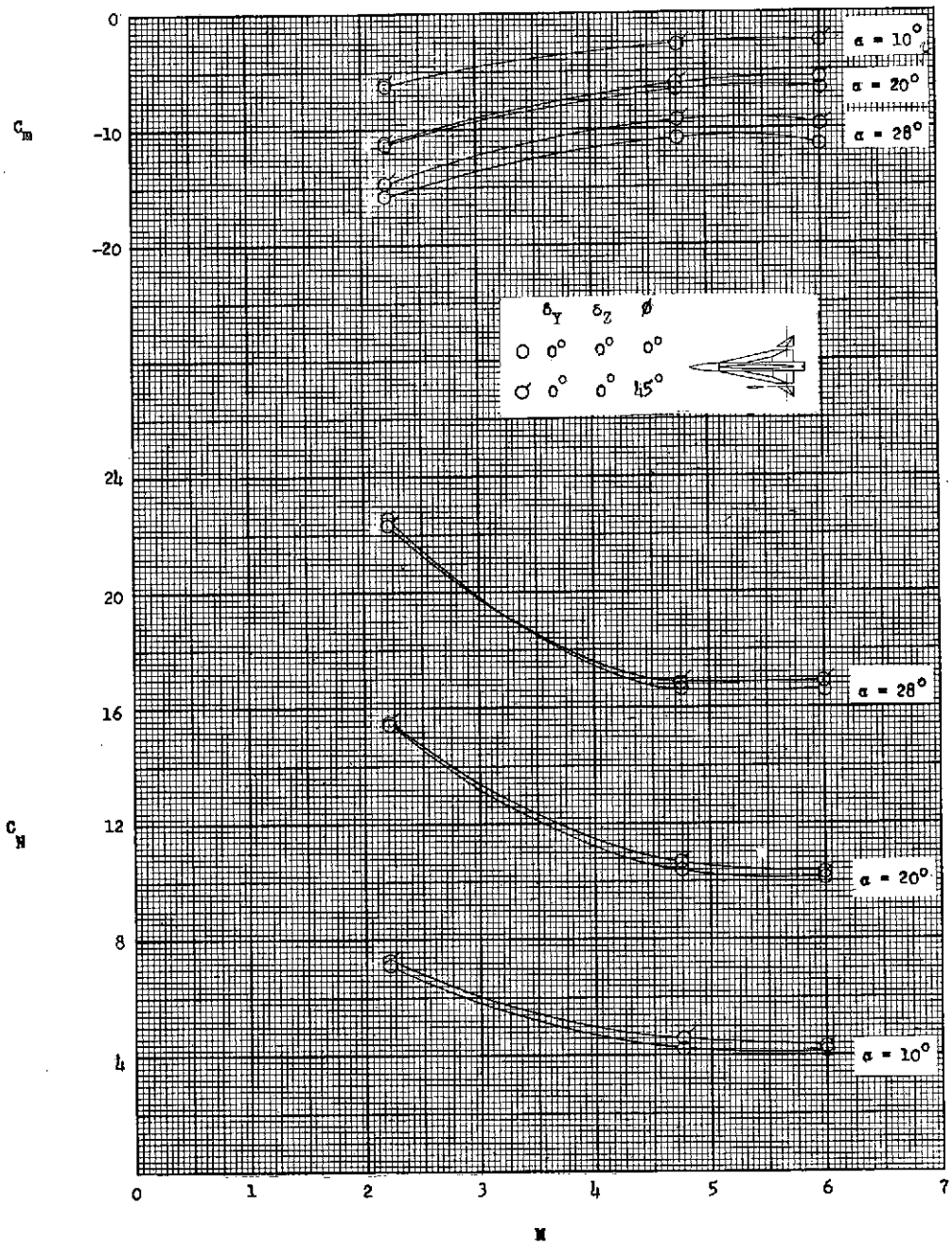

(b) Fins in forward position.

Figure 50.- Concluded.

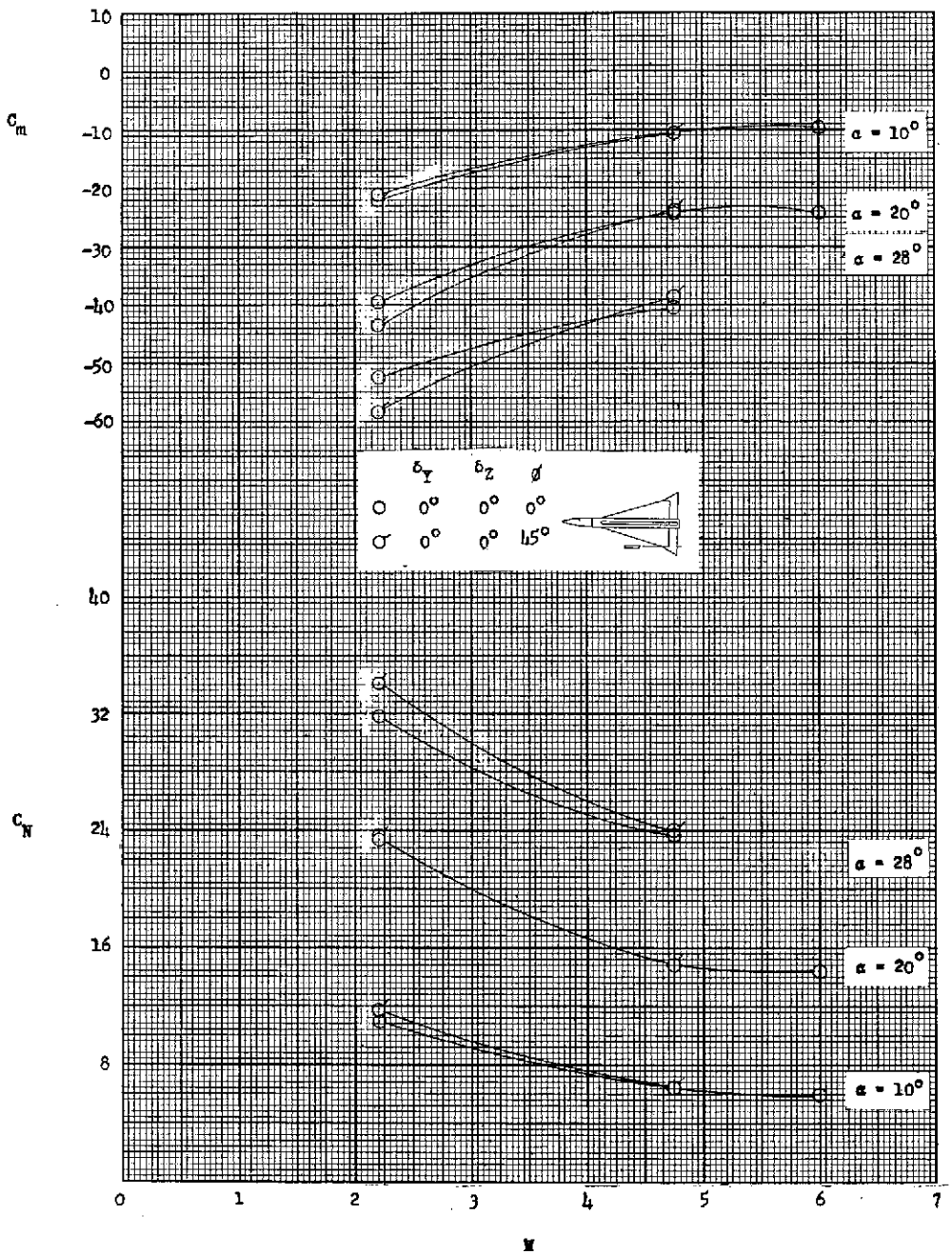

(a) Fins in rear position.

Figure 51.- Effect of Mach number. Variation of the aerodynamic characteristics of configuration I-3-7 with Mach number at roll angles of 0° and 45° and angles of attack of 10°, 20°, and 28°. Data at Mach numbers 2.21 and 4.76 are from unpublished Jet Propulsion Laboratory tests.

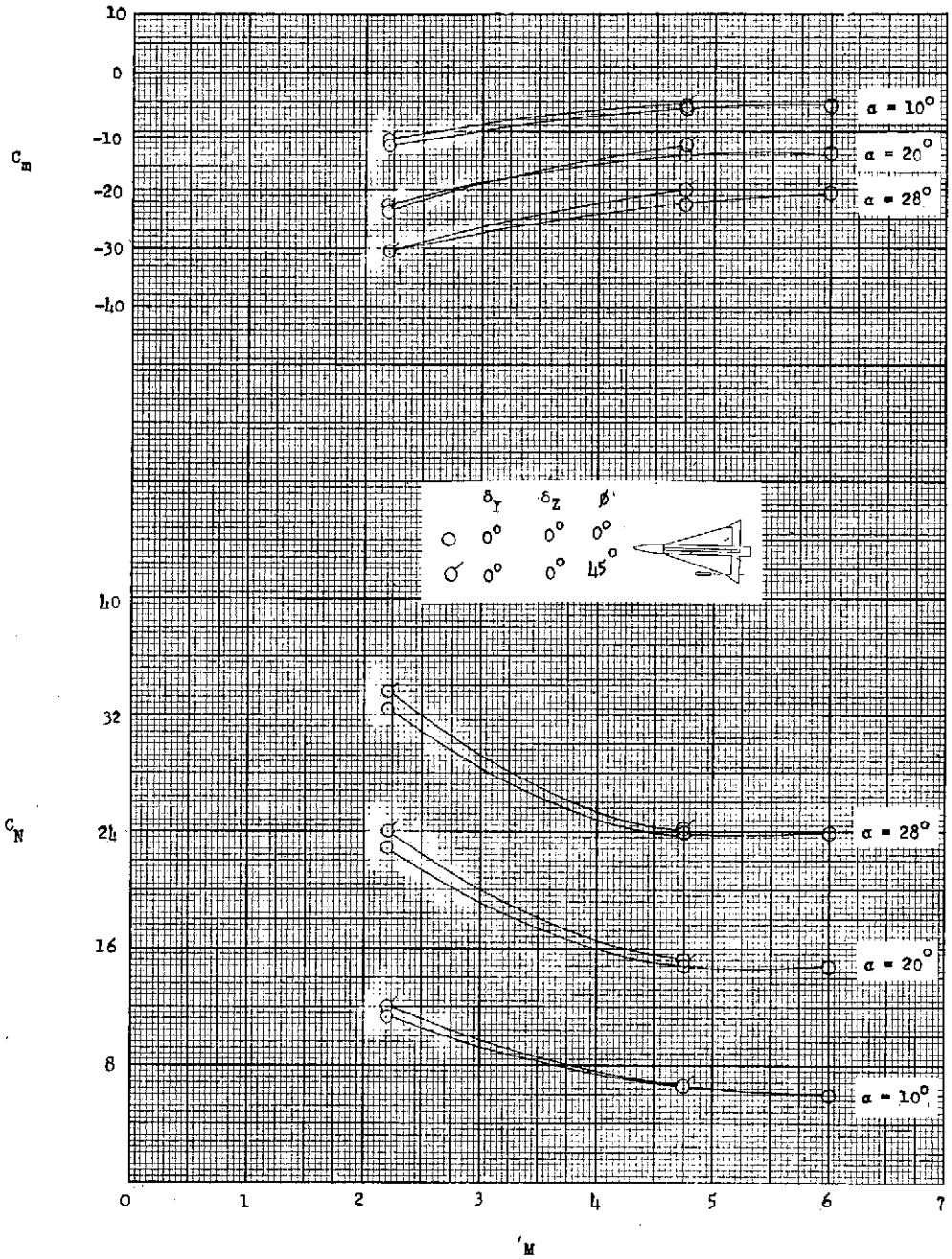

(b) Fins in forward position.

Figure 51.- Concluded.

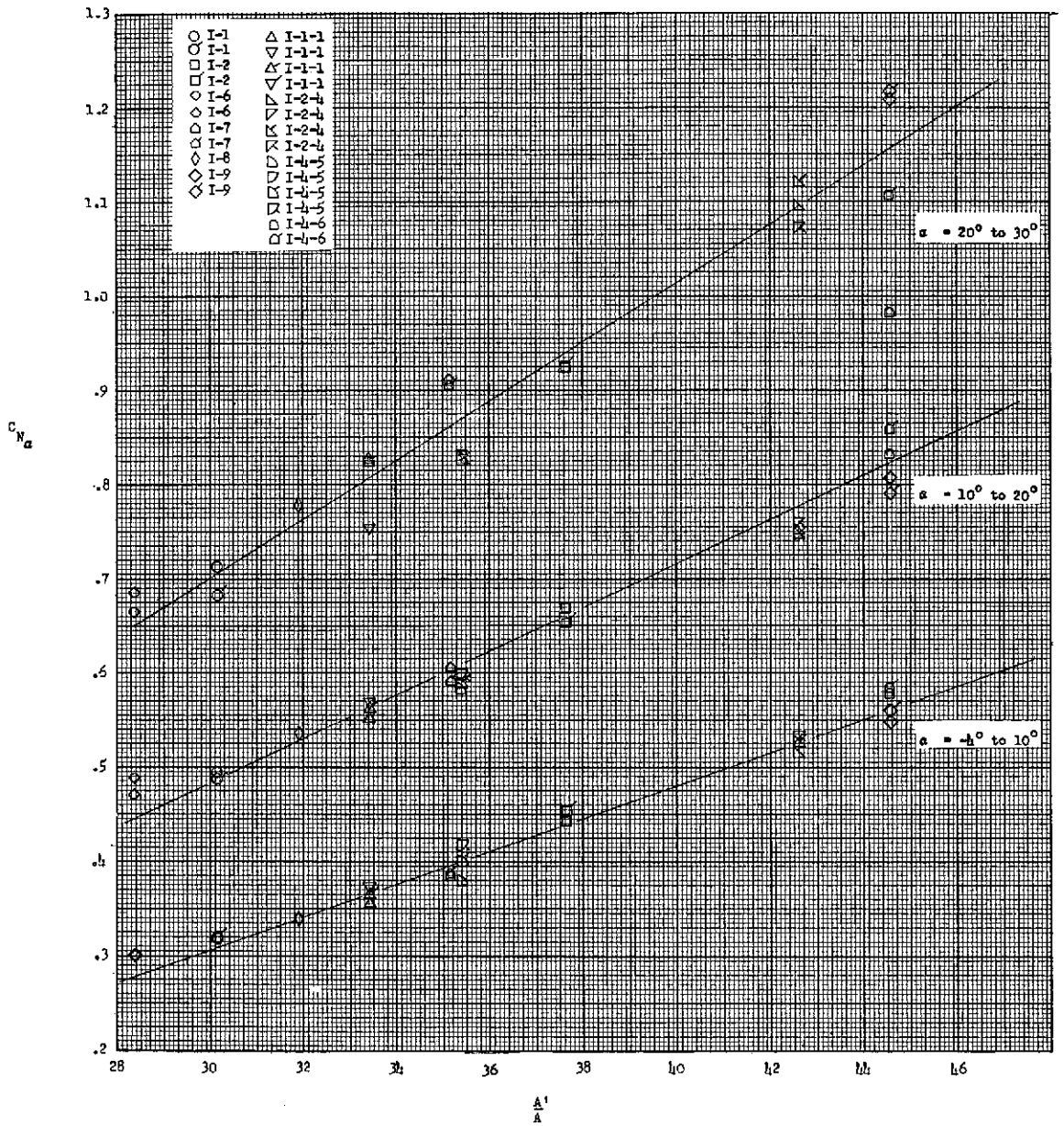

(a) M = 6.01.

Figure 52.- Correlation of slope of the normal-force curve with planform area. Variation of C_{N_α} with planform area in the angle-of-attack ranges -4° to 10°, 10° to 20°, and 20° to 30° for the majority of the test configurations. Inverted symbols indicate a roll angle of 45° and flagged symbols indicate the fins are in the forward position. Data at Mach numbers 2.21 and 4.76 are from unpublished Jet Propulsion Laboratory tests.

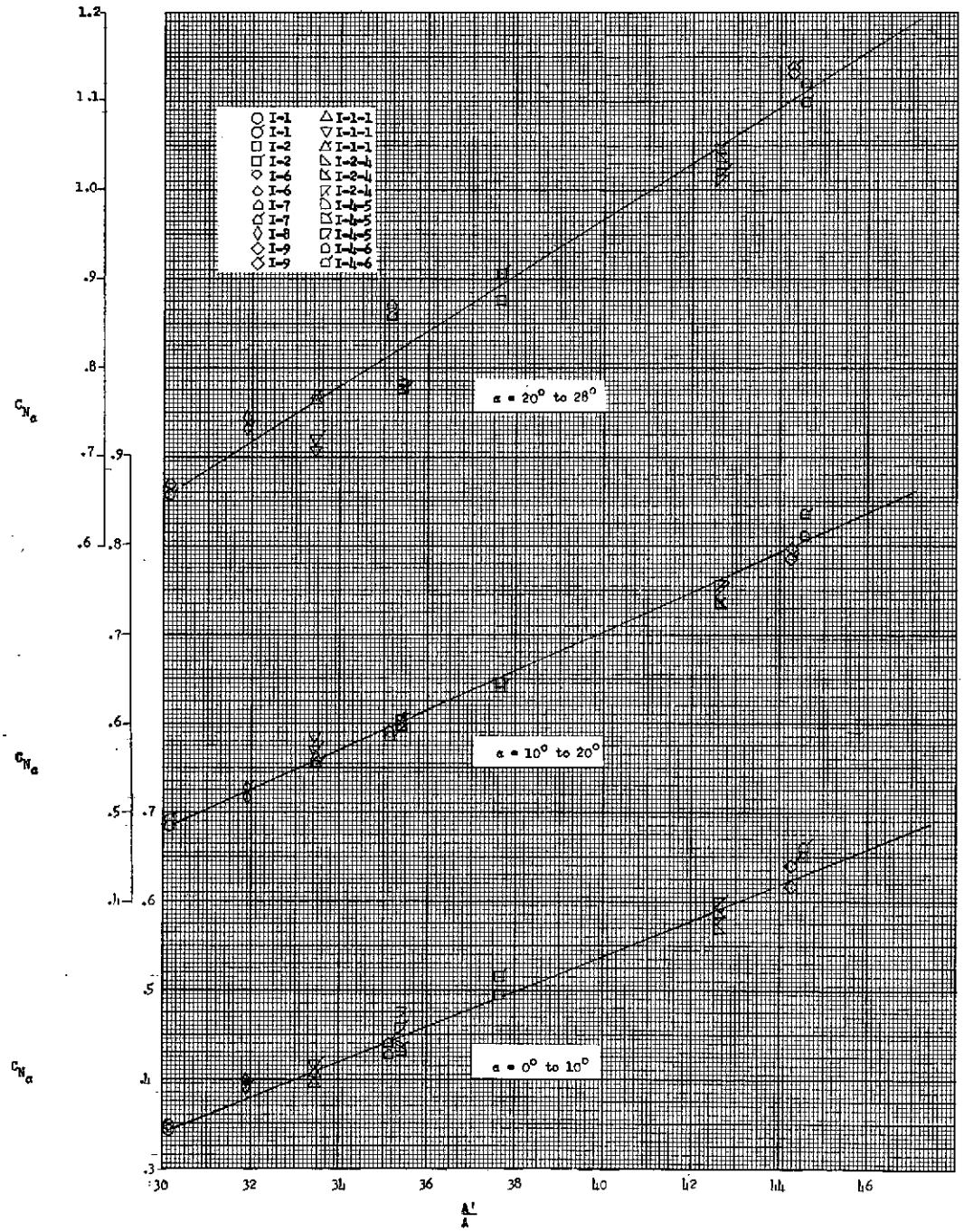

(b) M = 4.76.

Figure 52.- Continued.

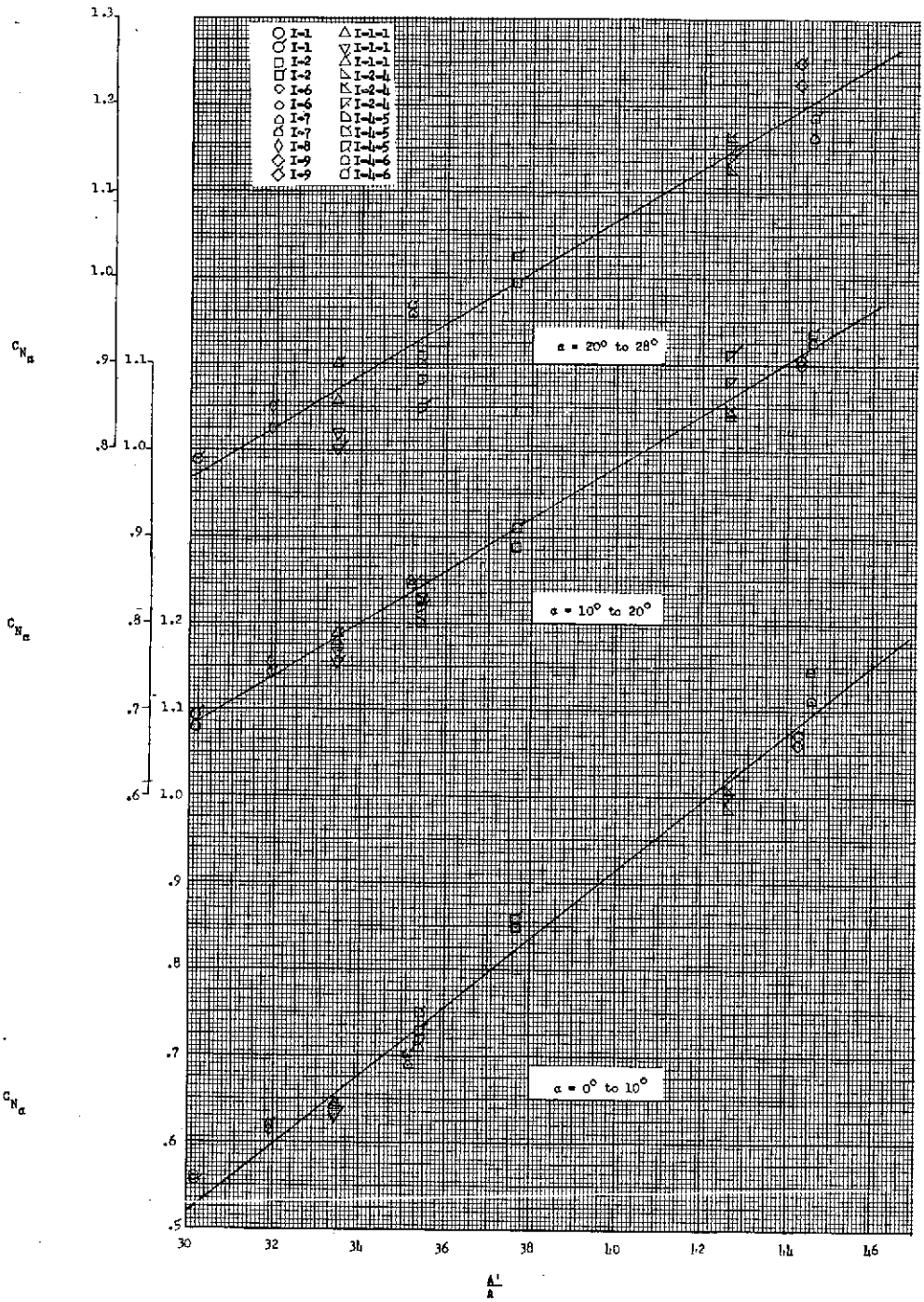

(c) M = 2.21.

Figure 52.- Concluded.

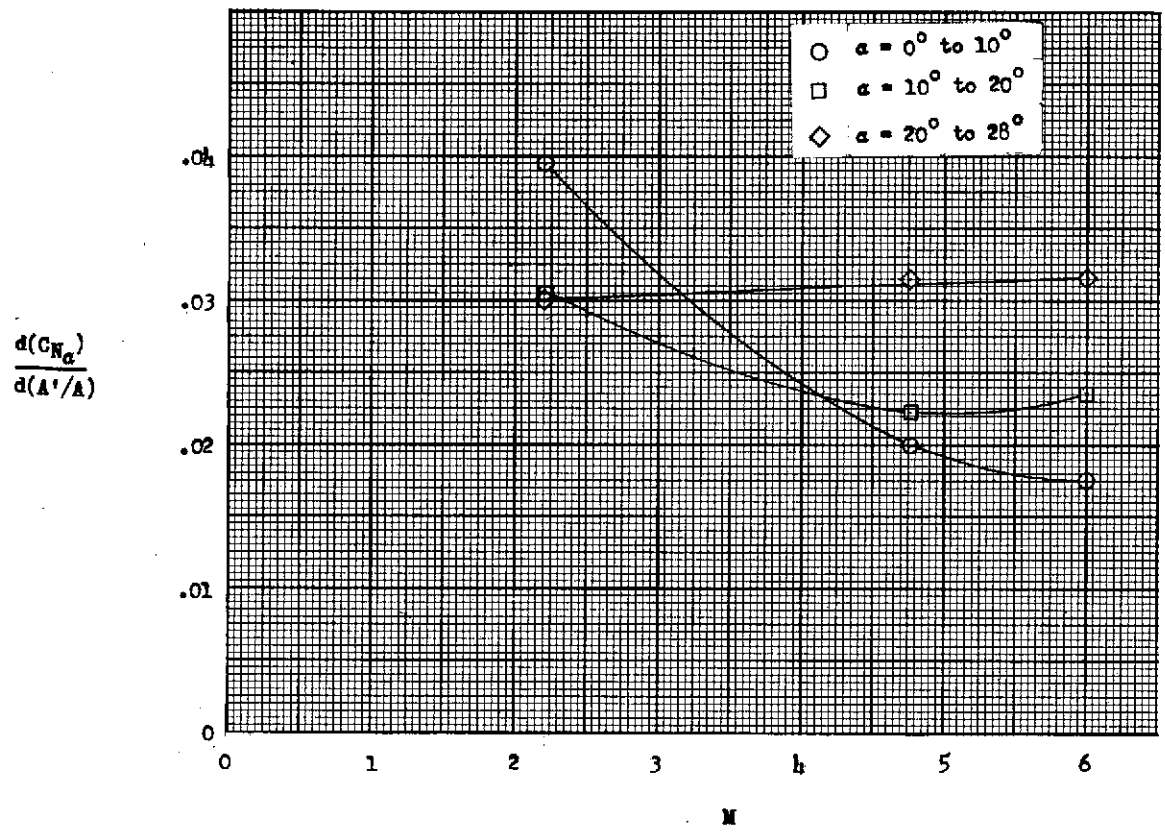

Figure 53.- Variation of the parameter $\frac{dC_{N_\alpha}}{d(A'/A)}$ for the angle-of-attack ranges of 0° to 10°, 10° to 20°, and 20° to 28°. Data at Mach numbers 2.21 and 4.76 are from unpublished Jet Propulsion Laboratory tests.

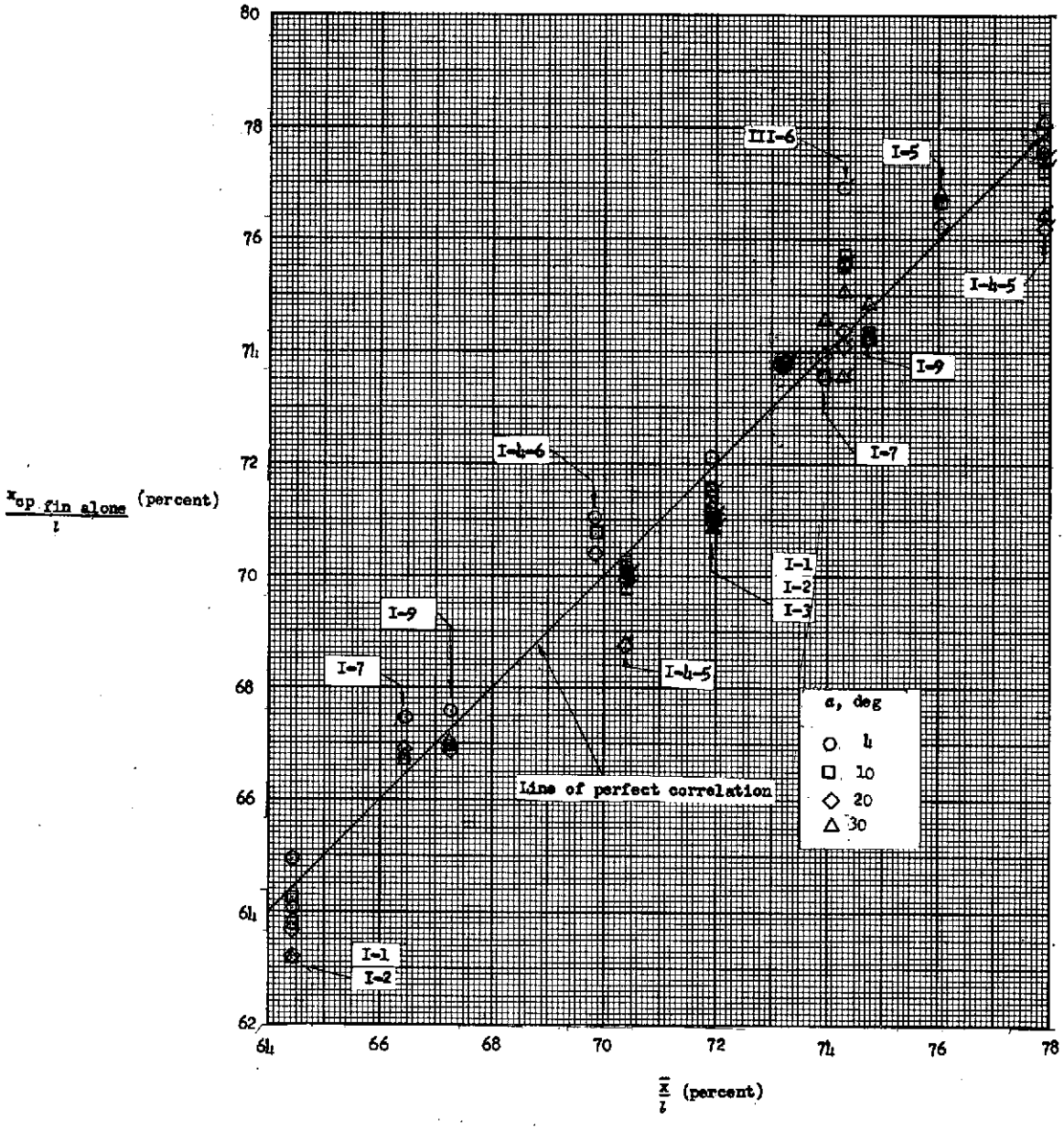

(a) M = 6.01.

Figure 54.- Variation of the center-of-pressure location of the fin with the centroid-of-area location of the fins for the majority of the test configurations at angles of attack of 4°, 10°, 20°, and 30°. Flagged symbols indicate roll angle of 45°. Data at Mach numbers 2.21 and 4.76 are from unpublished Jet Propulsion Laboratory tests.

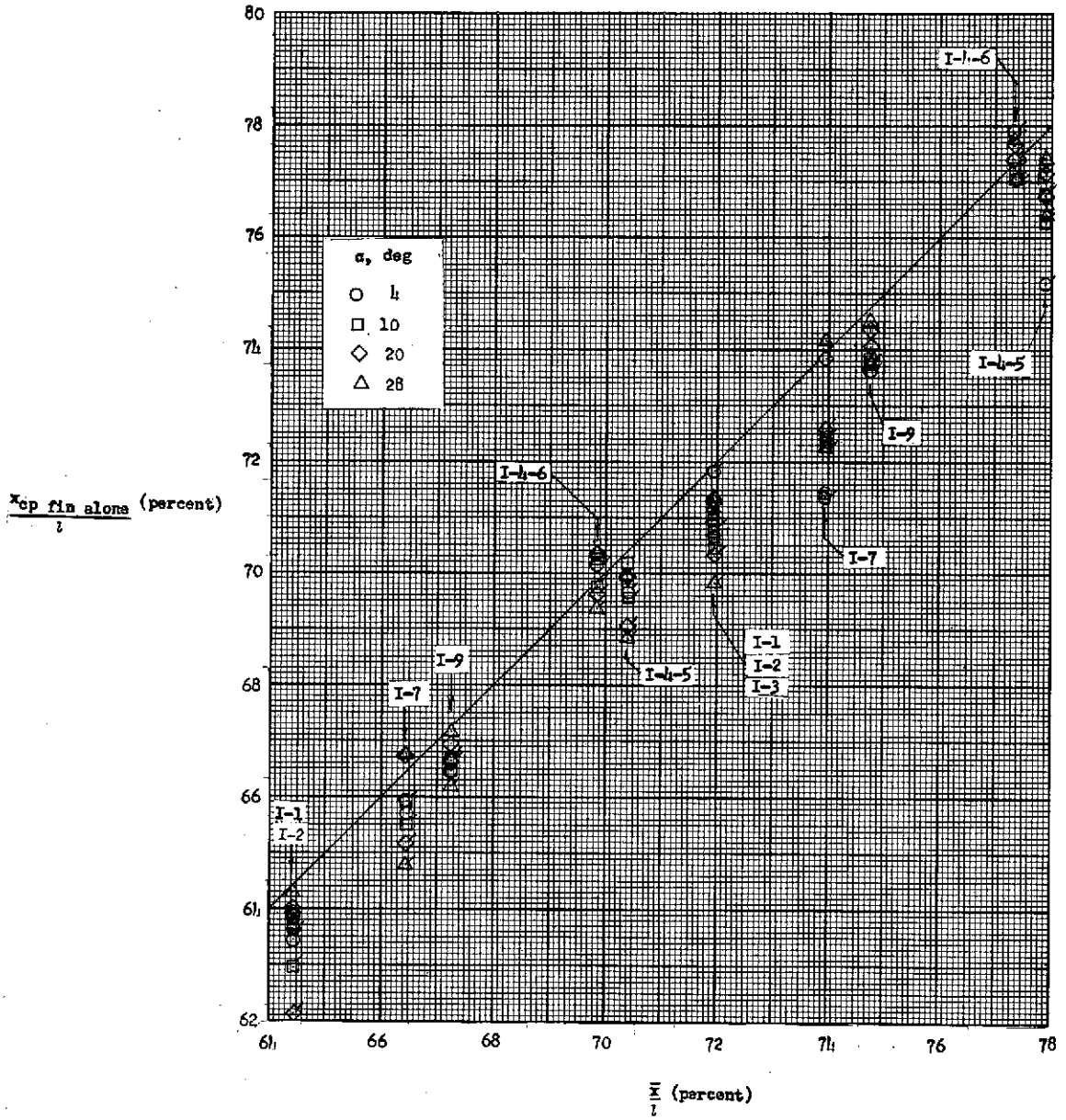

(b) M = 4.76.

Figure 54.- Continued.

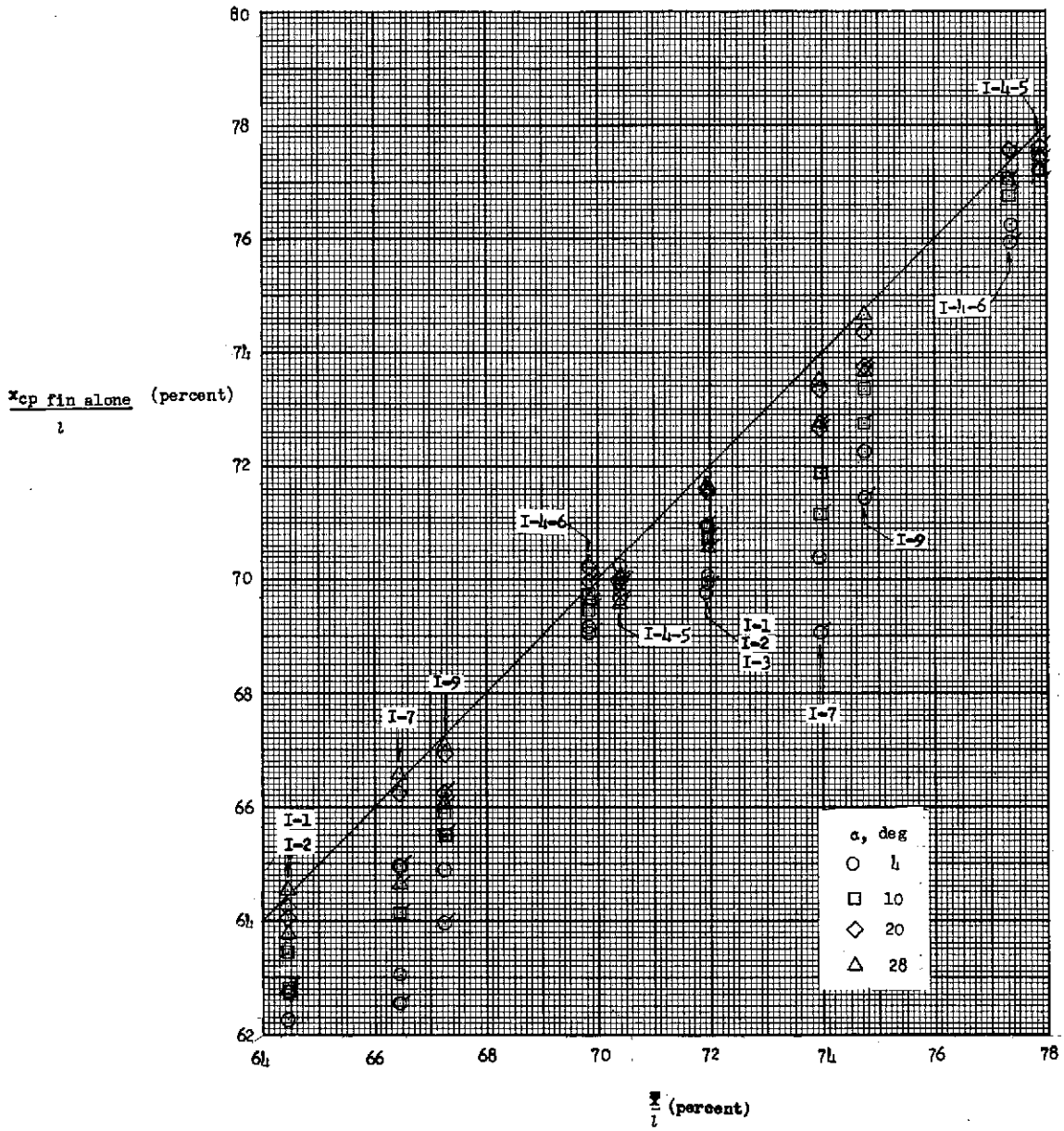

(c) M = 2.21.

Figure 54.- Concluded.

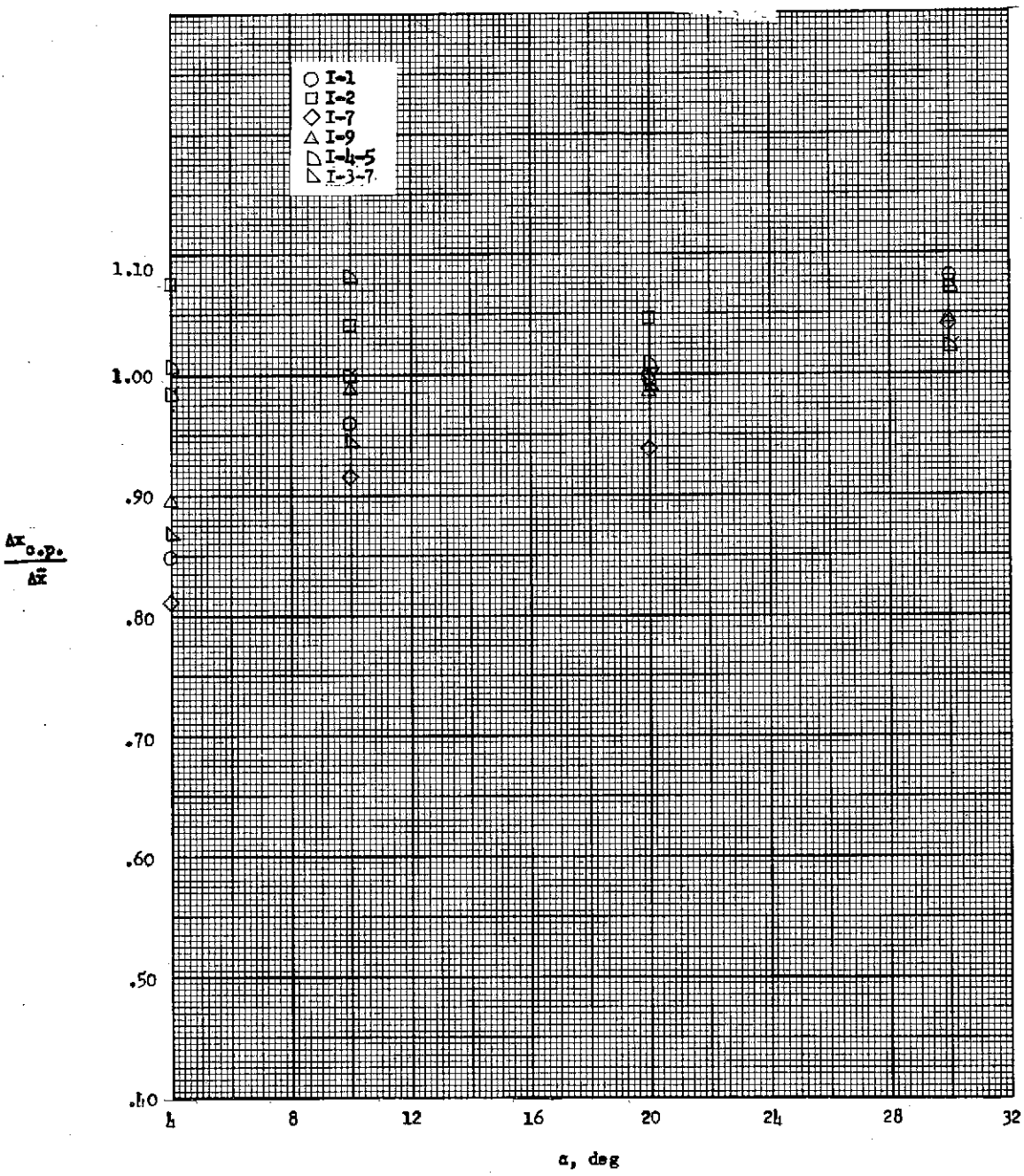

(a) M = 6.01.

Figure 55.- Correlation of fin center-of-pressure movement with fin longitudinal movement. Variation, with angle of attack, of the ratio of the fin center-of-pressure movement to the fin centroid-of-area movement for representative configurations. Flagged symbols indicate roll angle of 45°. Data at Mach numbers 2.21 and 4.76 are from unpublished Jet Propulsion Laboratory tests.

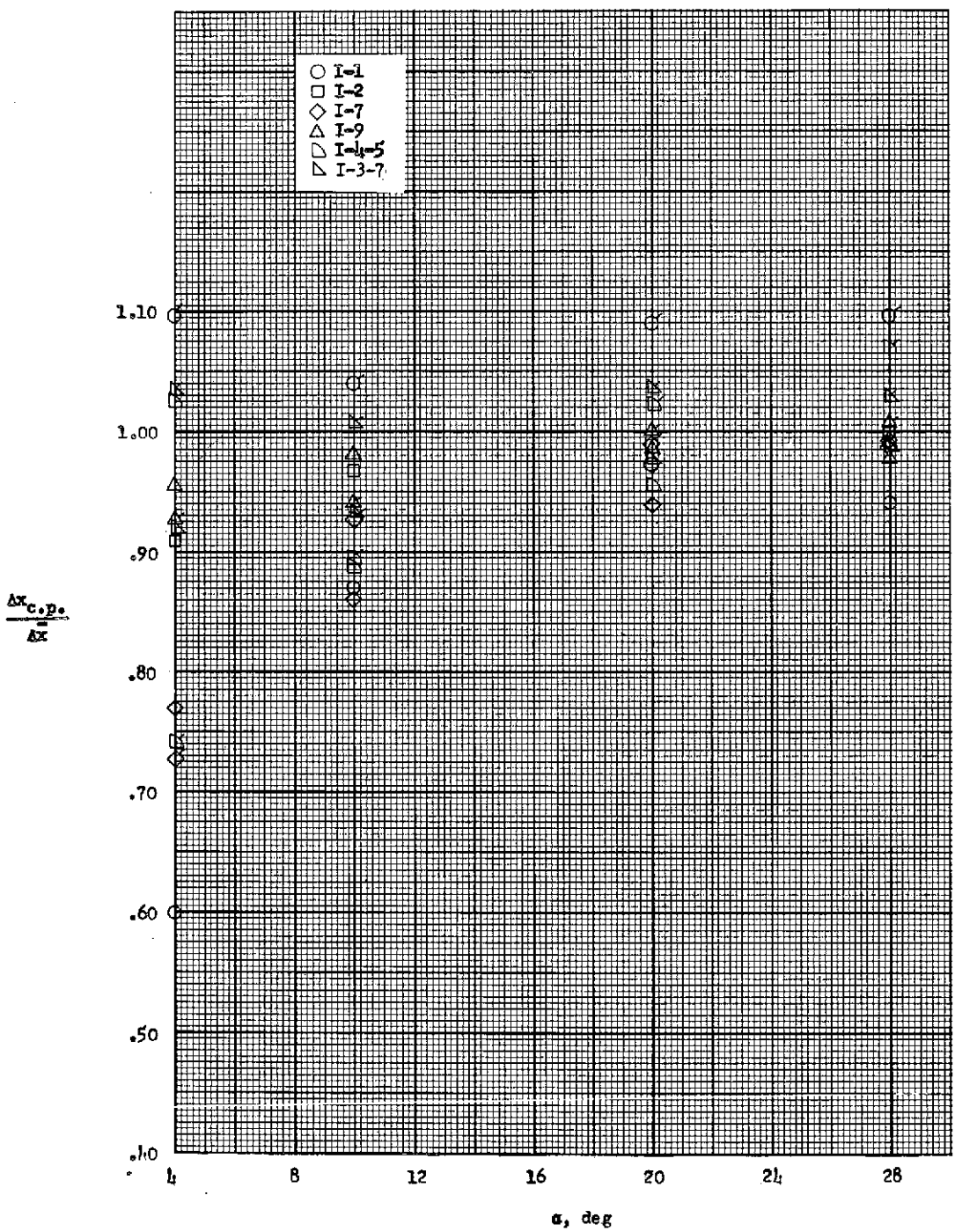

(b) M = 4.76.

Figure 55.- Continued.

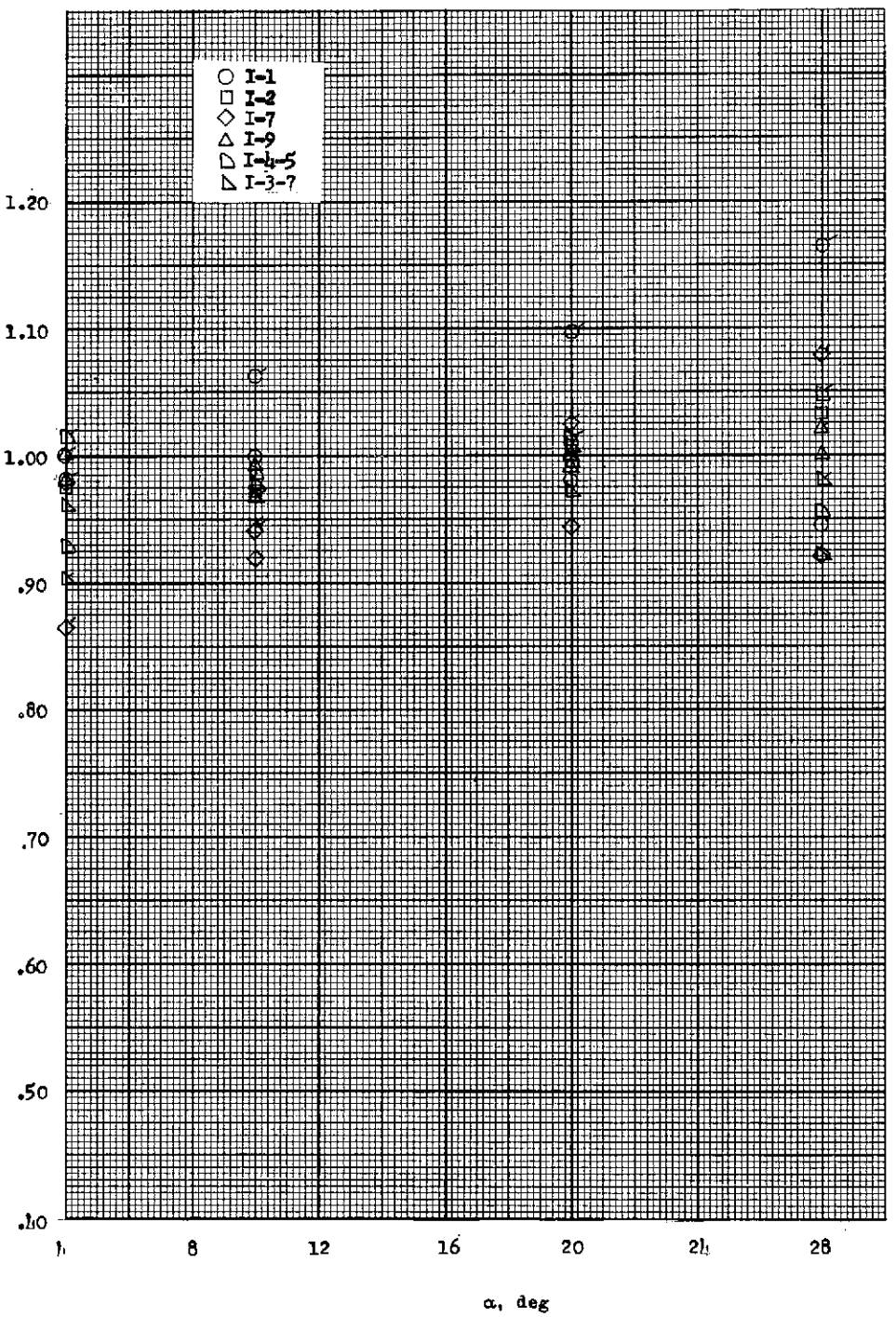

(c) M = 2.21.

Figure 55.- Concluded.

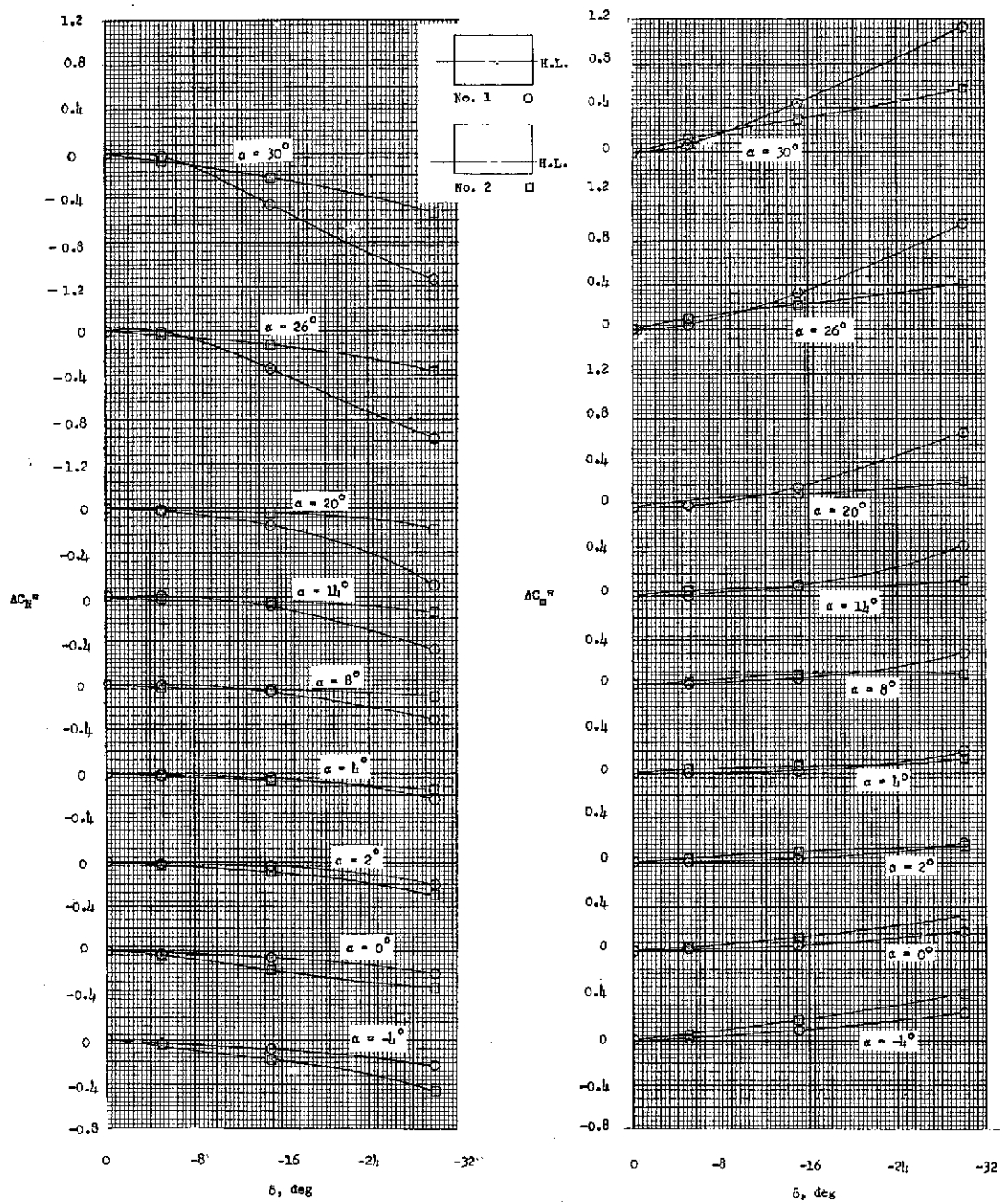

(a) $\phi = 0^{\circ}$.

Figure 56.- Effect of control hinge-line position. Comparison of $\Delta C_N''$ and $\Delta C_m''$ due to δ of control 1 with control 2 at angles of attack of -4° to 30° and Mach number of 6.01 for configurations I-1-1 and I-1-2.

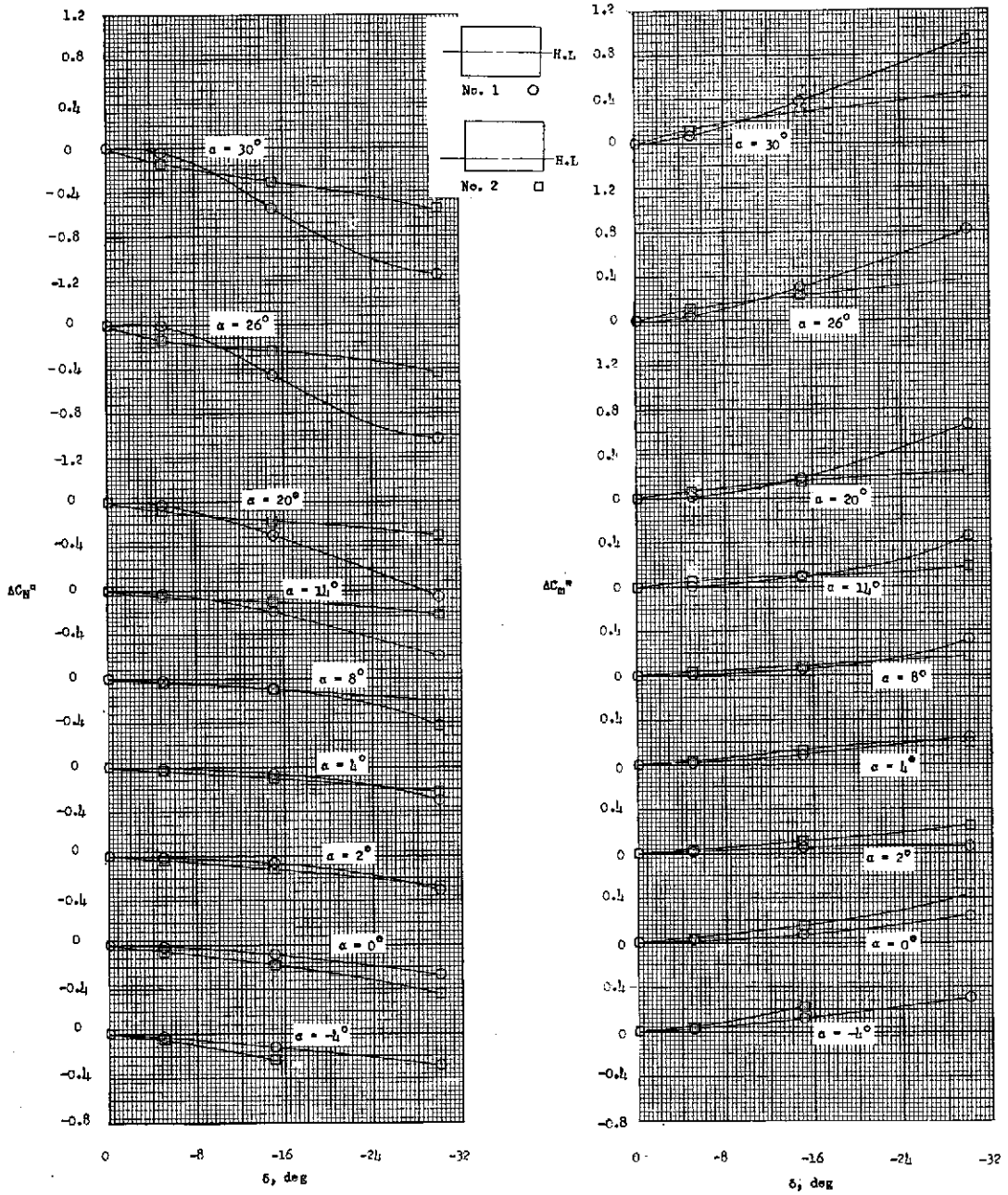

(b) $\phi = 45°$.

Figure 56.- Concluded.

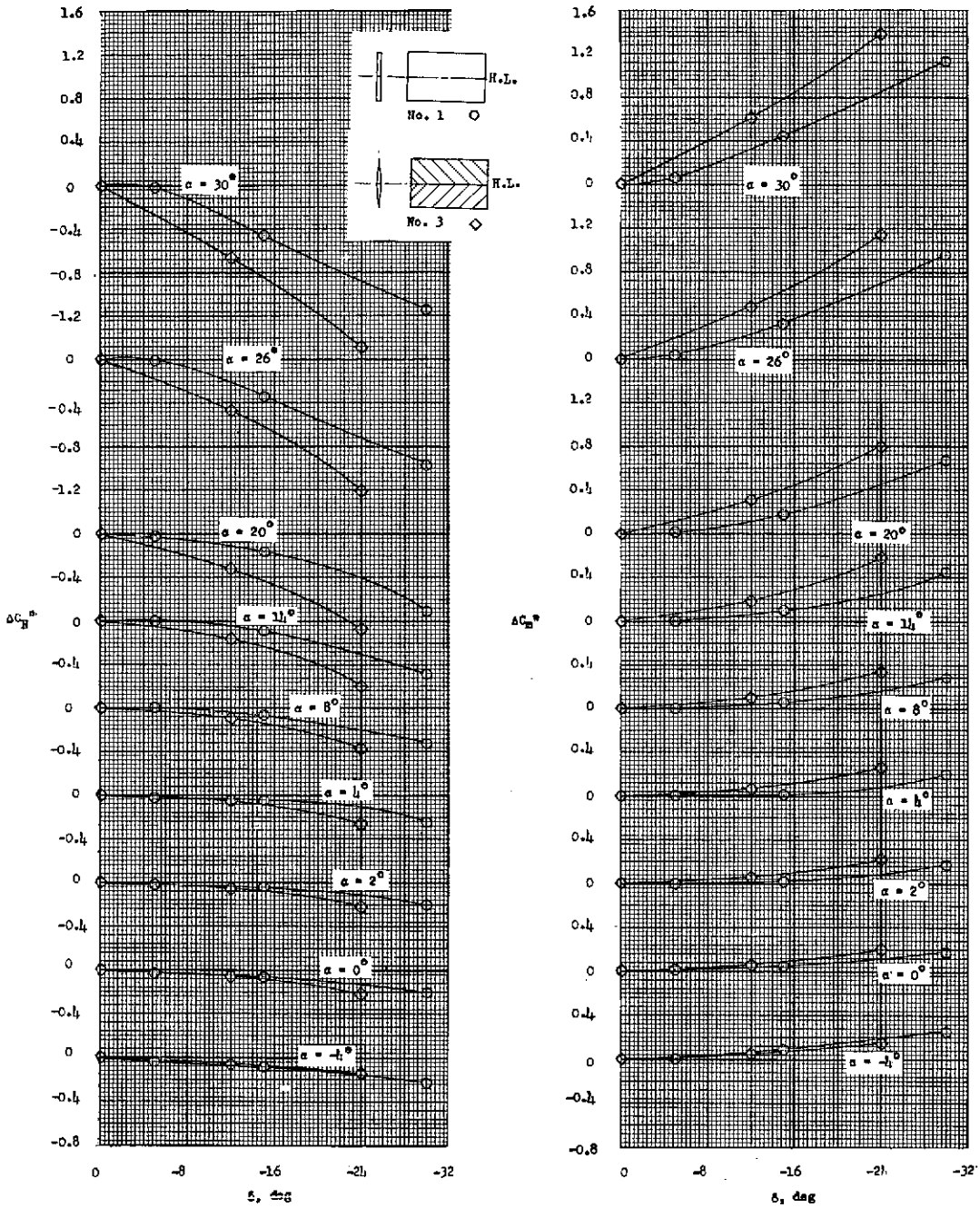

(a) $\phi = 0^{\circ}$.

Figure 57.- Effect of control profile. Comparison of $\Delta C_N''$ and $\Delta C_m''$ due to δ of control 1 with control 3 at angles of attack of -4° to 30° and Mach number of 6.01 for configurations I-1-1 and I-1-3.

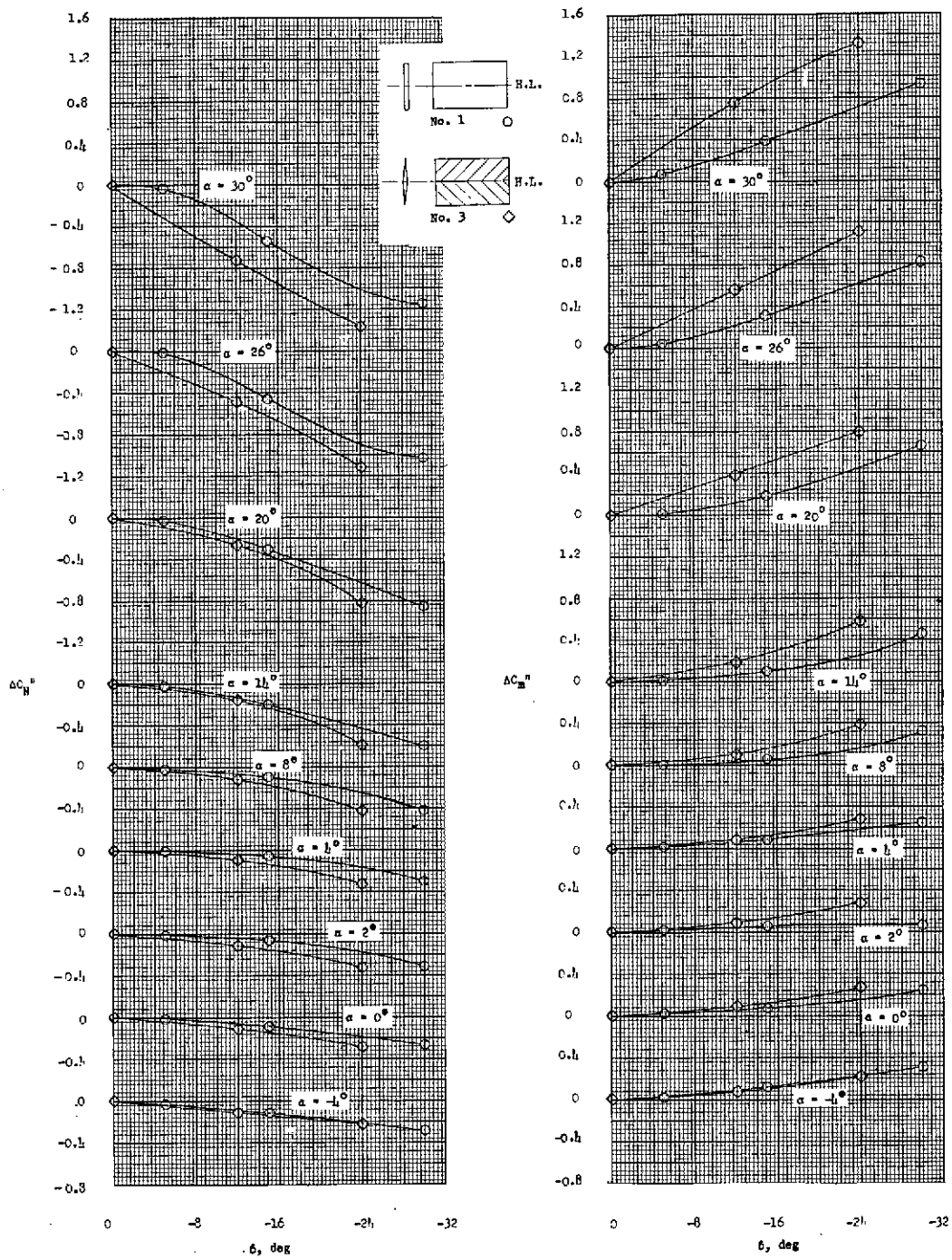

(b) $\phi = 45^{\circ}$.

Figure 57.- Concluded.

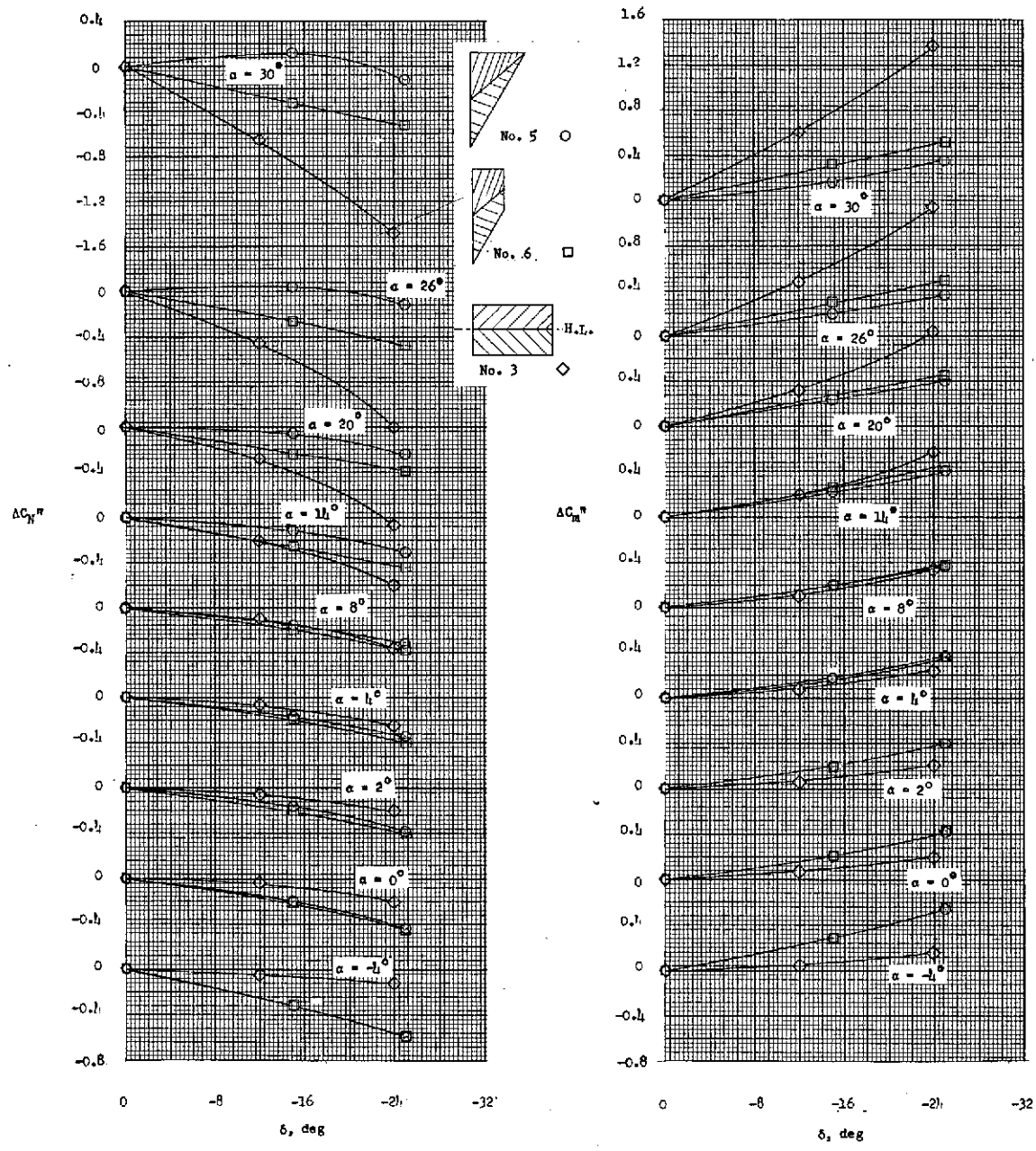

(a) $\phi = 0^\circ$.

Figure 58.- Comparison of trailing-edge and tip controls. Comparison of $\Delta C_N''$ and $\Delta C_m''$ due to δ of trailing-edge control 3 with tip controls 5 and 6 at angles of attack of -4° to 30° and Mach number of 6.01 for configurations I-1-3, I-4-5, and I-4-6.

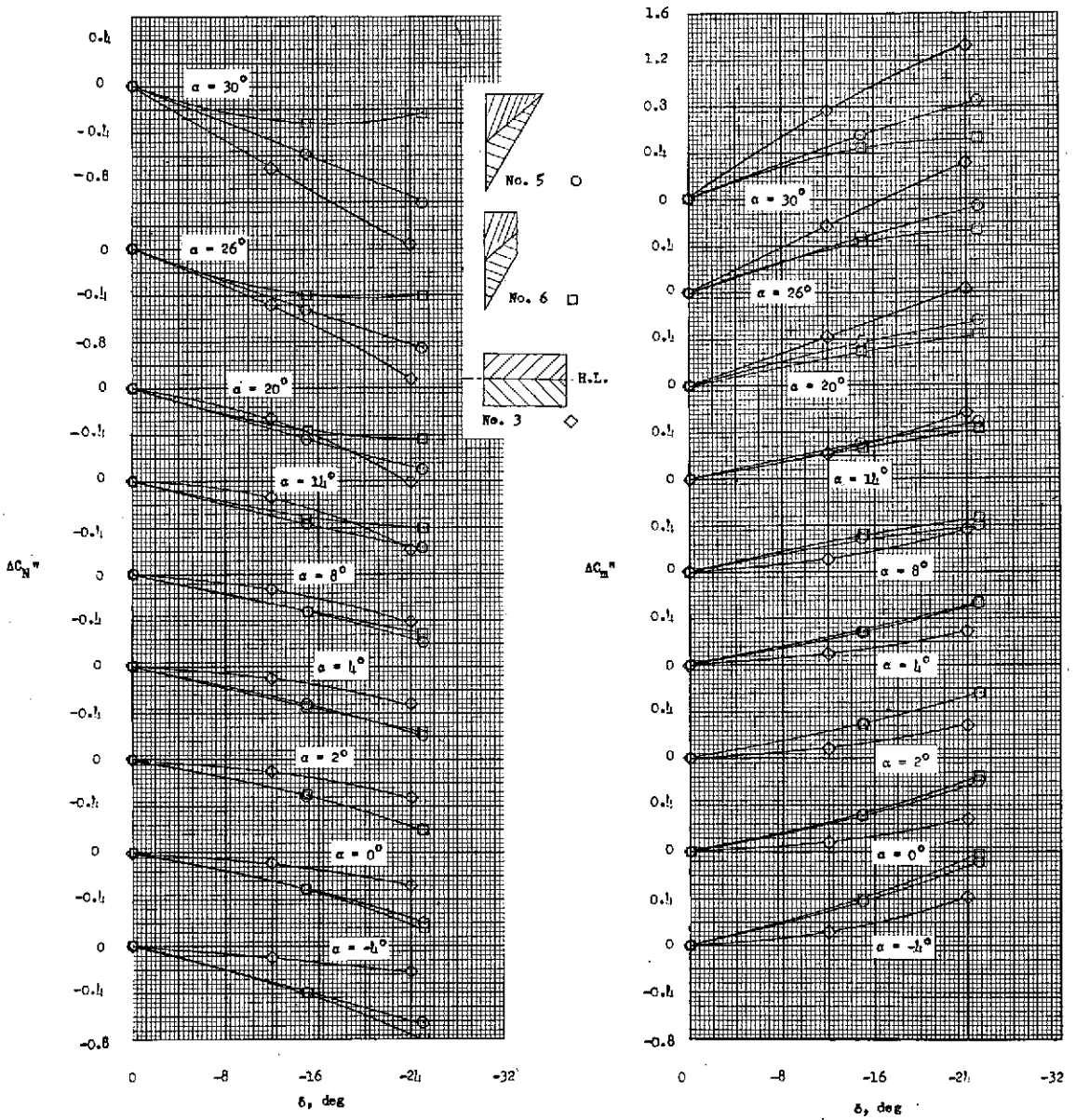

(b) $\phi = 45°$.

Figure 58.- Concluded.

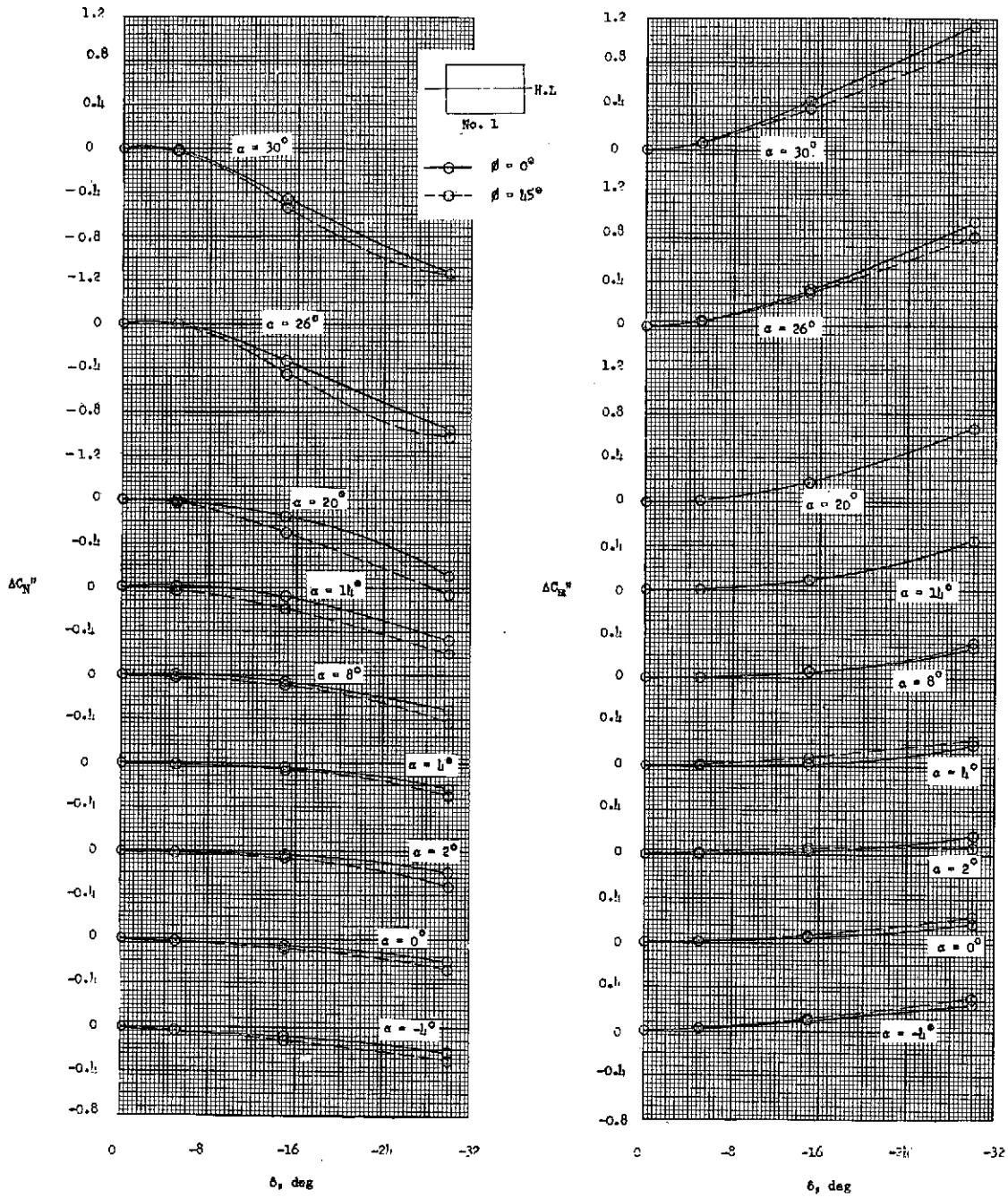

(a) Control 1; configuration I-1-1.

Figure 59.- Effect of roll. Comparison of $\Delta C_N''$ and $\Delta C_m''$ due to δ of control at $\phi = 0^\circ$ with control $\phi = 45^\circ$ for an angle-of-attack range of -4° to 30° and Mach number of 6.01.

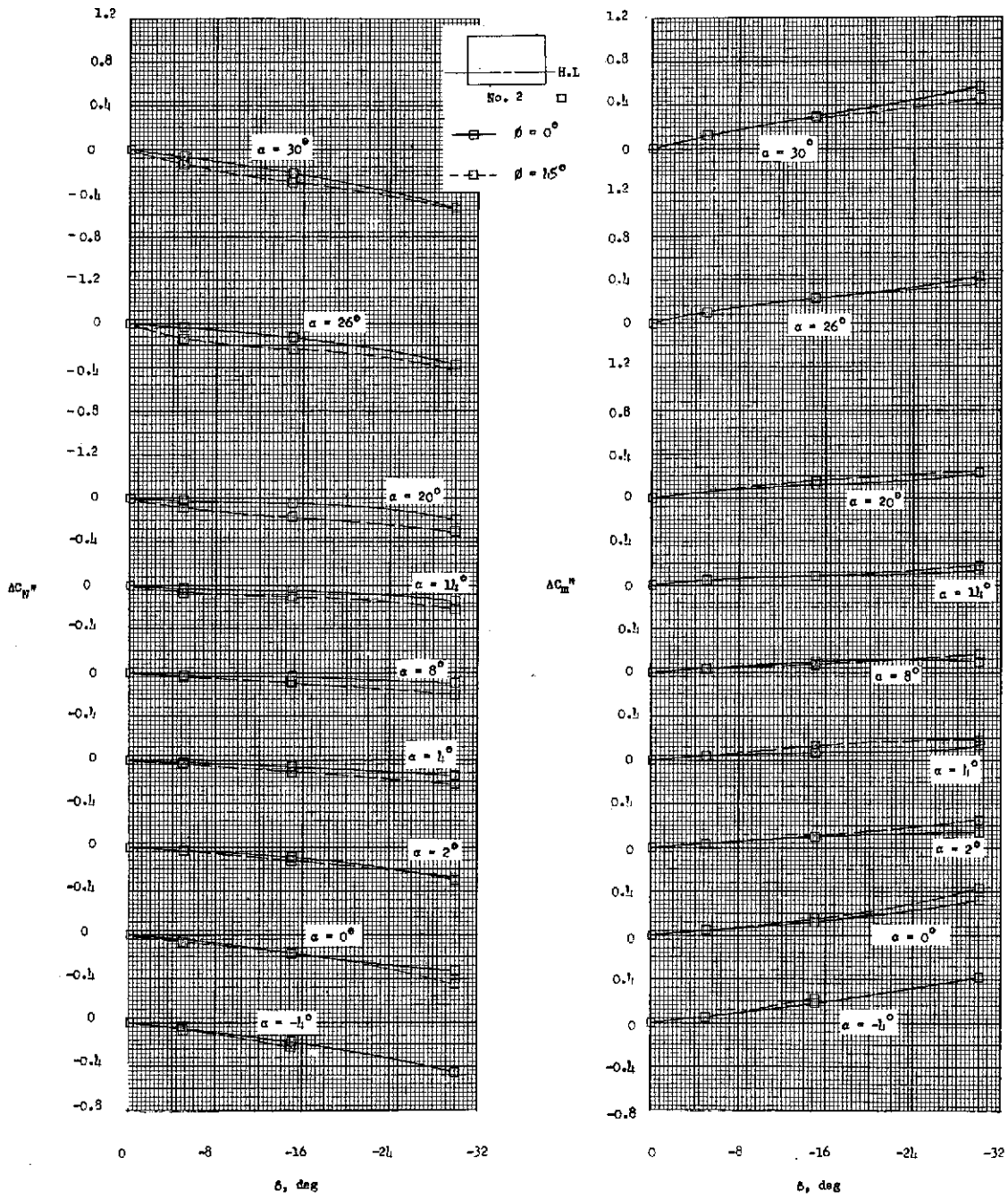

(b) Control 2; configuration I-1-2.

Figure 59.- Continued.

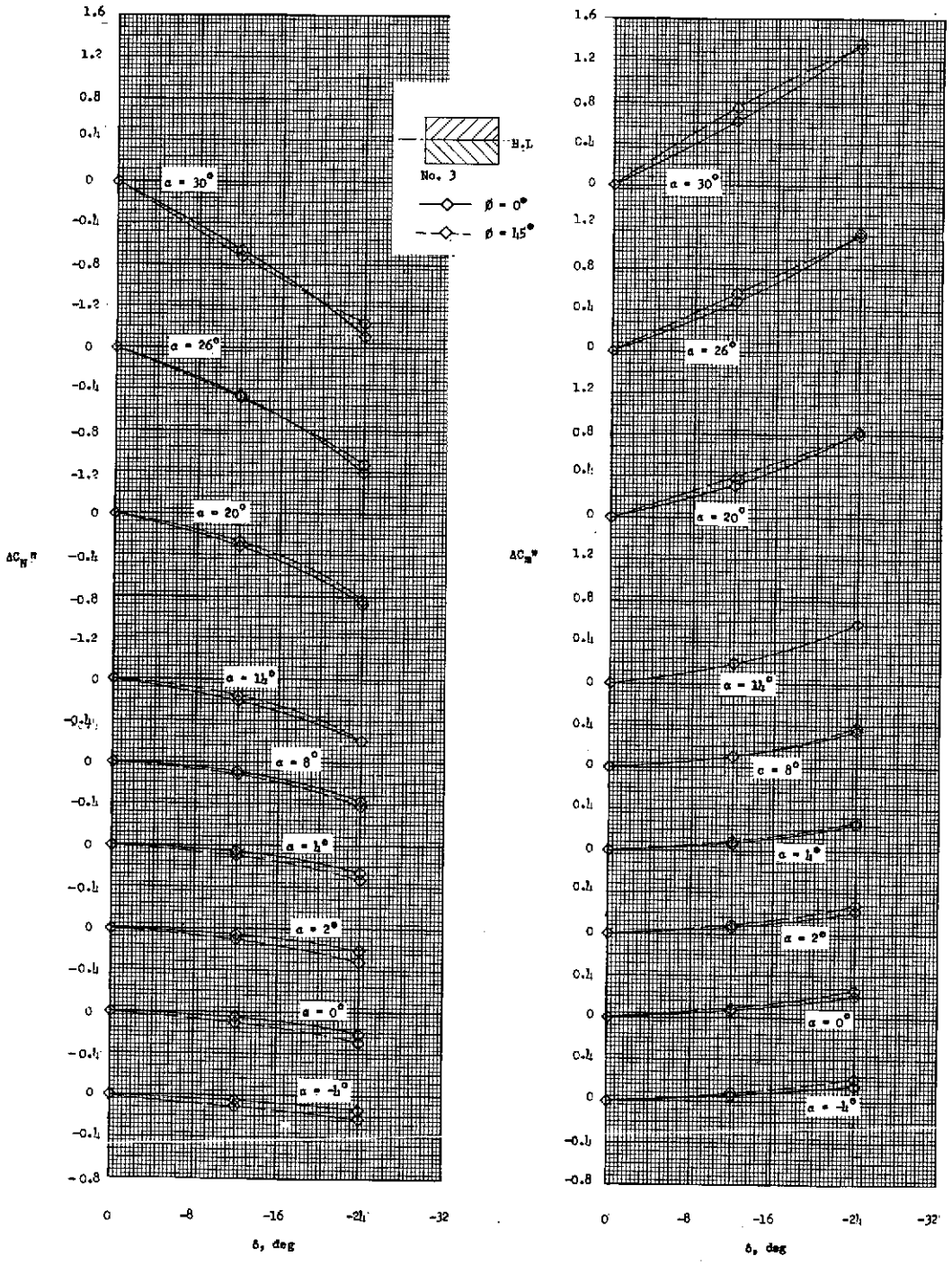

(c) Control 3; configuration I-1-3.

Figure 59.- Continued.

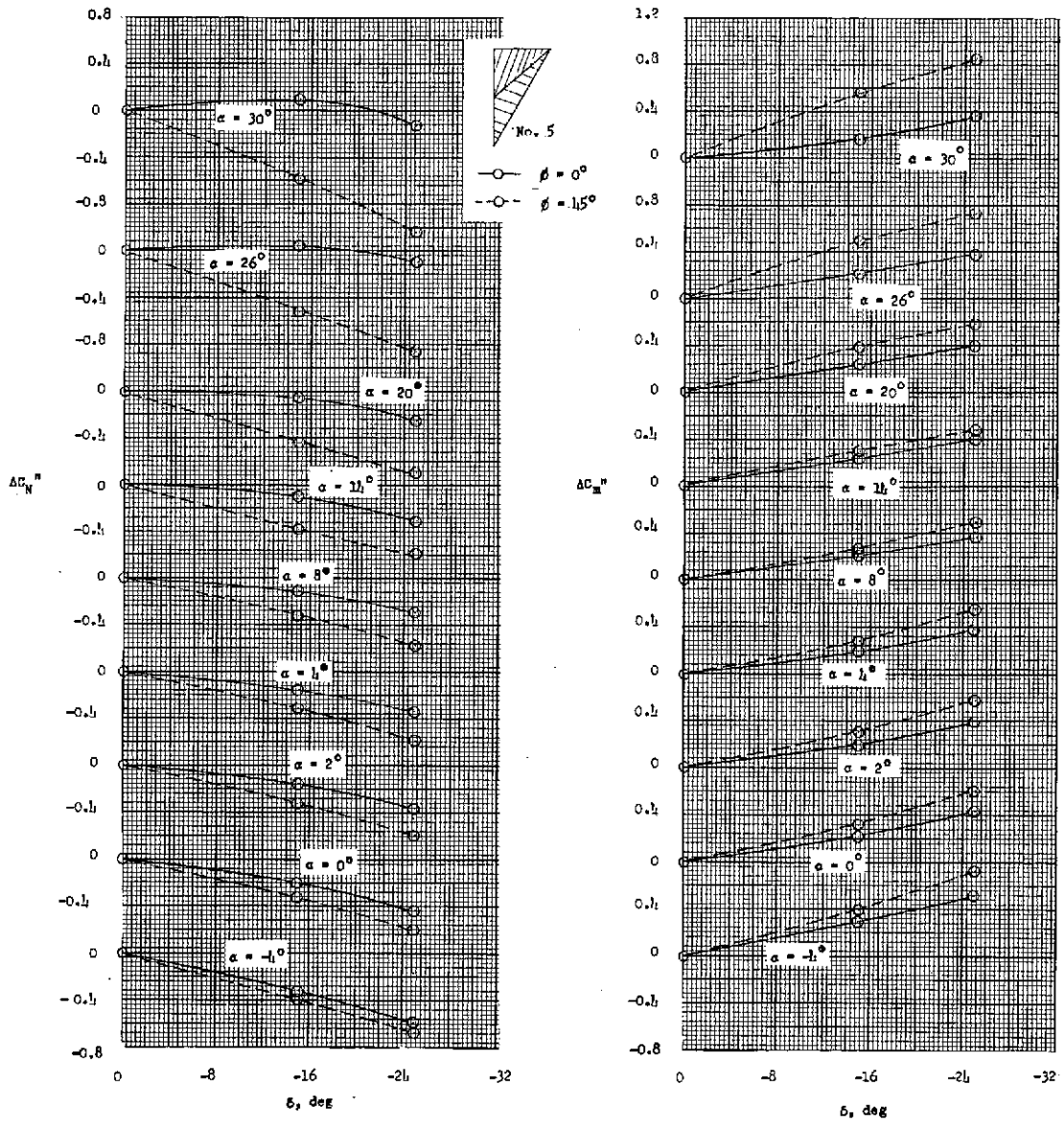

(d) Control 5; configuration I-4-5.

Figure 59.- Continued.

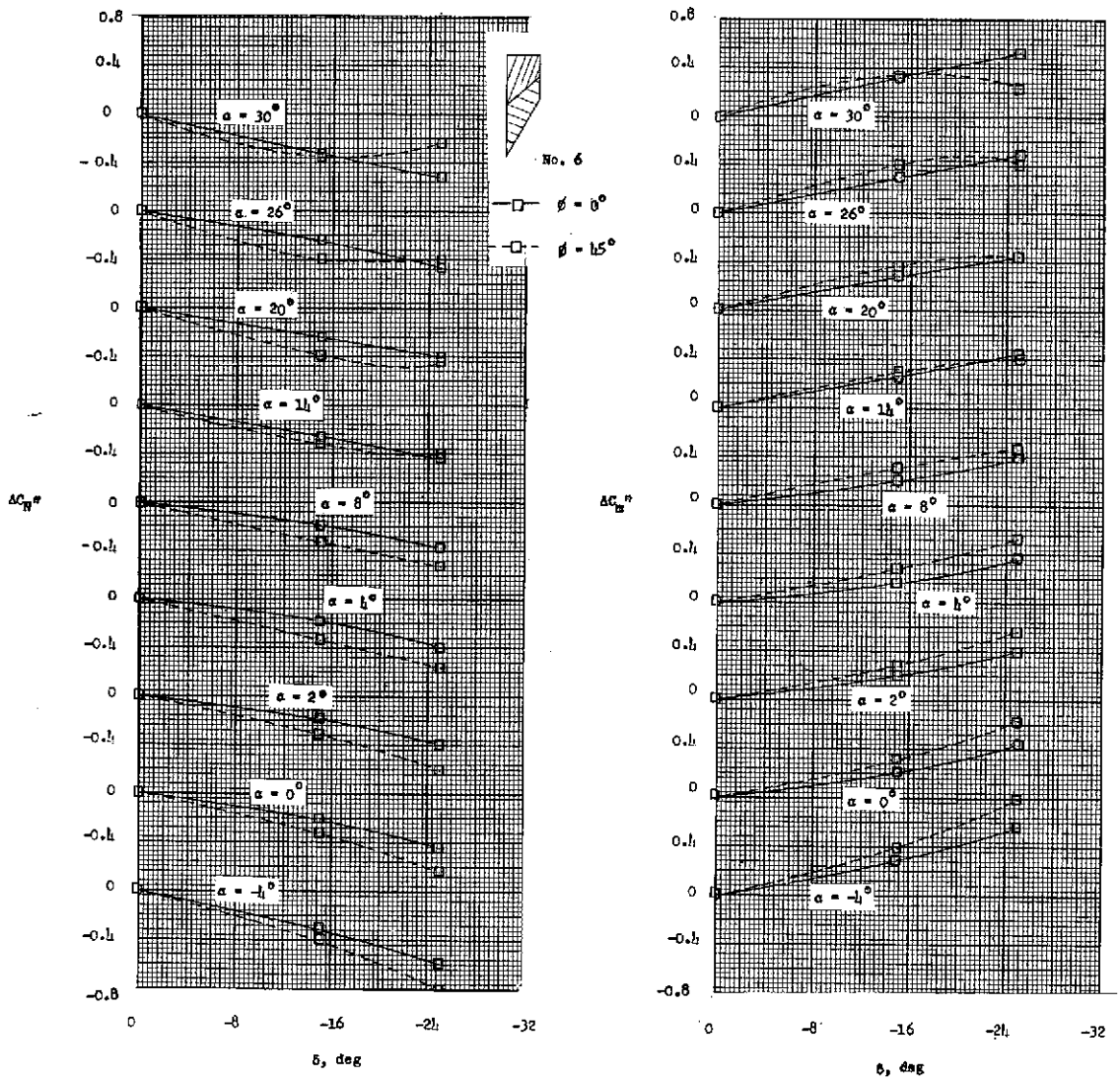

(e) Control 6; configuration I-4-6.

Figure 59.- Concluded.

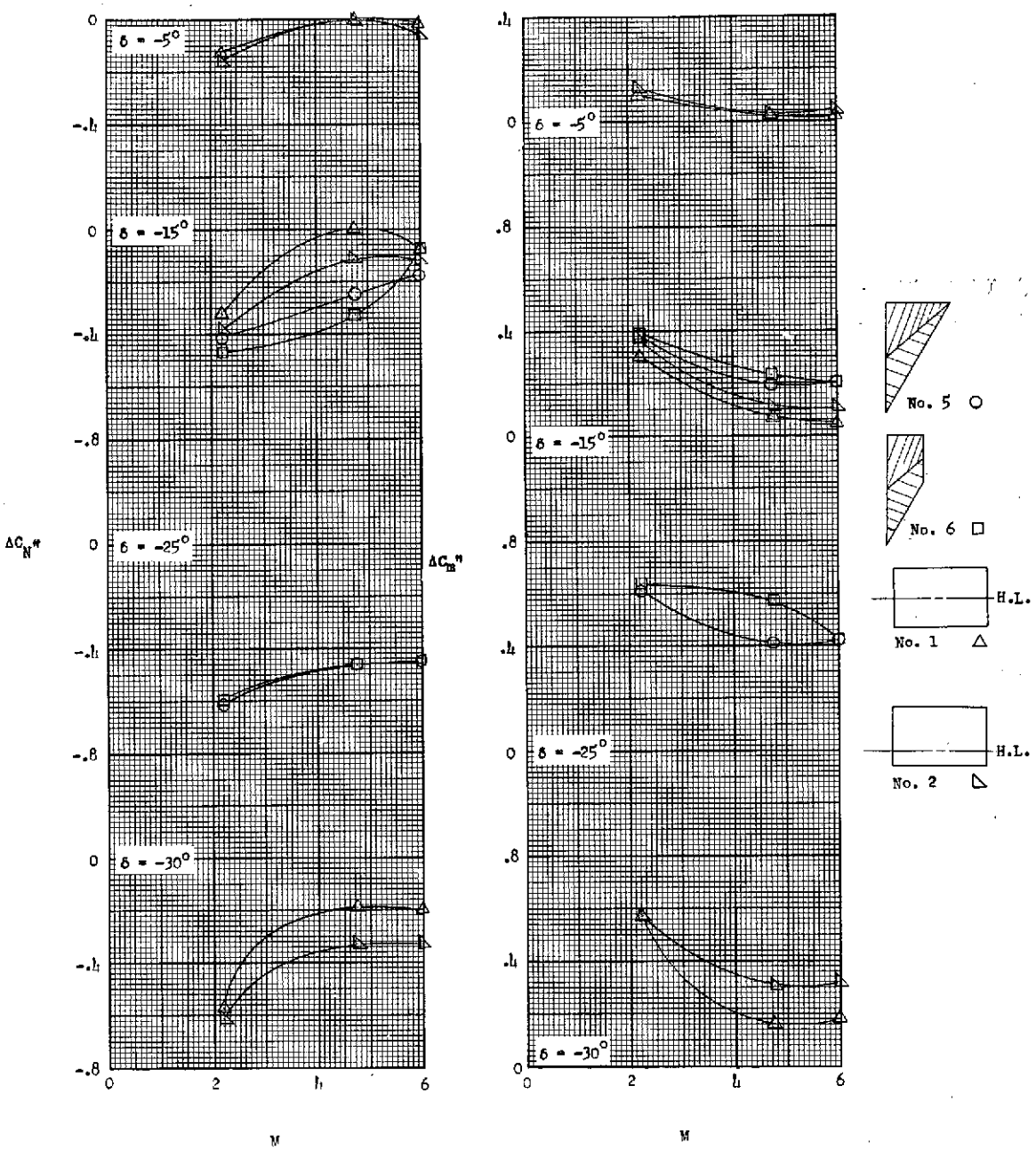

(a) $\alpha = 0^{\circ}$; $\phi = 0^{\circ}$.

Figure 60.- Influence of Mach number on control effectiveness. Comparison of variation of $\Delta C_N"$ and $\Delta C_m"$ with Mach number of controls 1, 2, 5, and 6 at control deflections from -5° to 30°. Configurations I-1-1, I-1-2, I-4-5, and I-4-6. Data at Mach numbers 2.21 and 4.76 are from unpublished Jet Propulsion Laboratory tests.

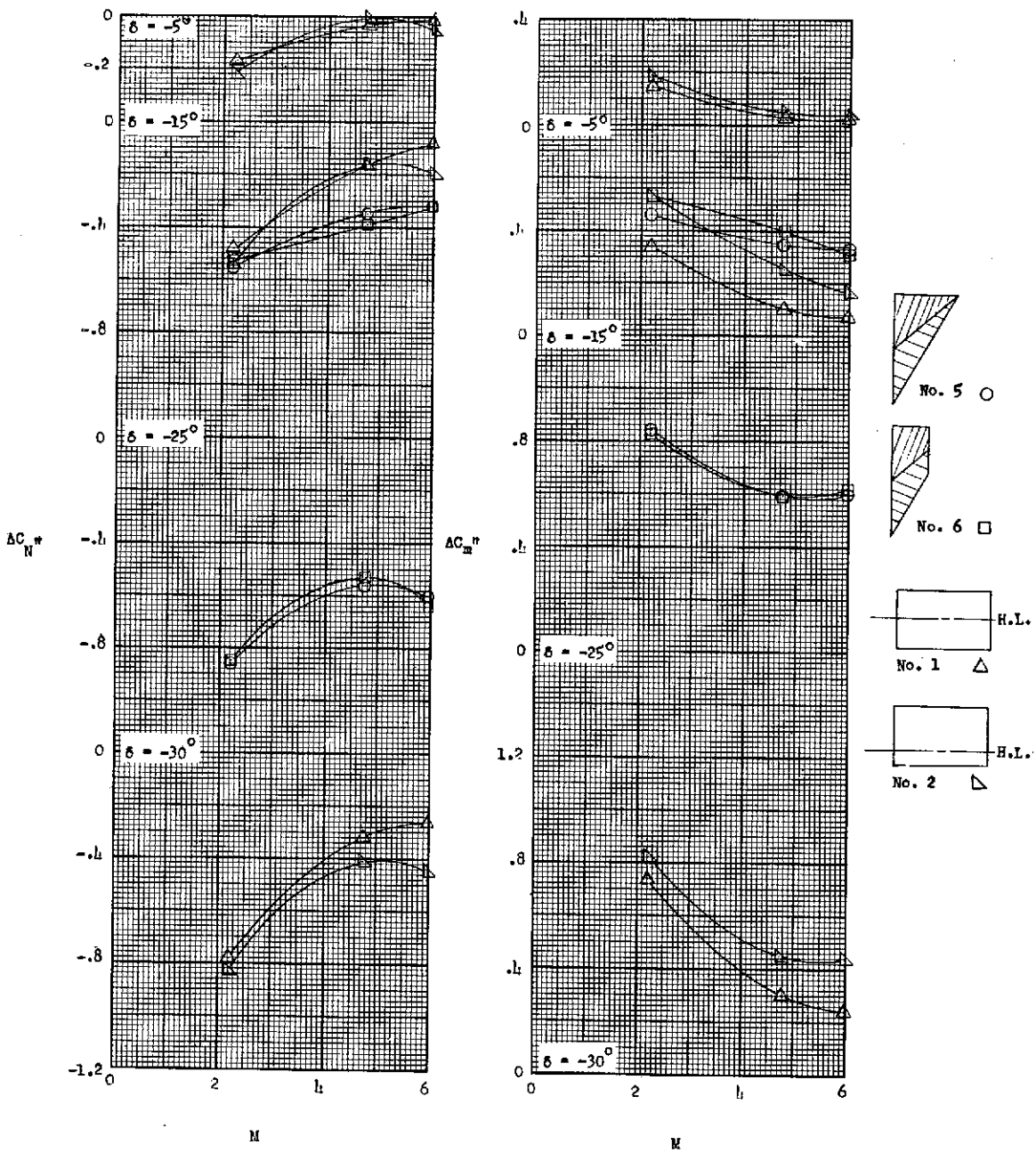

(b) $\alpha = 0^\circ$; $\phi = 45^\circ$.

Figure 60.- Continued.

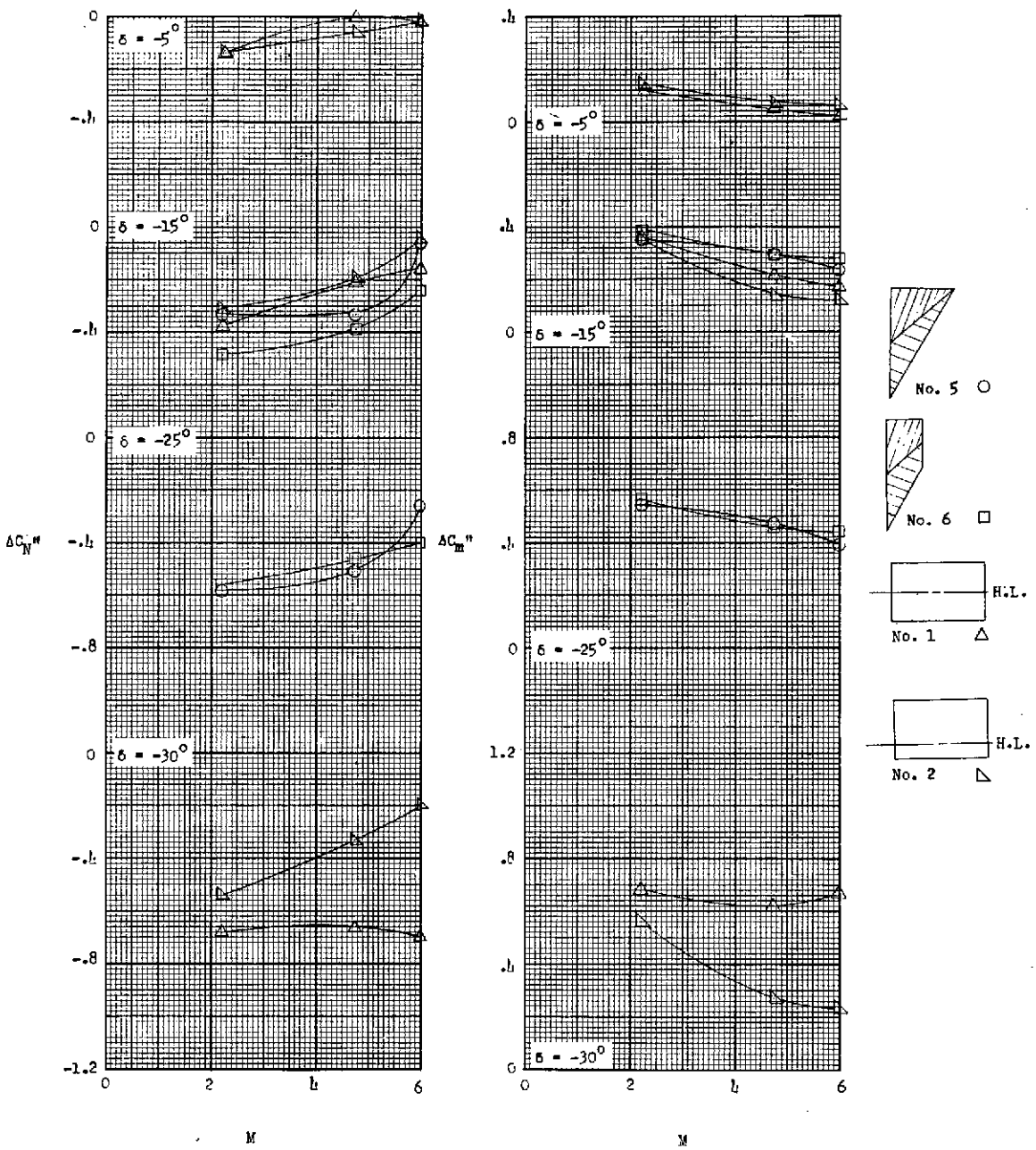

(c) $\alpha = 20^{\circ}$; $\phi = 0^{\circ}$.

Figure 60.- Continued.

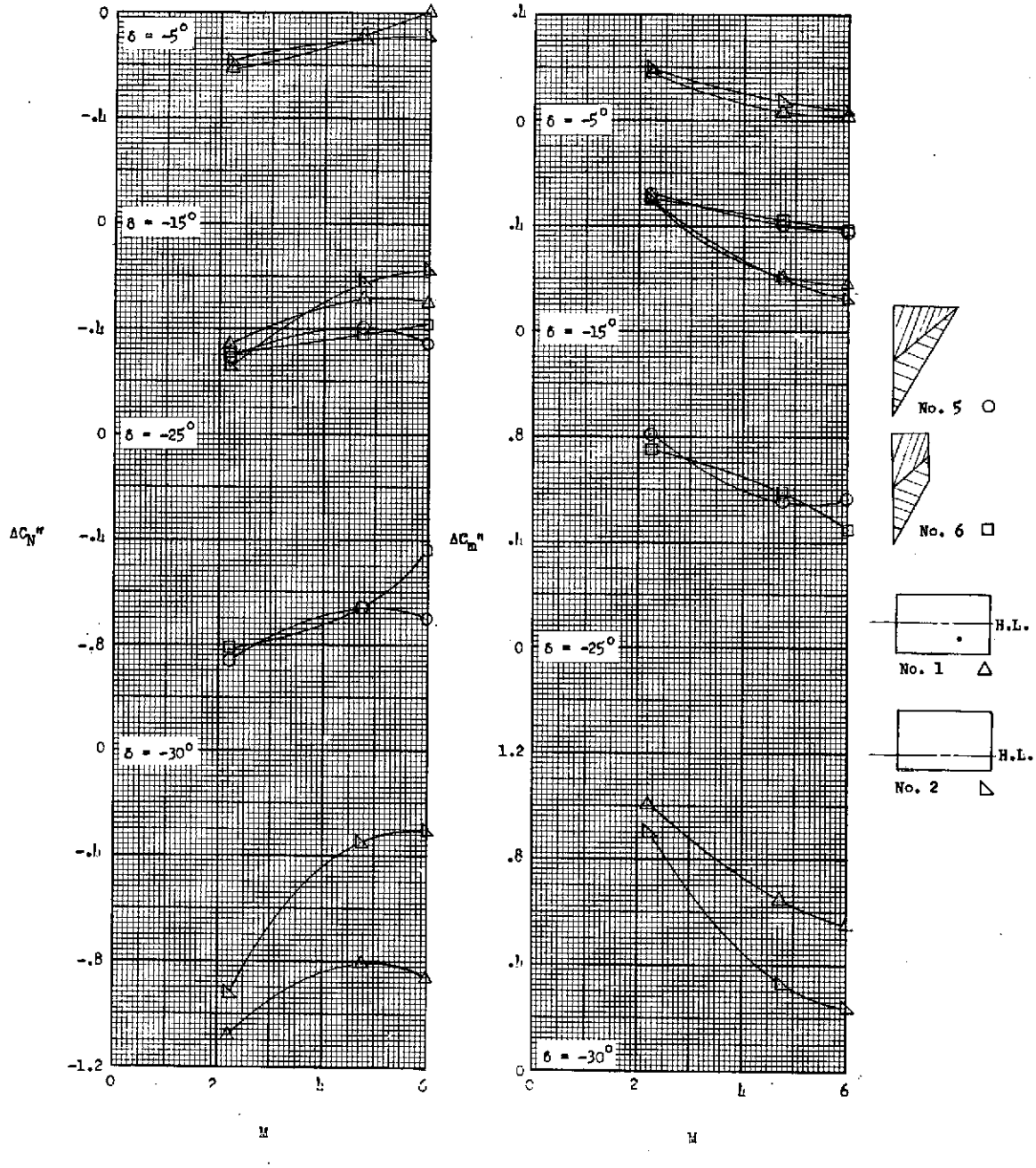

(d) $\alpha = 20^{\circ}$; $\phi = 45^{\circ}$.

Figure 60.- Concluded.

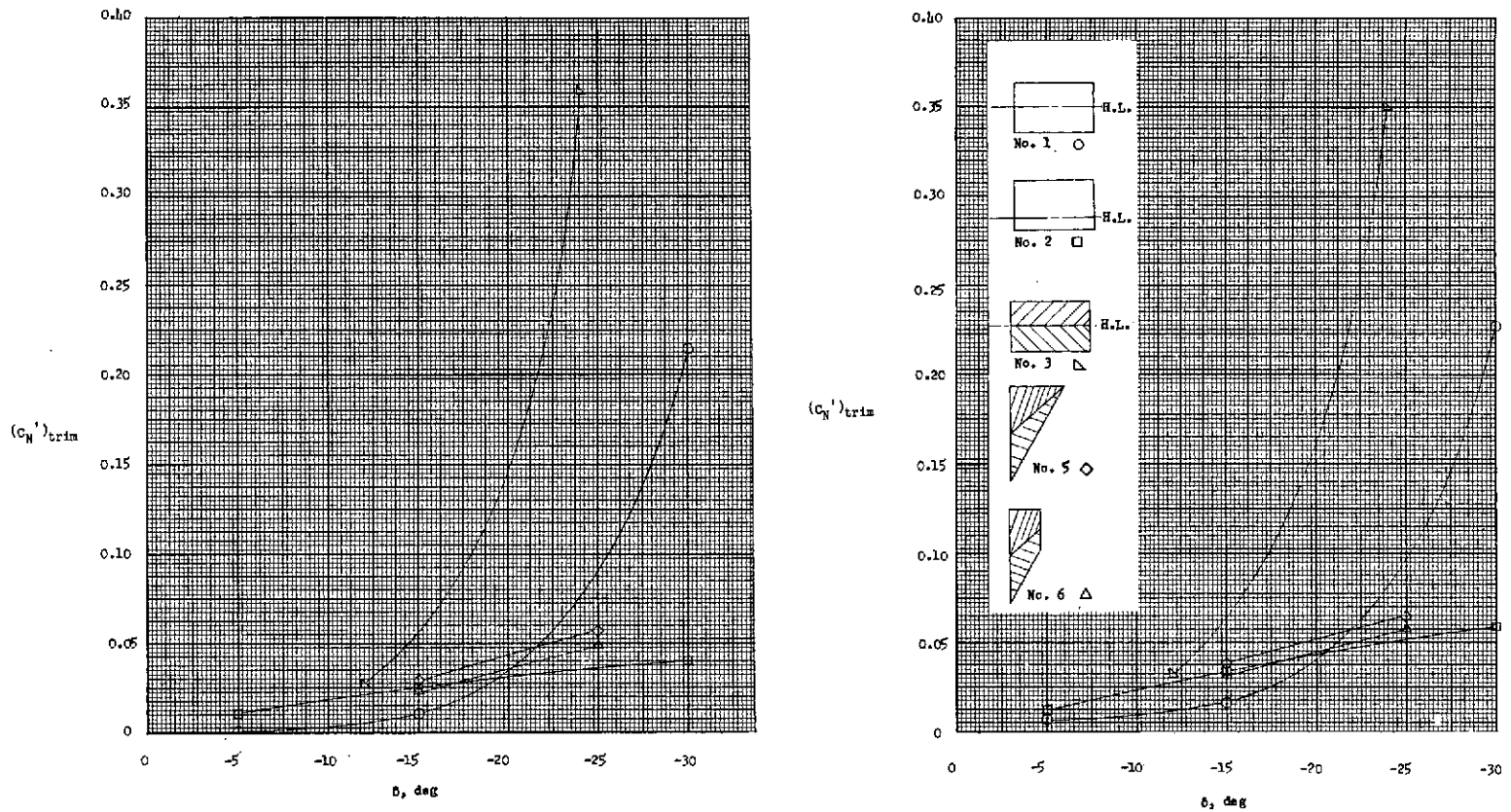

(a) $\phi = 0^\circ$.

(b) $\phi = 45^\circ$.

Figure 61.- Values of $(C_N')_{trim}$ at various control deflections for controls 1, 2, 5, and 6 and Mach number of 6.01. Configurations I-1-1, I-1-2, I-1-3, I-4-5, and I-4-6.

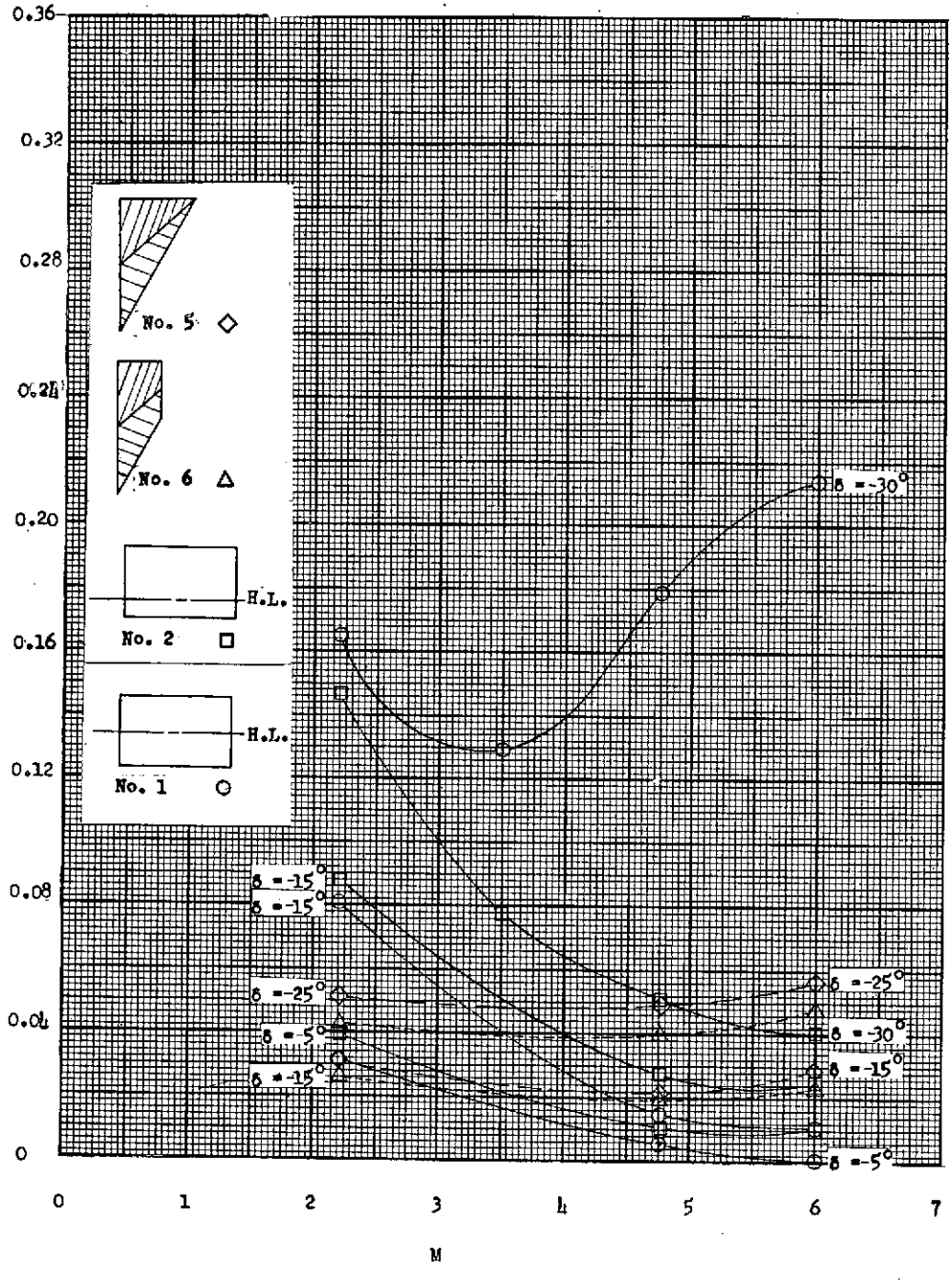

(a) $\phi = 0°$.

Figure 62.- Influence of Mach number on $(C_N')_{trim}$. Variation of $(C_N')_{trim}$ with Mach number for controls 1, 2, 5, and 6 at various control deflections. Configurations I-1-1, I-1-2, I-4-5, and I-4-6. Data at Mach numbers 2.21, 3.50, and 4.76 are from unpublished Jet Propulsion Laboratory tests.

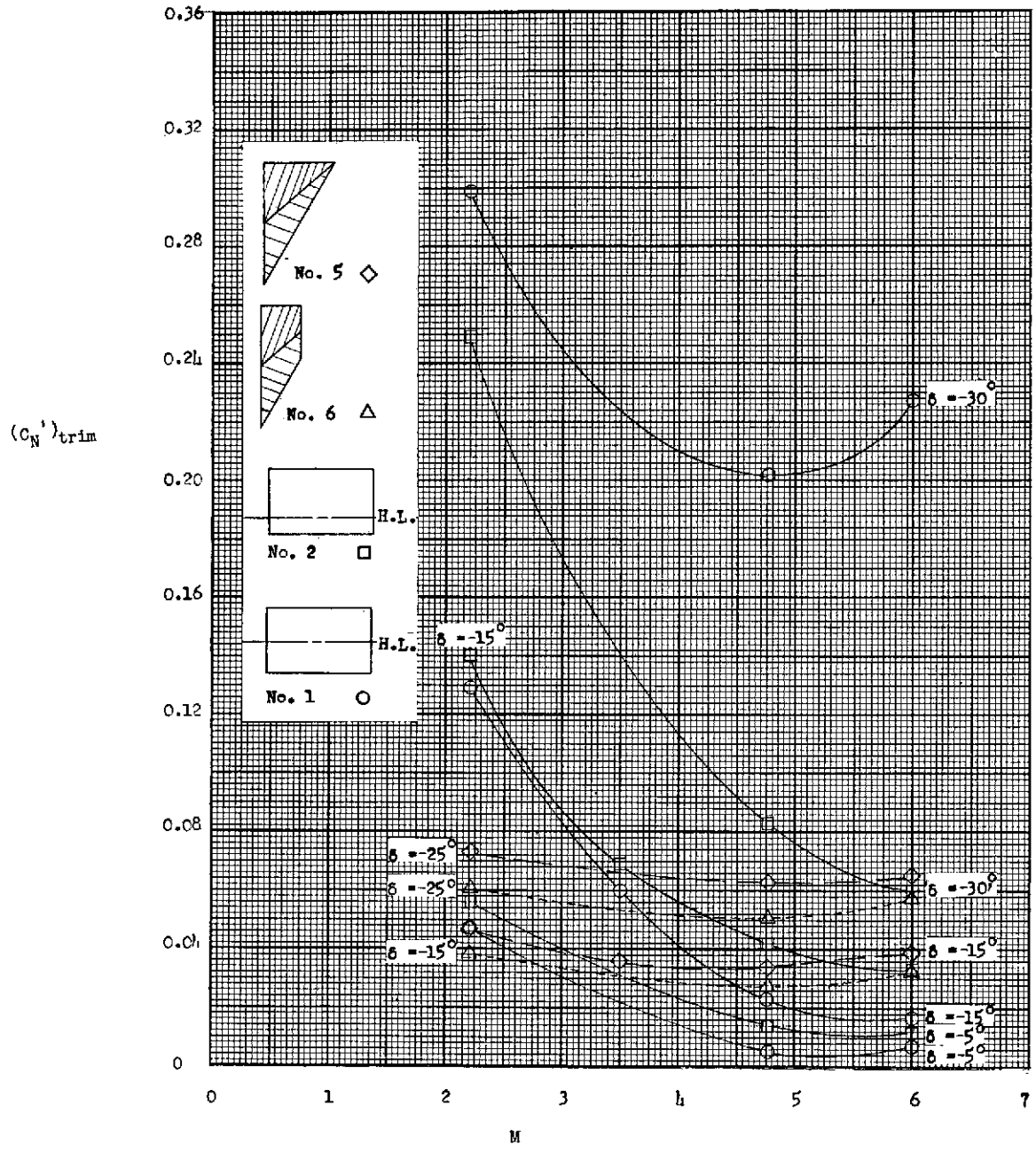

(b) $\phi = 45^\circ$.

Figure 62.- Concluded.

L-837